Detecting Sand Waves through Remote Sensing

Anne Mast

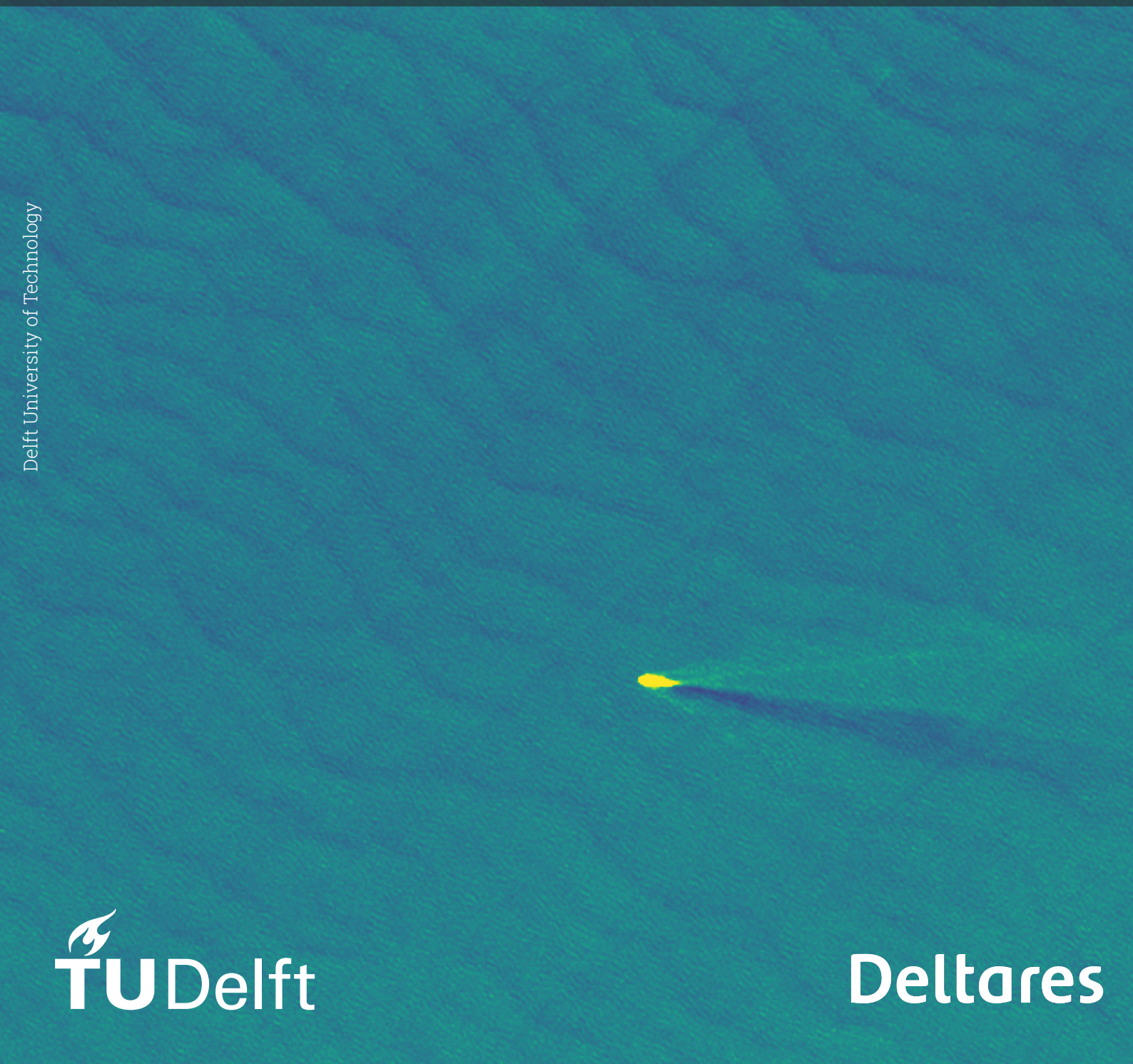

Delft University of Technology

TU Delft

Deltares

Detecting Sand Waves through Remote Sensing

by

Anne Mast

to obtain the degree of

Master of Science
in Civil Engineering

at the Delft University of Technology,
to be defended publicly on Monday January 25, 2024 at 15:00

Student number:	5448506	
Project duration:	March 2023 – January 2024	
Thesis committee:	Dr. Roderik Lindenbergh,	TU Delft
	Dr. Arjen Luijendijk,	TU Delft & Deltares
	Ir. Etiënne Kras,	Deltares

TU Delft

Preface

Before you lies the result of 10 months of research at Deltares, and concludes my master in Civil Engineering. This journey has been both challenging and enlightening, and I extend my gratitude to those who have played a great part in its materialization. I would like to thank all my supervisors, Roderik Lindenbergh, Arjen Luijendijk, and Etiënne Kras for providing me with the opportunity to undertake this thesis. Their guidance and expertise have been instrumental in shaping the trajectory of my research, and I am truly grateful for the invaluable learning experience. Furthermore, I would especially like to thank Etiënne for his guidance, discussions, multitude of ideas, and feedback throughout this process. I also want to express my appreciation to my family and friends for their continued support and encouragement.

This thesis is not just an individual achievement but a collective effort of those who have been part of this journey. As I present this work, I am deeply thankful to everyone who has contributed to its realization, making it a significant and fulfilling chapter in my life.

Anne Mast
Delft, January 2024

Summary

Sand waves can have a significant impact on offshore activities, and with the global push for sustainability and more renewable energy sources, these negative impacts will become more prevalent. Sand waves in the North Sea have a height up to a couple of meters and a wavelength between 100 and 1000 meters. The migration or change in asymmetry of sand waves can cause free spans in export cables leading to buckling or vibration causing failure. The migration can also cause cables to be exposed on the sea bed and in danger from offshore activities like anchors and fishing boats.

This research focuses on utilizing satellite data to determine sand wave characteristics. Satellites like Sentinel-1 and Sentinel-2 which are used in this research have global availability of data over multiple years at a 10 meter resolution. Sentinel-1 has a Synthetic Aperture Radar (SAR) which creates images by sending out microwave signals and recording the strength and the time delay of the returning signals. Sentinel-2 has an optical instrument which creates images by recording the reflected light from the sun on the earth's surface. Sand waves were detected through the change in Sea Surface Roughness due to the current interaction with the sea bed as described in the Alpers-Hennings Model. The difference in resulting sand wave characteristics between SAR and optical images were determined.

Three initial areas of interest off the coast of the Netherlands were chosen based on their different characteristics. Hoek van Holland contains short irregular sand waves. Holland Kust Zuid contains long regular sand waves. The third location is Alkmaar, which contains no sand waves and was used to determine the results of the methodology when a location has no sand waves present. The first step was to determine the environmental conditions necessary for sand waves to be visible in satellite images. Image collections for an area of interest over a set period of time were filtered based on the environmental parameters. These parameters include mean glint angle and cloud cover for optical images, and wind and current speed for both optical and SAR images. Threshold values were determined through literature. The wind speed should be between 3 and 12 m/s, the current speed should be greater than 0.4 m/s, and the mean glint angle for the latitude of the North Sea is less than 56 degrees. The image collection for the year 2021 for the three different areas of interest was filtered based on these parameters. The final collection after filtering was then manually checked for the visibility of sand waves. This number was lower than the initial filtered collection which means that there are additional factors that need to be accounted for.

A methodology was created to determine the sand wave characteristics over an area by applying a Fast Fourier Transformation (FFT) and calculating the sand wavelength and wave angle from the resulting signal. This was first applied to the three different areas of interest within the North Sea, Hoek van Holland, Holland Kust Zuid, and Alkmaar. Using the resulting image collection at these locations the sand wave characteristics were calculated. Although there are no sand waves at Alkmaar, due to the methodology, sand wave characteristics are still calculated. Also, the methodology works better at Holland Kust Zuid with long regular sand waves compared to at Hoek van Holland where sand waves are shorter and irregular.

To determine at which scale the satellite images should be viewed at to obtain information on the sand wave characteristics, the data was split into different area sizes and a FFT performed. The resulting average values and spread of the sand wavelength and wave angle were compared at different area sizes for optical and SAR images, as well as Multi-Beam Sonar (MBES). This resulted in an area of 5 by 5 kilometers which allows for the correct signals to be read across different possible sand wavelengths. Also, the effect of different sources of noise on the FFT and calculation of the sand wave characteristics for optical and SAR images was determined. From this it was seen that ships within a satellite image containing sand waves introduce a very strong signal within the FFT. This prevents the sand wave characteristics from being calculated correctly. Wind farms within a satellite image affect SAR images, and not optical images. Suspended sediment transport and clouds, which only occur within

optical images, have different effects. Optical images are not affected by sediment transport because the current direction will always be perpendicular to sand wave crests and therefore does not influence the calculation of sand wave characteristics. Clouds, similarly to ships, introduce a strong signal within the FFT which blocks the signal of the sand waves. Dark patches (like rain cells), which effect SAR images, block the visibility of sand waves within satellite images and therefore there no signal corresponding to sand waves within the FFT can be found.

Then, the area of interest was increased to the entire southern North Sea. Satellite images over the North Sea were downloaded in 5 by 5 km tiles for a single satellite pass over per year where the environmental parameters met the conditions necessary to view sand waves. As for the local scale cases, a FFT was applied to each tile and the sand wave characteristics were calculated including sand wavelength, wave angle, density, and spatial frequency. The differences in characteristics were compared from year to year. Typically, the difference is less than 200 meters in sand wavelength, however there are points where the difference is much larger. This is due to noise affecting the calculated value. Additionally, the data for wind speed and current speed for the date and time of the satellite image was determined. From this it is seen that optical images can contain sand waves at lower wind and current speeds, at the lower end of the boundary conditions. Sand waves are only visible in SAR images when the current speed is very high. Also, the results were compared to the water depth of the North Sea. At depths less than 40 meters which occurs on the Dutch Continental Shelf sand waves are almost always visible with the correct environmental parameters. At depths greater than 40 meters, which occurs on the West side of the sand wave field, sand waves are not visible consistently. The calculated sand wavelength over the North Sea was also compared to wavelength obtained from MBES. This resulted in low correlation values for both optical and SAR. As a result, noise present in satellite images should be taken into account.

By both applying the methodology to smaller scale cases and to the entire North Sea, it is possible to detect sand waves in different environments. Using the change in sea surface roughness due to sand waves it is possible to see sand waves in both optical and SAR satellite images. By applying the Fourier transformation the average sand wave characteristics over an area can be calculated. The methodology is limited by environmental parameters and noise that can be present in the satellite images. SAR and optical images require specific wind and current conditions, while optical images also requires specific mean glint angles and a low cloud cover. Different sources of noise also have a negative impact, adding signals to the FFT that do not correspond to the sand waves. Although the methodology proposed in this thesis is successful in determining the average sand wave characteristics over an area, more research for this topic would increase the possibilities. This includes using additional conditions for filtering image collections for sand waves, removing sources of noise, utilizing higher resolution satellite data, and testing the methodology on different sand wave fields that have different characteristics, such as symmetry. There are still many possibilities that can be explored in using satellite images to determine sand wave characteristics.

Contents

Nomenclature

Abbreviations

Abbreviation	Definition
AH Model	Alpers-Hennings Model
ALK	Alkmaar
AOI	Area of Interest
DCSM	Dutch Continental Shelf Model
FFT	Fast Fourier Transformation
HKZ	Holland Kust Zuid
HvH	Hoek van Holland
MBES	Multi-Beam Sonar
OPT	Optical
POI	Period of Interest
SAR	Synthetic Aperture Radar
SSR	Sea Surface Roughness

1 Introduction

1.1. Motivation

1.1.1. Energy Transition

Climate change and the increase of global temperature effects many of the natural processes in the world. To combat the negative impacts that this increase will cause, the Paris Agreement was introduced in 2015. 194 countries, including the European Union, have entered a legally binding international treaty to set the long-term goal of limiting the global temperature increase to 2 degrees Celsius (UNFCCC, 2015). The Netherlands has taken this a step further and has committed to being carbon neutral by 2050. Offshore wind farms are a desired source of sustainable energy, and the Netherlands plans to increase the capacity from the current 4.5 GW to 11.5 GW in 2030, which will account for 40% of the Dutch energy demand. The Netherlands eventually aims to have 70 GW capacity of offshore wind energy in 2050 (Rijksoverheid, 2018). Figure 1.1 shows current and planned wind farms in the North Sea. The North Sea is an ideal location due to its shallow waters, favorable wind climate, and a much larger available sea area compared to land area. Important information necessary for determining the location of offshore wind farms includes the seabed, wind speeds, and water data (Rijksoverheid, 2020).

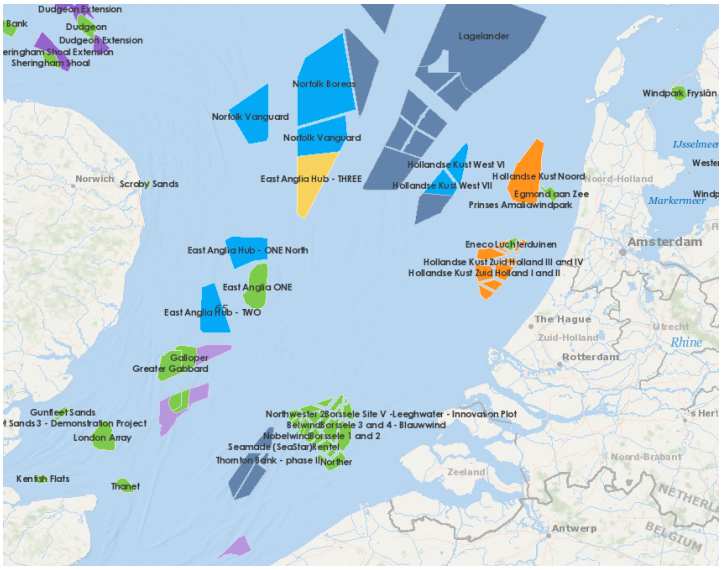

Figure 1.1: Global Offshore Renewable Energy Map for North Sea. Wind farms shown in green are fully commissioned, in orange/yellow are under constriction, blue has consent authorised, purple represents concept/early planning stage, and gray is a development zone (4COffshore, n.d.)

1.1.2. Sand Waves

Knowledge of the seabed is important because of the possible presence of sand waves which can have a negative impact on offshore wind farms, especially on the cables that connect the structures to land. Sand waves are bed forms that have a height range of 1-10 meters, length range of 100-1000 meters, and can migrate several meters per year. The North Sea has an extensive sand wave field that affect current and possible future offshore activities in the area as seen in Figure 1.2.

Figure 1.2: Observed sand wave occurrence in the southern part of the North Sea (Nemeth, 2003)

Sand waves form due to small variations in the seabed, eventually forming residual current cells from tidal currents which causes the growth of sand waves. They only occur in shallow sandy seas when there are strong tidal currents. Tidal sand waves have been found in the North Sea as well as the coastal waters of Japan and Canada, the shelf off Argentina, the shelf near Cadiz, southwest Spain, and the Irish Sea. Offshore sand waves are also observed in straits, such as Torres Straight north of Australia, Taiwan Straight in the Chinese Sea, and Messina Strait in the Mediterranean, and in tidal inlets in Denmark, and USA (van Santen et al., 2011). Sand waves are a global threat to offshore activities such as wind farms.

1.1.3. Detection of Sand Waves

The most practiced method to map seabed topography and to detect sand waves is through Multi-Beam Sonar (MBES). However, this method has a long measurement period, a limited range, specific in-field conditions that must be met, and high costs. To supplement MBES data or provide information in data poor areas remote sensing with satellite data can be used. Data from satellites is continuous, covers a large area, and is freely available (He et al., 2014). Data captured from satellites can easily be processed in Google Earth Engine, which has an expansive data catalog of remote sensing images and strong computational capabilities that can be accessed through the platform (Gorelick et al., 2017).

There are two methods of remote sensing through satellites further explored in this thesis, Synthetic Aperture Radar (SAR) and optical imagery. SAR is an active sensor which works by emitting microwave pulses and creating images based on the strength and time delay of the returned signal (Gagliardini et al., 2004). The first application of this method was by Alpers and Hennings in 1984 with a SAR sensor mounted on an airplane (Alpers & Hennings, 1984). The second method, optical imagery, is a passive sensor that takes the visible and near-visible part of the electromagnetic spectrum from reflected sun radiation from the surface. Although it is possible to use optical images in clear shallow water to see sand waves, when the water is deeper or less clear sun glint is needed as a medium. Sun glint is defined as “the specular reflection of light from water surfaces” and occurs when the water surface orientation causes the sunlight to be reflected directly towards the sensor (Kay et al., 2009). Both methods require strong tidal currents and moderate wind speeds.

Remote sensing offers another option in obtaining data over not only a large area but it also has the ability to look back in time for decades. Sentinel 1 and 2 were launched in 2014 and 2015 respectively, and Landsat 4 in 1984 with five additional Landsat satellites launched since. All these satellites have global coverage allowing for large scale observation (Gorelick et al., 2017). Utilizing remote sensing for the detection of sand waves will increase the amount of available data and allow for the further understanding of sand wave characteristics and migration at different locations, whether previously data rich or poor.

1.2. Problem Statement

1.2.1. Sand Wave effect on Cables

Sand waves are an important influencing factor on the construction and performance of offshore wind farms over the lifetime. Seabed topography is needed to determine the ideal location for construction and the threats posed by sand waves to cables. Cables when located in sand wave fields are in danger when migration or changing asymmetry of sand waves occurs as seen in Figure 1.3. This can cause free spans to form which can result in buckling due to gravity or vibration due to turbidity of flow around the free span. Exposure of the cables also put it at risk of offshore activities such as fishing equipment and anchors (Roetert et al., 2017). On the contrary, deep burial of the cable can lead to a temperature increase causing thermal stresses.

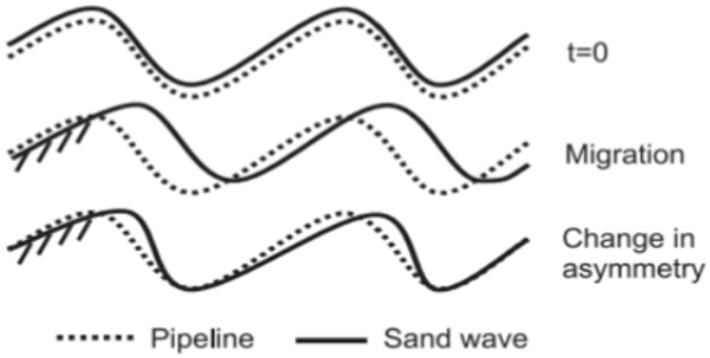

Figure 1.3: Illustration of a free span pipeline along a cross section of the seabed, due to the migration and change in asymmetry of sand waves. The solid line denotes the sand wave in which the pipeline, represented by the dotted line is buried. Note the exaggeration of the vertical scale compared to the horizontal scale (Nemeth, 2003)

1.2.2. Remote Sensing of Sand Waves

Currently, the most common method of obtaining seabed topography is MBES, a sensor placed on a ship that records information as it moves over the seabed. This method is expensive, is labour intensive, takes time, is only a snapshot of what is occurring and covers a limited area (He et al., 2014). Remote sensing using satellites offers an alternative method for the detection of sand waves by using the relationship between bed forms and the sea surface roughness (SSR). This can provide higher frequency data over a large area which is freely available. Methods for satellite remote sensing that can be applied include SAR and optical imagery, however the methods are dependent on different sensors and therefore might result in different outcomes.

Currently, remote satellite sensing has been used to detect sand waves in the North Sea (Jackson & Alpers, 2010; Kras et al., 2022), San Matías Gulf in Argentina (Gagliardini et al., 2004), and in the Taiwan Banks (He et al., 2014; Li et al., 2010; Shao et al., 2011, 2014; Zhang et al., 2014; Zhang, Yang, et al., 2015; Zhang et al., 2018). As stated before, there are two methods to remotely sense sand waves, SAR and optical imagery. Both methods rely on the same underlying mechanism off measuring sea surface roughness (SSR) however SAR directly measures SSR while optical imagery uses the amount of sun glint in relation to SSR to detect sand waves. Due to the differences outlined below both methods are dependent on different factors. Optical imagery with sun glint requires images to be taken during the day and cloud free as well as optimal current and wind conditions, it also is dependent on the imaging geometry which includes solar azimuth and zenith angle (Shao et al., 2011). While SAR is not dependent on cloud free daylight conditions it is still dependent on optimal current and wind conditions and can miss low frequency features due to noise speckling (Gagliardini et al., 2004).

To best detect sand waves through remote sensing the two different methods, SAR and optical imagery, should be compared for accuracy and the limitations of each method when applied to different sand wave fields needs to be assessed. By comparing crest location and wavelength of sand waves detected from satellite data compared to MB data, the accuracy of each method can be determined and the limitations in the temporal and spatial scale can be compared. Also, at this point in time there

is no automatic process available that takes satellite images from an area of interest and can detect the presence of sand waves in different sand wave fields around the world, which is the obvious next step in remote sensing of sand waves.

1.3. Objective

The aim of this study is to further the research and to understand the spatial and temporal limitations as well as the accuracy of the detection of offshore sand waves through remote sensing. The purpose of this research is to answer the following research question:

To what extent can satellite data be used to detect sand waves in different environments?

Sub-questions:

1. What methods are there for detecting sand waves through satellite data and what are the different processes they require?
2. How can these methods be applied to sand wave fields in different environments?
3. What is the accuracy of the methods and what are the limitations regarding spatial and temporal scale?

1.4. Thesis Outline

The following chapter contains the background information on sand waves and how remote sensing can be utilized in which the first sub-question is answered as part of the literature study. The third chapter contains the methodology for obtaining satellite images containing sand waves in an area of interest as well as the post processing to get sand wave characteristics. The fourth chapter will contain the results from following the methodology in the previous chapter, comparing the results from the different remote sensing methods and validation compared to MBES data along with the upscaling of the methodology. Chapter five will contain the discussion of results while chapter six will contain conclusions about the research. Finally, the last chapter will contain recommendations for further research.

2
Background Information

2.1. Sand Waves

Sand waves can be described by four characteristics: wavelength, wave angle, migration, and wave skewness. Sand waves typically have a height range of 1-10 meters, wave length range of 100-1000 meters, and can migrate up to several meters per year (Hulscher, 1996). They only occur in shallow sandy seas when there are strong tidal currents such as in the North Sea as well as the coastal waters of Japan and Canada, the shelf off Argentina, the shelf near Cadiz, southwest Spain, and the Irish Sea. Offshore sand waves are also observed in straits, such as Torres Straight north of Australia, Taiwan Straight in the Chinese Sea, and Messina Strait in the Mediterranean, and in tidal inlets in Denmark, USA, and the Netherlands" (van Santen et al., 2011).

Sand waves form due to small variations in the seabed, eventually forming residual current cells from tidal currents as seen in Figure 2.1 which causes the growth of sand waves. The environmental parameters effecting sand waves includes water depth, median grain size, and amplitude and ellipticity of the depth averaged tidal current. There exists an inverse relationship between sand wave length and tidal current, where wavelength decreases as the tidal current increases, however the wavelength increases when the water depth increases (van Santen et al., 2011). The timescale for the growth of sand waves is between 5 and 10 years (Hulscher & Dohmen-Janssen, 2005).

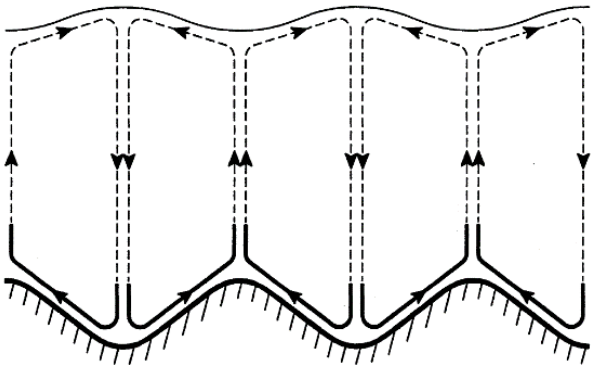

Figure 2.1: Strong near-bed circulation which supports the growth of the bottom perturbation. The backward circulation in the upper flow part uses a larger part of the water column and is weaker (Hulscher, 1996)

Migration, as pictured in Figure 2.2 (b), occurs due to residual currents which can be induced from tide, wind, or wave currents, or due to tidal asymmetry and typically migrates downstream in the direction of the residual current (Besio et al., 2008). The migration rate of sand waves also depends on the maturity of wave, as a fully grown sand wave migrates slower than an infinitely small sand wave. Asymmetry occurs when a steady current causes accumulation of sediment on one side of a sand wave and erosion on the other, which can cause migration (Nemeth, 2003).

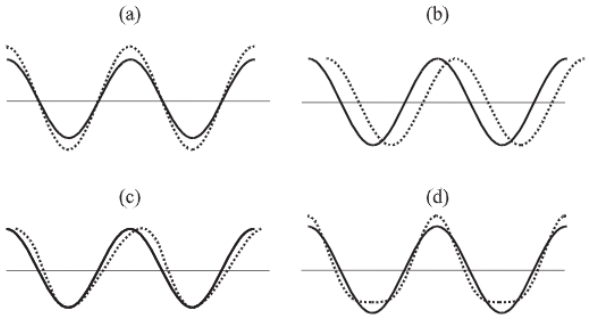

Figure 2.2: Changes in sand wave profile: (a) growth, (b)migration, (c) change in horizontal asymmetry and (d) change in vertical asymmetry (Nemeth, 2003)

2.2. Detecting Sand Waves

Historically, Single-Beam Sonar were used however data obtained through this method does not allow for a full understanding of complicated three dimensional sand wave fields due to the limited horizontal scale. The most common method currently used to map seabed topography and to detect sand waves is through Multi-Beam Sonar (MBES) which can capture the full extent of sand wave characteristics and migration.

However, there are downsides to utilizing sonar such as having a long measurement period, a limited range, specific in-field conditions that must be met, and high costs. To supplement MBES data or provide information in data poor areas remote sensing with satellite data can be used. For example, Sentinel 1 and 2 were launched in 2014 and 2015 respectively and have global coverage allowing for large scale observation (Gorelick et al., 2017). In addition to covering a large area, the data provided is continuous and freely available (He et al., 2014). Data captured from satellites can easily be processed in Google Earth Engine, which has an expansive data catalog of remote sensing images and strong computational capabilities that can be accessed through the platform (Gorelick et al., 2017).

2.3. Remote Sensing of Sand Waves

Remote sensing can of sand waves can be performed in multiple ways, such as using the blue-green band of optical satellite images in shallow, clear waters because it penetrates much further into the ocean (Hennings et al., 1994). However this method is not applicable when water is turbid. Additionally, the breaking of waves in optical images due to sand wave formations has also been to determine seabed features (Zhang, Lou, et al., 2015). However, this research will focus on two remote sensing methods that utilizes the Alpers-Hennings (AH) Model.

The AH Model allows for the observation of sand waves through remote sensing in three steps. The first is that the current interacts with the bottom topography. Then, the surface current has variations due to the bottom topography which causes variations in the surface short waves and is controlled by a weak hydrodynamic interaction theory. The Sea Surface Roughness (SSR) is smoother on the fore side of the sand wave and rougher on backside with respect to the direction of the current as seen in Figure 2.3. SSR is then measured directly or indirectly through SAR or optical imagery respectively. To have the necessary small gravity and capillary waves present for this method to work there needs to be a low to moderate wind for the right SSR and a strong current speed (Gagliardini et al., 2004).

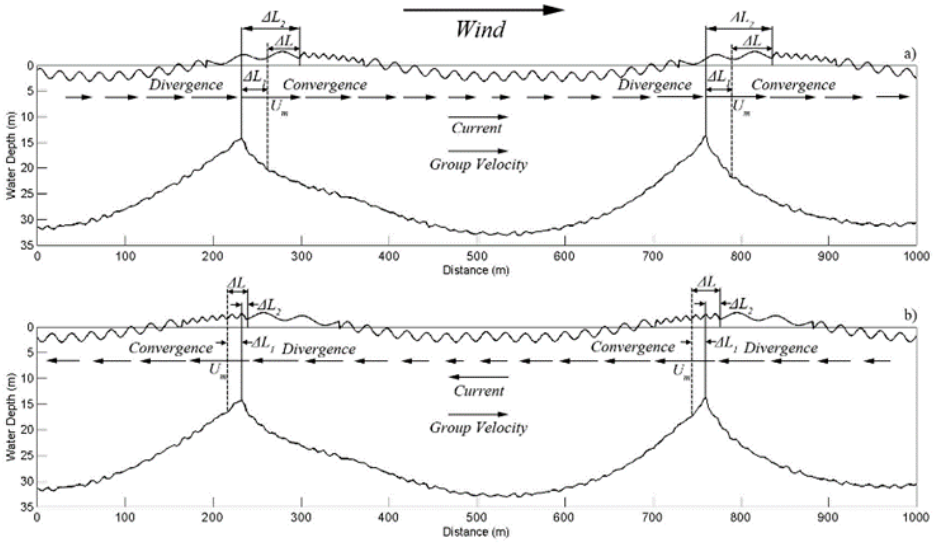

Figure 2.3: A schematic diagram of the advection effect (phase modulation) due to submarine topographic variations when the current is (a) in the same direction as and (b) opposite to the direction of the wave group velocity. ΔL_1 is the distance from a sand wave crest to the location of maximal surface current, ΔL_2 is the distance from the sand wave crest to the location where the modulation ratio of the action spectrum is equal to zero, and ΔL = ΔL_2 - ΔL_1 also know as the advection length for determining relaxation rate (Shao et al., 2011)

2.3.1. Optical Imagery

Optical imagery is a passive sensor that takes the visible and near-visible part of the electromagnetic spectrum from reflected sun radiation from the surface. As stated before, optical images can be directly used to determine sand wave location in clear, shallow water, however when the water is deeper or less clear, sand waves need to be indirectly measured.

When light travels through the atmosphere towards the sea surface there are multiple paths that can be taken as seen in Figure 2.4. To detect sand waves through optical satellite images using the AH model, sun glint is required to measure the amount of SSR. Sun glint is defined as “the specular reflection of light from water surfaces” and occurs when the water surface orientation causes the sunlight to be reflected directly towards the sensor (Kay et al., 2009). Typically, sun glint is undesirable in optical images because it can contaminate images because sun glint measures as a much greater value than the radiance from the water surface. However, the amount of reflectance measured by the sensor directly relates to measure of SSR and can therefore determine the locations of sand waves within a field. To determine whether the conditions to use sun glint for using satellite images is met, the mean glint angle is used. The mean glint angle is the angle between the incident sunlight that reflects off the sea surface and the sensor.

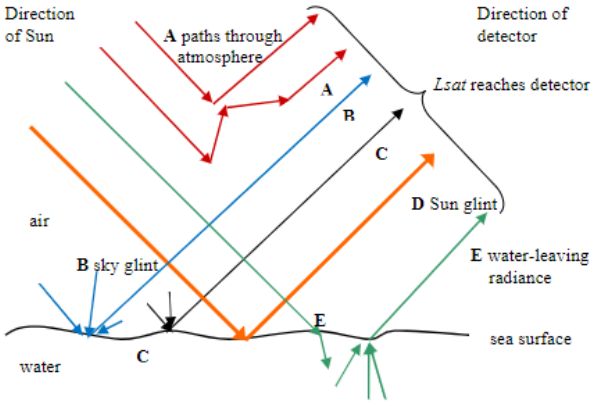

A Single or multiple scattering in the atmosphere, by molecules or aerosols

B Scattering from the atmosphere to the water surface and then reflection to the detector—often termed "sky glint"

C Reflection from whitecaps on the sea surface

D Specular reflection from water surface, with direct transmission through the atmosphere from the sun to the surface and from the surface to the detector—this is termed 'sun glint' in the context of this review.

E Transmission through the atmosphere and air-water interface followed by scattering or reflection below the water surface and transmission back through the atmosphere to the detector.

Figure 2.4: Schematic diagram showing routes by which light can reach a remote sensing detector (Kay et al., 2009)

In addition to requiring low to moderate winds and a strong tidal current which is required for the process in the AH model, optical imagery also requires cloud free conditions and daylight. Clouds can block the view of sand waves in an image when the cloud cover is high or when cloud cover is low it can introduce noise in the image, blocking other signals. Other sources of noise are ships, wind farms, and suspended sediment transport.

To decrease the amount of noise in an optical satellite image a Gaussian filter is used. This primarily smooths the image based on the Gaussian distribution in two dimensions and removes high frequency noise. It is useful in this case because it preserves the edges of an image while removing noise (Basu, 2002). The sand waves in optical satellite image are presented as edges and it is important to maintain these features after smoothing away other noise.

2.3.2. SAR

Synthetic Aperture Radar, or SAR, is an active sensor which works by emitting microwave pulses and creating images based on the strength and time delay of the returned signal (Gagliardini et al., 2004). Using the AH model, SAR is a direct measurement of the SSR and can detect sand waves this way. SAR requires the same wind and current conditions as optical images do, however has no such requirements for low cloud cover, daylight, high solar azimuth, and high zenith angle months (Shao et al., 2011). A disadvantage of using SAR is that images can contain error due to speckle noise which optical images do not have (Agrawal & Khairnar, 2019). SAR experiences speckle noise due to the back-scatter or interference of the returning microwave signals. Speckle noise can hide weaker signals of sand waves present in SAR images.

To mitigate the effects of speckle noise within a SAR image a filter can be applied. Common filters include Lee, Frost, and GMAP filters. In this case the Lee filter will be used because it smooths speckle noise and retains edges and textures (Painam & Manikandan, 2021). The texture of an image is the information about the spatial arrangement of intensity in an image which is how the SSR due to sand waves is presented ins satellite images. The Lee filter works by using a small window size where the

value of the center pixel is based on the mean value of all the pixels and the weight based on variance of the pixels and the variance of the speckle noise (Taskesen, 2020).

2.4. Fourier Transformation

To determine sand wave characteristics from satellite images, a Fourier transformation is used. A Fourier transformation is a technique used to decompose complex signals into the different sinusoidal components of the different frequencies. This is done by transforming the spatial domain into the frequency domain. In a Fourier transformation the low frequency components shows coarser signals while high frequency components shows more details. To determine the different signals derived from sand waves present in satellite images a two-dimensional Fourier transformation was applied using the Fast Fourier Transformation (FFT) algorithm.

Sand waves are assumed to have a sinusoidal shape and therefore represent a sinusoidal signal in a satellite image. Therefore, the aim of applying the FFT to the satellite image is to decompose the image into the different signals and identify the signal due to the sand waves present. Sinusoidal signals are represented in a two-dimensional Fourier transformation by two points that are equidistant from the center of the image as seen in Figure 2.5. By determining the distance d of the point from the center

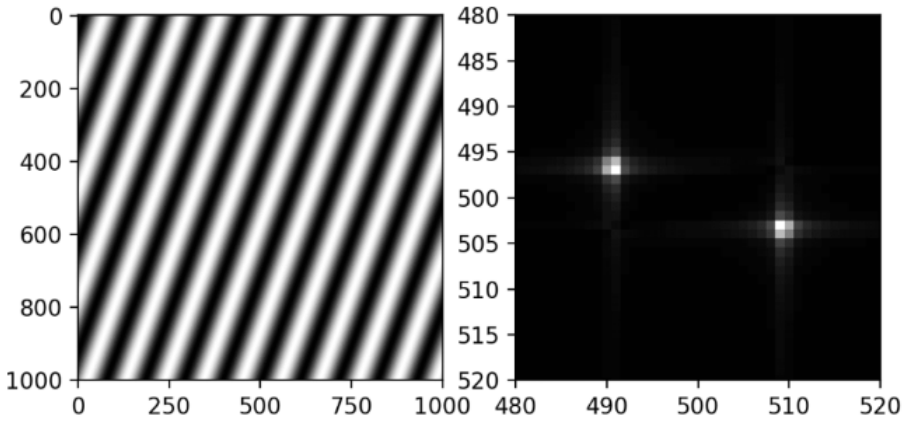

Figure 2.5: Fourier transformation performed on image containing sinusoidal grating in spatial domain (left) to the spectral domain (right) (Gruppetta, 2021)

of the figure, the wavelength can be determined by taking 1/d to get the value from the frequency to the spatial domain and is visualized in Figure 3.9. Similarly, the wave angle of the sand waves can be determined by taking the angle between the x-axis and the point.

2.5. Data Sources

This section will discuss the origin of the data that is used in order to detect sand waves. This data includes satellite data from Sentinel 1 and 2, MBES data for validation, wind and current speed data necessary for filtering, and lastly sand wave characteristic data for the Dutch Continental Shelf.

Satellite Data

The Google Earth Engine (GEE) database and API is used to process the image collections from satellites Sentinel 1 and Sentinel 2. The Sentinel 1 satellite has a synthetic aperture radar that sends out microwave pulses and then captures the returning signal. The satellite was launched in April of 2014 by the European Space Agency and since then has been monitoring the Earth's surface. The vertical transmit/vertical receive (VV) band with a 10 meter resolution was used for SAR because it is the best method to determine height variation in the ocean surface compared to vertical transmit/horizontal receive (VH) band. Sentinel 2 was launched in 2015 and since then has been monitoring the Earth's surface. Bands two through four corresponding to the blue, green and red band with a 10 meter resolution each was used.

MBES Data
Two sets of Multi-Beam Survey data is obtained for the Dutch Exclusive Economic Zone which covers the Dutch Continental Shelf. The first is from 2018 and the second from 2019. The resolution for both data sets is 25 meters, which is lower than the resolution of satellite data.

Wind Speed Data
The wind speed time series is obtained from ERA5 hourly data on single levels from 1940 to present. ERA5 is a European Centre for Medium-Range Weather Forecasts reanalysis of global climate and weather since 1940. The data is a combination of model data and global weather and climate observations. The resolution is 0.25 degrees. The 10 meter u and v components of wind were downloaded and composed into a time series for a point within the AOI.

Current Speed Data
The current speed data is obtained from the results of the Dutch Continental Shelf Model (DCSM). It is a depth-averaged hydrodynamic model based on Delft3D Flexible mesh software with coverage for the extent of the North Sea. It contains hourly measurements for the u and v component of the current to the from the year 1978 to 2022.

Sand Wave Characteristics North Sea
To compare the resulting sand wave characteristics over a large area in the North Sea, the results from Damen et al., 2018 were used to compare. The sand wave characteristics were obtained by applying a 2-D Fourier transform on bathymetry data of the Dutch Continental Shelf from the Bathymetric Archive System of the Netherlands Hydrographic Office with a spatial resolution of 5 by 5 m or 25 by 25 m.

3 Methodology

The overall methodology needed to answer all the sub-questions is shown in 3.1. Each of the following subsections will go into further detail about the locations that are used for each of the case studies, the filtering of satellite image collections, and post processing of the resulting images to determine sand wave characteristics.

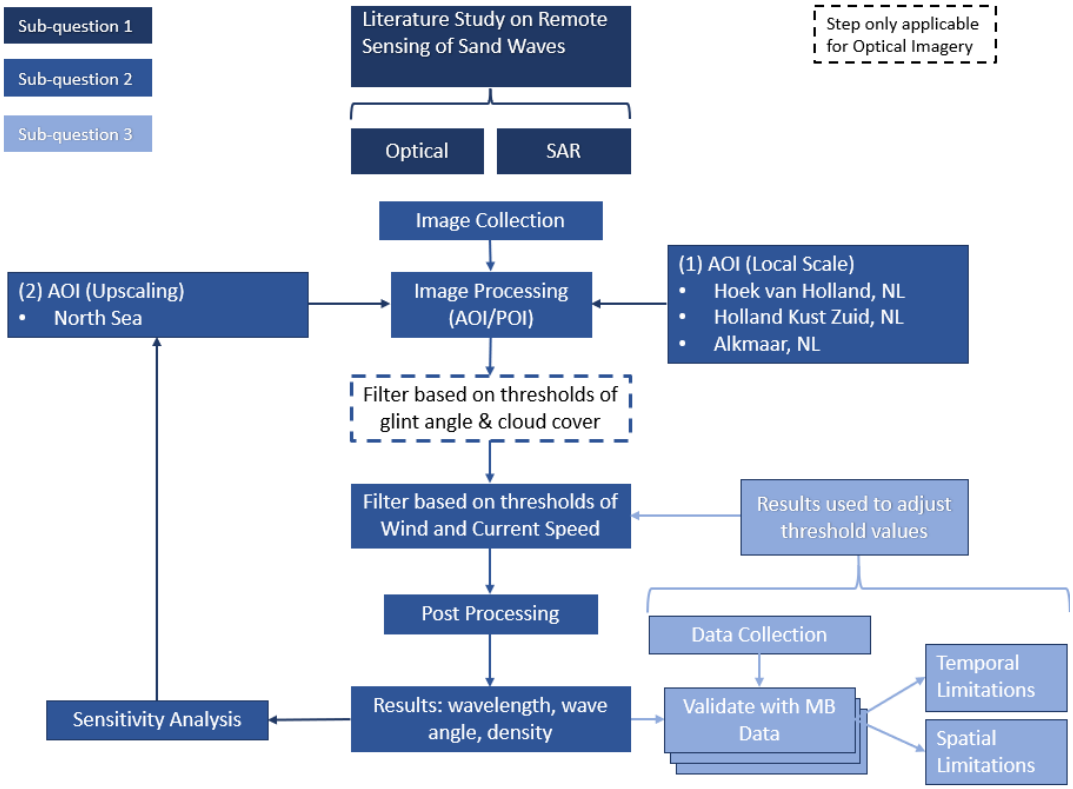

Figure 3.1: Framework for answering research question through sub-questions split into two main phases, where the first phase will compare the methods of remote sensing sand waves and the second phase will be the automation and upscaling of the process.

To answer the first research question, to determine which methods there are for detecting sand waves through satellite data and what are the different processes they require, is answered with a literature study found within the Background Information in Chapter 2. The methodology for the second research question, to determine how these methods can be used to determine sand wave characteristics, is looped through twice. The first time through the process, the area of interest the methodology is applied to is three smaller areas within the North Sea. The results for the local case are used to perform a sensitivity analysis for the effects of different area sizes considered and different sources of noise. The second time it is looped through the area of interest is up-scaled to the entire North Sea. The third research question, determining the accuracy as well as the spatial and temporal limitations, is answered using the results from the second research question, including filtering of the image collection and the calculated sand wave characteristics.

3.1. Areas of Interest

The framework of this research is set up to understand the limitations of the two remote sensing methods that are based on the Alpers Hennings model. Multiple case studies will be investigated due to unique properties in the sand wave fields and the surrounding environment that causes noise. These difference are described in the following confusion matrix shown in Figure 3.2. The matrix contains four categories which includes detecting sand waves through remote sensing when they are present in MBES, not detecting sand waves when they are not present in MBES, detecting sand waves when there are none present or not detecting sand waves when they are present in MBES.

	Positive Sand Waves Detected	Negative No Sand Waves Detected
Positive Sand Waves Present	1. Hoek van Holland, NL 2. Holland Kust Zuid, NL	
Negative No Sand Waves Present		3. Alkmaar, NL

Figure 3.2: Confusion matrix with corresponding locations

Hoek van Holland, Netherlands

The first case study is located off the coast of the Netherlands by the Hoek van Holland (HvH). The area has a width of 0.2 degrees and a height of 0.1 degrees, centered around the point (3.54, 52.07). The sand waves found here are highly irregular with shorter wave lengths as seen in Figure 3.3 The depth ranges from 25 to 30 meters at this AOI. The median cloud coverage for the Netherlands in Sentinel-2 images is about 60% annually (Bergsma & Almar, 2020).

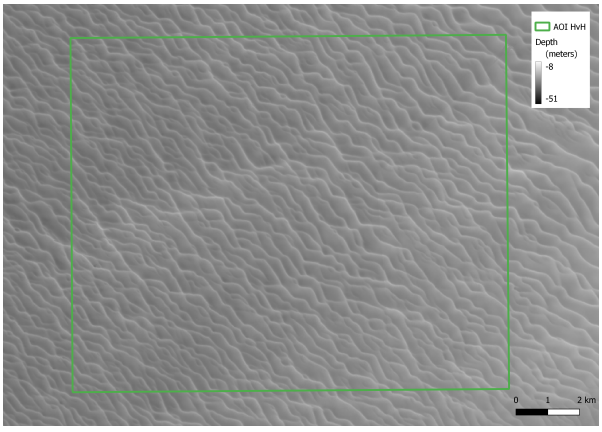

Figure 3.3: Area of Interest Hoek van Holland from MBES

Holland Kust Zuid, Netherlands

The second case study is located at Holland Kust Zuid (HKZ) off the coast of the Netherlands. The sand wave field here is highly regular with longer wave length as seen in Figure 3.4 The average depth

at this location is about 20 meters. The area has a width of 0.2 degrees and a height of 0.1 degrees and is centered around the point (4.15, 52.3).

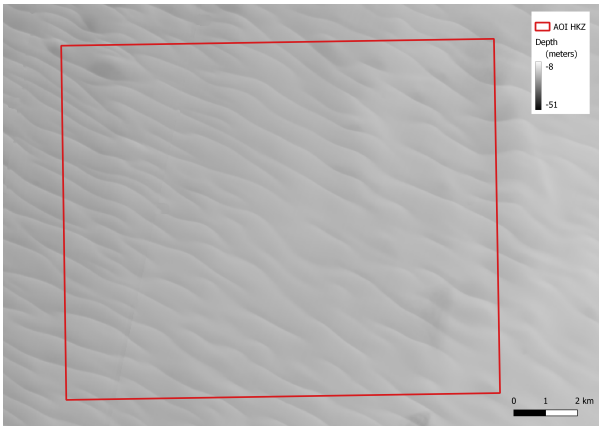

Figure 3.4: Area of Interest Holland Kust Zuid from MBES

Alkmaar, Netherlands
A location without the presence of sand waves as seen in Figure 3.5 was chosen off the coast of the Netherlands by Alkmaar. The water depth is about 20 meters at this location, equivalent to the depths found at Holland Kust Zuid, and is centered round the point (4.4, 52.54) with the same dimensions as the other areas.

Figure 3.5: Area of Interest Alkmaar from MBES

3.2. Filtering Image Collection

This section will describe the filtering process for the image collections for mean glint angle and cloud cover for optical, and for environmental parameters for both optical and SAR images as seen in Figure 3.1. Unlike SAR satellite images, to determine if sand waves are visible in optical satellite images there are additional filtering steps needed as discussed in Subsection 2.3.1. The first is mean glint angle, or the angle between the receiving satellite, the sea surface, and the sun which is determined by the following equation (Giglio et al., 2003).

$$cos\theta_g = cos\theta_v cos\theta_s - sin\theta_v sin\theta_s cos\phi$$

θ_g represents the mean glint angle, θ_v is the view angle while θ_s is the solar zenith angle, and $\Delta\phi$ is the relative azimuth angle as seen in Figure 3.6. The mean glint angle is calculated by getting the necessary values from the meta data of the satellite image, calculating using the formula, and adding the result back as meta data.

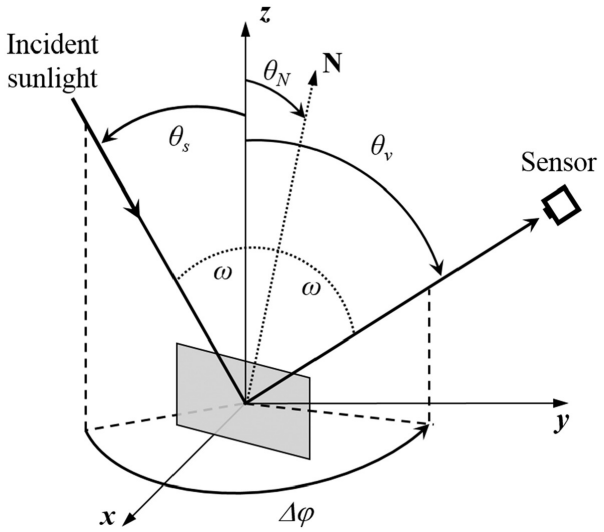

Figure 3.6: Coordinate system and definition of the relevant geometry parameters: θ_s and θ_v are the solar and the viewing angles, respectively, $\Delta\varphi$ is the relative azimuth angle (Harmel et al., 2018)

In Kras et al., 2022 the relationship between the latitude and mean glint angle was determined for Sentinel-2 over the year 2021 to as seen in Figure 3.7. The threshold value for filtering was set as the minimum mean glint angle found during the winter months based on the assumption that no sun glint images are found during this time period. This angle is 56 degrees for the latitudes of the North Sea which is a higher angle value than what would be found near the equator at lower latitudes.

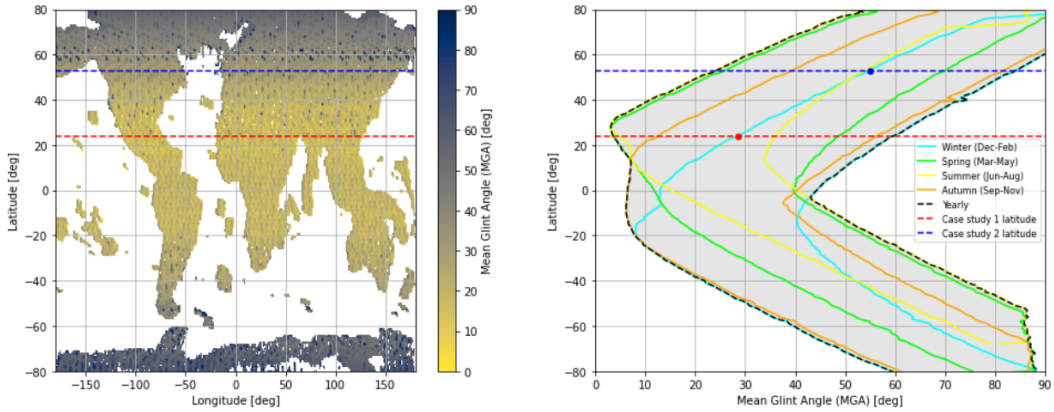

Figure 3.7: Relation between latitude and mean glint angle for Sentinel-2 collection based on the data between the 1st of January 2021 and 1st of January 2022. The minimum mean glint angle found for any longitude and latitude combination (left) and ranges of the mean glint angle as function of the latitude for each season (in the Northern Hemisphere) and for the whole year (right) (Kras et al., 2022)

Clouds are only a pertinent factor for optical satellite images as SAR microwaves do not pick up on clouds. For optical images clouds can range from completely blocking all available data to adding noise to the image with clouds containing high reflectance values compared to the surrounding ocean surface. Therefore, to remove satellite images that contain a significant number of clouds the collection was filtered for a threshold of 20% cloud cover.

Wind and current speeds are added to the meta data of the satellite images in the image collection based on the nearest hour of the date and time the satellite image is taken. As discussed in Section 2.3, for the Alpers-Hennings Model, to be able to detect sand waves in a satellite image the current speed needs to be strong enough for the current moving over the bed form to effect the sea surface roughness. Also, the wind speed needs to be strong enough that the sea surface is not flat, but not too strong where the surface is too rough and the signals from the sand waves can no longer be detected.

The initial thresholds set for wind speed is between 3 and 12 m/s and current speeds about 0.4 m/s (Gagliardini et al., 2004). During the phase of obtaining an image collection containing only satellite images with sand waves present the thresholds for wind speed and current speed will be determined with more precision. Considering that sand waves should never be detected at Alkmaar, the collection was filtered for the environmental parameters and then satellite images will be used for the same date and time where sand waves are detected at the nearest area of interest, Holland Kust Zuid.

3.3. Post Processing for Sand Wave Characteristics

Figure 3.8 shows the expanded methodology for the post processing used to acquire the sand wave characteristics from a satellite image. This methodology can also be applied to a MBES to determine the sand wave characteristics over an area. The input images are obtained by following the filtering process described in the previous Subsection 3.2.

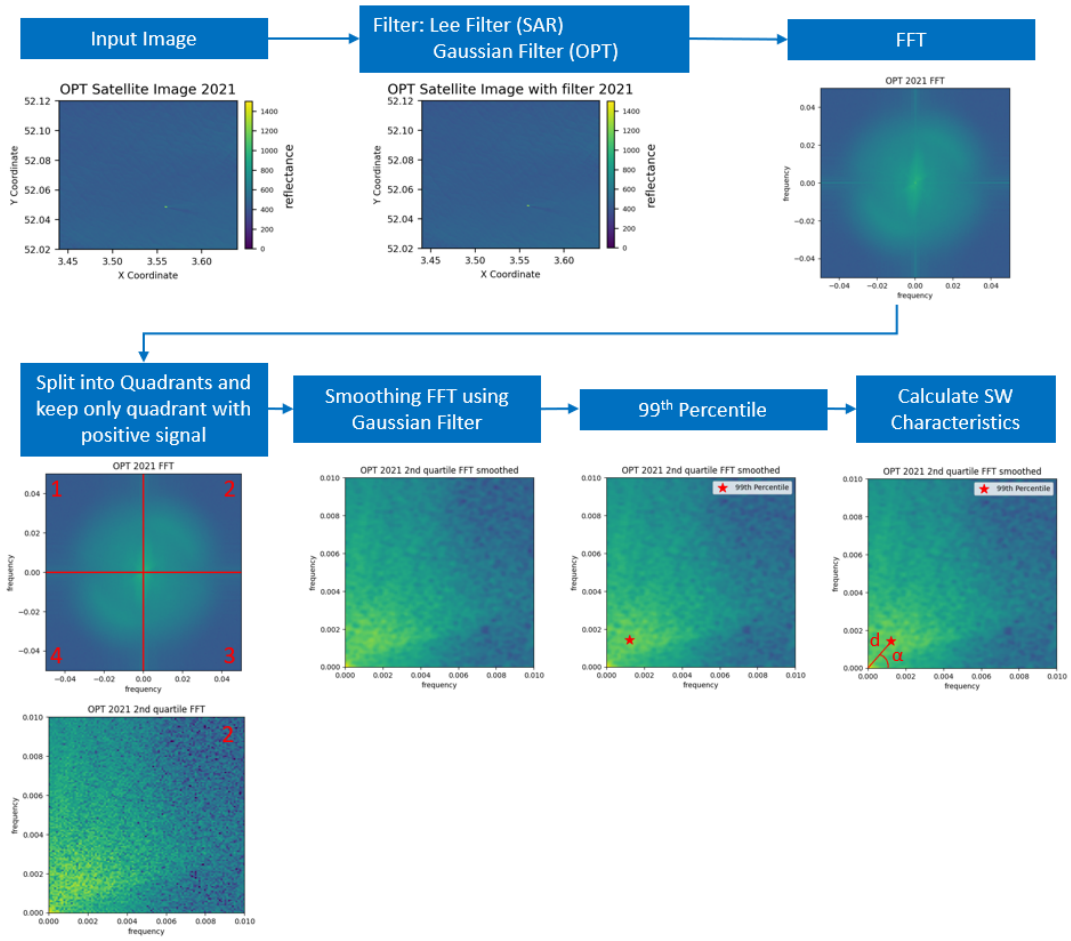

Figure 3.8: Framework for post processing step in Figure 3.1. A resulting satellite image from filtering the image collection containing sand waves is then filtered for noise. Then a 2D FFT is applied. The resulting image is split into four quadrants and the quadrant containing the positive signal is taken. This is then smoothed for noise using a Gaussian Filter and the 99th percentile of points is taken to get the center of the signal. From this point the sand wave characteristics can be calculated.

The output collection of both SAR and Optical images are filtered to remove noise. For SAR images, the Lee filter is used and for optical images the Gaussian filter is used which is further discussed in Subsection 2.3.2 and 2.3.1 respectively. A 2D Fast Fourier Transformation (FFT) is performed on the entire satellite image as described in Subsection 2.4. From the signal in the FFT the wavelength and wave angle can be determined by taking the 99th percentile of the data points of the quadrant containing the signal of the sand waves. The four quadrants are shown in Figure 3.9, and the second quadrant is used which contains the positive part of the sand wave signal. This method was tested in Appendix A to determine which parameters to use to most accurately determine the center of the signal. The

wavelength is determined by converting the distance from the origin to the point from frequency back into meters. The angle is defined as the angle formed between the positive x axis and a line drawn from the origin to the point, and therefore with respect to due East. These values provide an average value for wavelength and wave angle over the considered area. This method was create and tested for the first area of interest, Hoek van Holland and then later applied to the other AOIs to test the limitations.

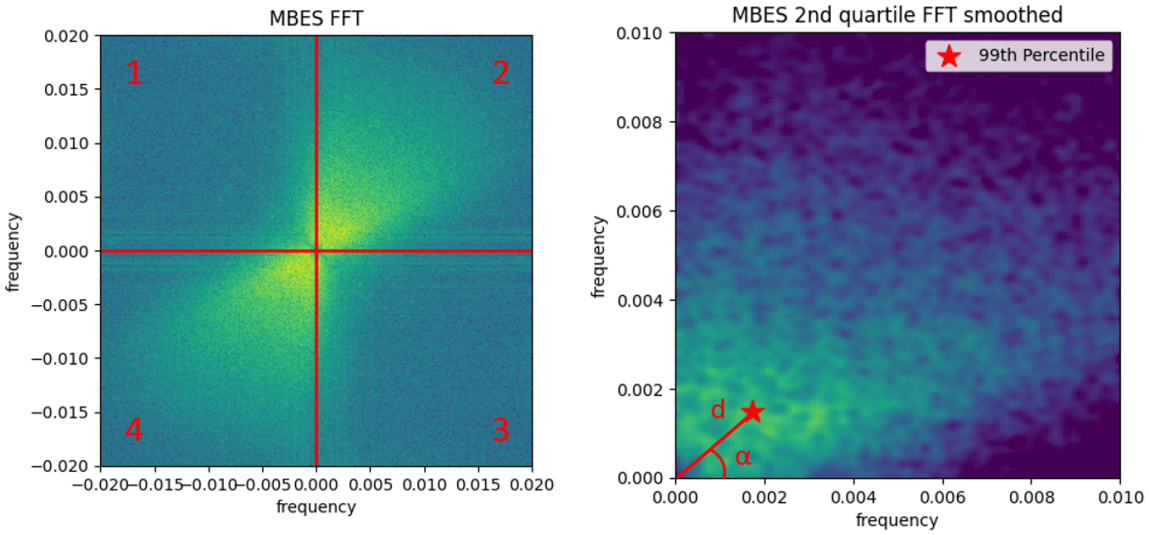

(a) Quadrants definition

(b) Sand wave characteristics determination in quadrant 2

Figure 3.9: Splitting the FFT for MBES of Hoek van Holland into four quadrants then determining sand wavelength d is frequency and wave angle α

Before the upscaling can occur, a sensitivity analysis was performed on the results for the local scale areas of interest. This was done to determine the effect that different sources of noise that can be present in satellite images such as ships and clouds, have on the FFT and calculated sand wave characteristics. Also, the satellite images for each of the AOIs as well as the MBES, were split into smaller area sizes with measurements of 1, 2, 3, 4, and 5 kilometers to determine which tile size is appropriate for the upscaling. After splitting the images into tiles, a 2D FFT was applied and the wavelength and wave angle were calculated for each tile. To understand the variance in data between the results from SAR, optical, and MBES, the distribution of the tiles for each year is compared using box plots. The area size that had the least amount of spread and the most accurate average value was then used for the upscaling. Depending on the area size and the sand wave characteristics in an area, different signals are present within the FFT which would alter the results.

To perform the upscaling of the methodology to obtain sand wave characteristics of a larger area a single pass over of the satellite was used. A date is chosen on which sand waves are visible through the filtering process. Then, using a grid created over the entire North Sea, the images were downloaded in tile size increments. Once all the tiles for a single pass were downloaded over the grid, the wavelength and wave angle were calculated using the methodology in Figure 3.8. Additionally, a density map of each AOI was made by using the calculated sand wavelength and the distance within the tile inline with the wave angle to calculate the number of sand waves per tile. The wind speed and current speed data was added to the information for each point in the grid to better understand the effects of each parameter on the visibility of sand waves. By comparing all the factors such as wind speed, current speed, depth, and different sources of noise, the limitations of the methodology will be understood.

4
Results

The results are split into two parts, based on which Area of Interest (AOI) is used as input. There are the local scale cases: Hoek van Holland (HvH), Holland Kust Zuid(HKZ), and Alkmaar (ALK), and the second AOI is the entire North Sea and is considered the upscaling of the methodology.

4.1. Areas of Interest

For each of the areas of interest discussed in Section 3.1, first, the image collection was filtered to obtain images containing sand waves, then the post processing to obtain the sand wave characteristics. Finally the effect of noise over an area for calculating sand wave characteristics was observed.

4.1.1. Filtering Image Collection

The processing of filtering the original image collection is performed for each AOI for the year 2021. First, to determine the effect that each environmental parameter has, the image collection was filtered for a single parameter which is shown in the following figures for the Hoek van Holland. Then, to determine the final amount of images per year containing sand waves, the image collection was filtered in series for the environmental parameters. This order is: mean glint angle (applicable for optical images only), wind speed, current speed, and cloud cover (applicable for optical images only).

Unlike SAR, the optical images also depend on the mean glint angle and the amount of cloud cover. For both parameters the entire image collection for the year 2021 at HvH was filtered to determine how many images per year meet these conditions as seen in Figure 4.1. The original image collection for Sentinel-2 is 144 images and when filtered for mean glint angle, 82 images remain, about 57% of the original collection. The remaining images in the collection are between the months of March and August where the sun makes the correct angle between the sea surface and the satellite sensor. When filtered for cloud cover threshold of 20%, the remaining number of images is 29 or 20% of the original collection. Considering the typical weather found at the North Sea which consists of a lot of cloud cover, a low number of images that pass the conditions is expected. The low threshold value for cloud cover is necessary to apply the FFT, which is discussed later when looking at different examples of noise.

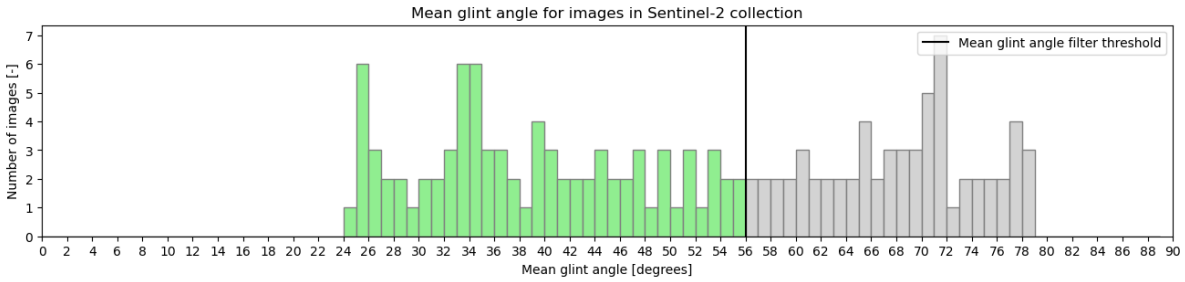

(a) Mean Glint Angle Filtering OPT

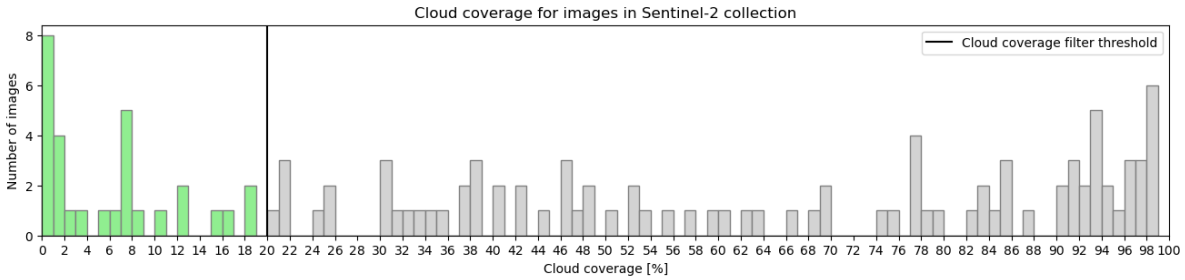

(b) Cloud Cover Filtering OPT

Figure 4.1: The result of filtering the entire Sentinel-2 image collection for AOI Hoek van Holland over the year of 2021 for mean glint angle (a) and cloud cover (b)

The image collection for SAR contains 290 images, which makes it seem as though the Sentinel-1 satellite passes over the North Sea about twice as often, however this is not always the case. The higher amount is due to the splitting of the images in Google Earth Engine as a result of their size which happens to be split over the Hoek van Holland for SAR and not for Optical, doubling the amount of images. The probability density function for wind and current speed is shown in Figure 4.2. It is observed that for the majority of time in 2021, the wind speed at this point falls within the minimum and maximum thresholds of 3 to 12 m/s. The data for the current speed shows that the threshold condition of 0.4 m/s is fulfilled more than half the time. This shows that the North Sea has relatively favorable conditions based on these two environmental parameters.

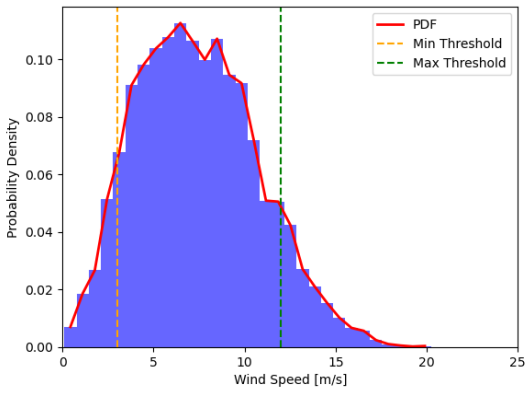

(a) PDF Wind Speed

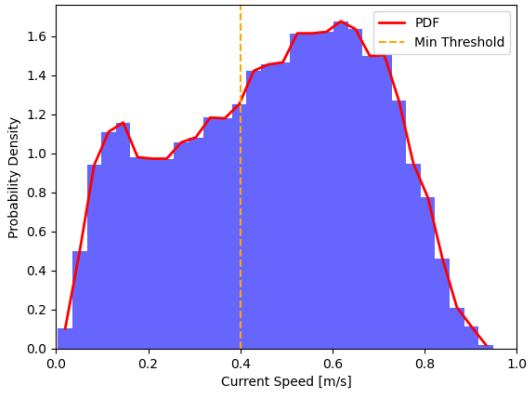

(b) PDF Current Speed

Figure 4.2: The Probability Density Function for wind speed from ERA5 and current speed from DCSM with thresholds from literature (Gagliardini et al., 2004) for filtering for a point within the AOI Hoek van Holland for the entire year of 2021.

When filtering the SAR and Optical image collections for wind speed as seen in Figure 4.3, the amount of images left in the collections is 243 and 117, or 84% and 81% respectively. This corresponds to the values in the Probability Density Function of wind speed seen in Figure 4.2, where a large amount of the wind speed values fall between the thresholds. Wind direction has no impact on the results as the wind direction for the passing images has no specific trend.

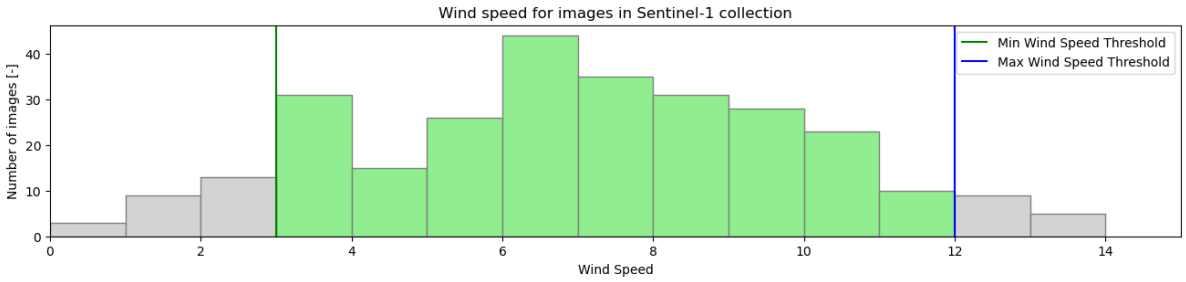

(a) Wind Speed Filtering SAR

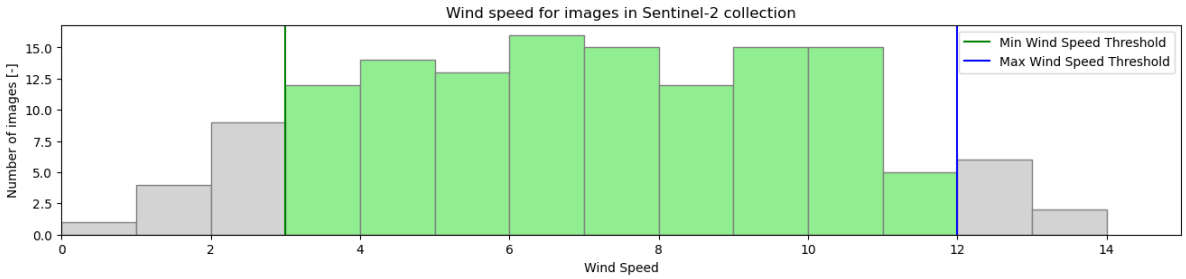

(b) Wind Speed Filtering OPT

Figure 4.3: The result of filtering the entire Sentinel-1 (a) and Sentinel-2 (b) Image Collections for AOI Hoek van Holland over the year of 2021 for the wind speed thresholds

When filtering the image collections for current speed as seen in Figure 4.4 the remaining amount of images in the collections for SAR and Optical is 192 and 98 images respectively, or 66% and 68%. Like the results of wind speed filtering, the percentage of images left is comparable to the Probability Density Function of the current speed seen in Figure 4.2 which satisfies the condition.

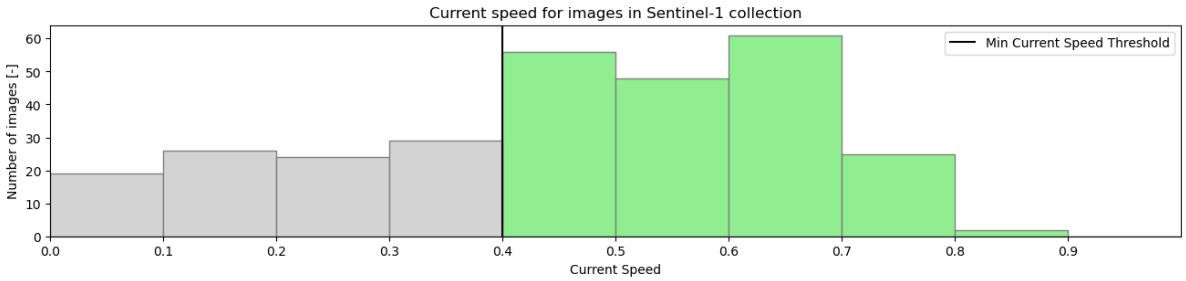

(a) Current Speed Filtering SAR

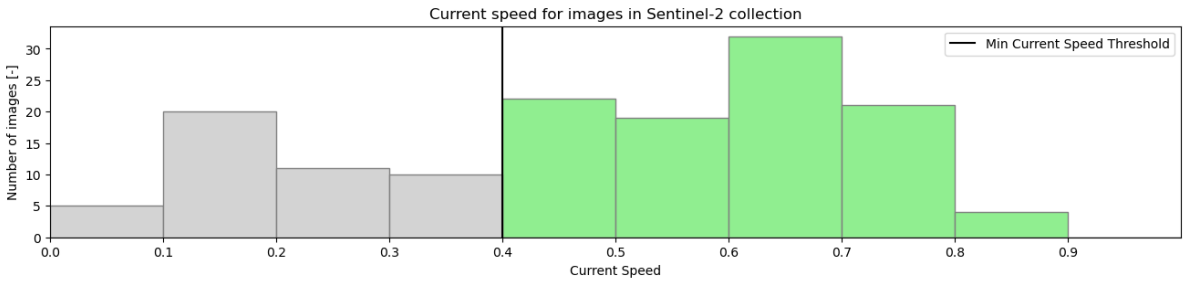

(b) Current Speed Filtering OPT

Figure 4.4: The result of filtering the entire Sentinel-1 (a) and Sentinel-2 (b) image collections for AOI Hoek van Holland over the year of 2021 for the current speed thresholds

To find the resulting image collection containing sand waves, the collection was filtered for all the thresholds. Table 4.1 shows the resulting number of images in an image collection after applying all the filters in order. However, the final image collection after filtering based on the parameters has shown that not all resulting images actually contain sand waves, and the true number of images containing sand

waves is shown in the last column of the table. The values in the final column were found by manually checking the final image collection for sand wave signals.

Table 4.1: The results for filtering image collections for optical and SAR for the three AOIs based on environmental parameters in series for the year 2021. The Final total containing sand waves was determined manually. SAR does not need to be filtered for mean glint angle or cloud cover

	Location	Image Collection	Mean Glint Angle	Wind Speed	Current Speed	Cloud Cover	Final Total	Final Total actually containing Sand Waves
OPT	HvH	144	82	69	49	14	14	2
	HKZ	288	161	136	97	30	15	1
	ALK	144	79	67	48	16	16	-
SAR	HvH	290	-	243	166	-	166	10
	HKZ	236	-	202	132	-	132	10
	ALK	266	-	228	150	-	150	-

The reason the true final total that actually contains sand waves has fewer images than what is the result of the filtering process is due to multiple factors. One of these factors is that the parameters of wind and current speed need to be adjusted to be stricter and can differ between optical and SAR. Also, the speckle noise present in SAR will cover weaker signals such as sand waves if the conditions are not exactly ideal.

When comparing the amount of satellite images containing sand waves for SAR and optical, there is a higher percentage of images left for SAR at about 3.5% and 7.6% compared to 1.4% and 0.7% for optical. This is due to the additional parameters required, the mean glint angle and cloud cover percentage, to detect sand waves in optical images. SAR has viable satellite images containing sand waves throughout the year as seen in Figure 4.5. The resulting optical images for 2021 is in April and June only. For multiple years it was observed that optical images fall between the months of April and July due to the mean glint angle and the favorable weather conditions.

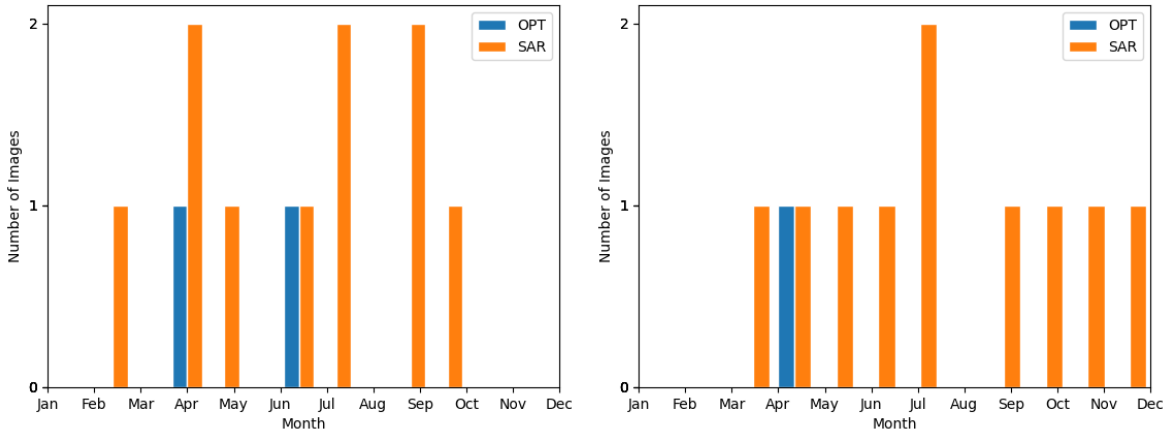

(a) Hoek van Holland

(b) Holland Kust Zuid

Figure 4.5: Distribution of dates per motnh that satellite images where taken containing sand waves in the year 2021

4.1.2. Post Processing for Sand Wave Characteristics

Results for the Three AOI

After the process of filtering the original image collection to a smaller collection containing images with sand waves an image was chosen at each of the AOIs. First, the AOI of Hoek van Holland was considered and was used to create and test the methodology to calculate sand wave characteristics. A Gaussian filter was applied to the optical image and a Lee filter to the SAR image to remove noise in the images. In both images in Figure 4.6, ships, which are labeled with A, are present which is a common occurrence for images at this location due to traffic. The sand waves are very distinct in the optical image and the irregularity of the waves can be seen. In the SAR image there is speckle noise

present which gives the image a grainy appearance. Also, the sand waves are clearer in the southwest of the image and not very visible in the northeast of the image.

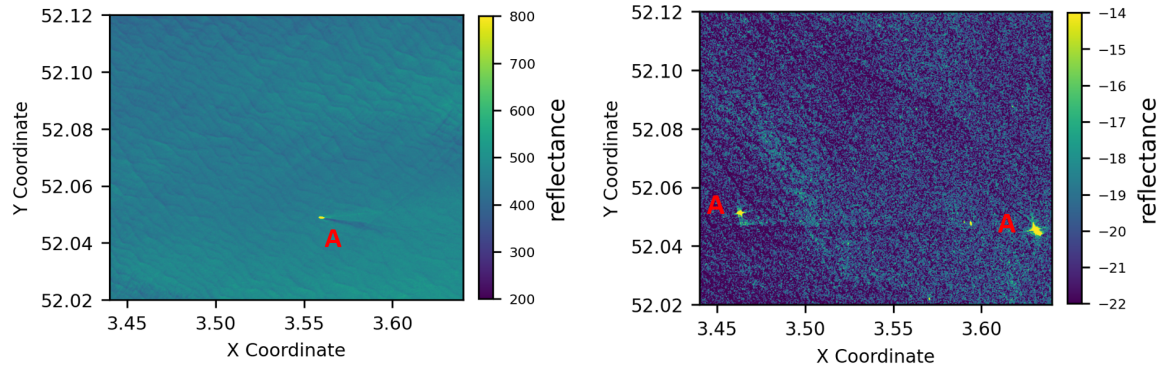

(a) Optical Satellite Image with Gaussian Filter

(b) SAR Satellite Image with Lee Filter

Figure 4.6: Optical and SAR Satellite Images at Hoek van Holland 2021 with Gaussian and Lee Filter Respectively. Effect of filter visually is very small so only the filtered image is shown.

The signal derived from the sand waves present in each of the images is shown in Figure 4.7. In the FFT from SAR image the only distinct signal is that from the sand waves marked by the letter A. However, in the optical image in addition to the signal due to sand waves marked by the letter B, there is evidence of a larger signal on top of the signal of the sand wave labeled with A. The source of this additional signal will be further explored in Section 4.1.3 and is due to the ship. The signal from the sand waves is also larger and more spread out for the optical image than the SAR image.

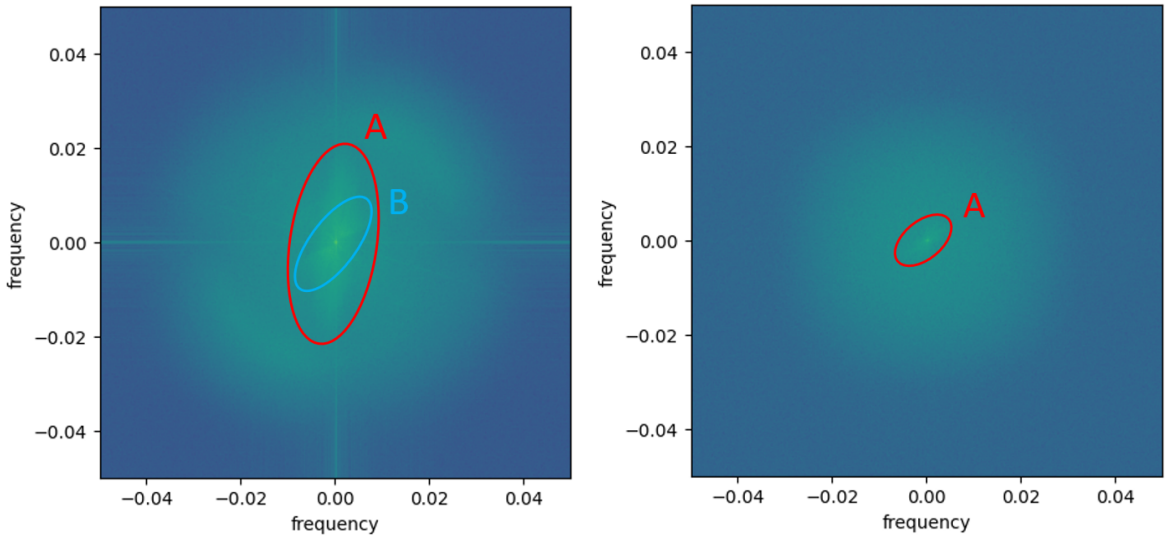

(a) FFT of Hoek van Holland Optical Image

(b) FFT of Hoek van Holland SAR Image

Figure 4.7: Comparison of FFT results between Optical and SAR satellite images

The overall FFT was split into four quadrants and the quadrant containing one of the pair of points resulting from the sand waves was used to calculate the characteristics as seen in Figure 3.9. First, the resulting quadrant was smoothed using a Gaussian Filter the peak values are less extreme with less outliers and the methodology to get the center of the signal is more accurate as seen in figure 4.8. The peak location detected visually matches the center of the signal from the sand waves. The wavelength and wave angle calculated is an average value over the entire area, and the wave angle is calculated with respect to due East. The use of a low/high pass filter from 100 to 1000 meters was explored. However, due to the amount of noise in the FFT signal for the sand waves it was chosen not

to use a low/high pass filter. The reason to ignore this filter is that the filter often cuts out parts of the FFT signal. This leads to a shift in the calculated center of the signal, which does not visually agree with the location of the center of the signal. However, to make sure that only the correct signal is read, the bright signal at the origin of the FFT is removed when calculating the center of the signal.

The resulting wavelength and wave angle for optical is 533.2 meters and 49.6 degrees, and for SAR is 561.9 meters and 29.1 degrees. The wavelength from the optical image is about 30 meters smaller than the from the SAR image. Also, the angle calculated from the SAR image is 20 degrees smaller than the optical image. This is because the optical image has more visible sand waves than the SAR image when comparing visibility in Figure 4.6. With more waves present, including smaller waves between larger waves, the resulting FFT signal will be shorter. The waves are also very irregular and due to wind and current conditions the angle angle the sand waves make in the image changes.

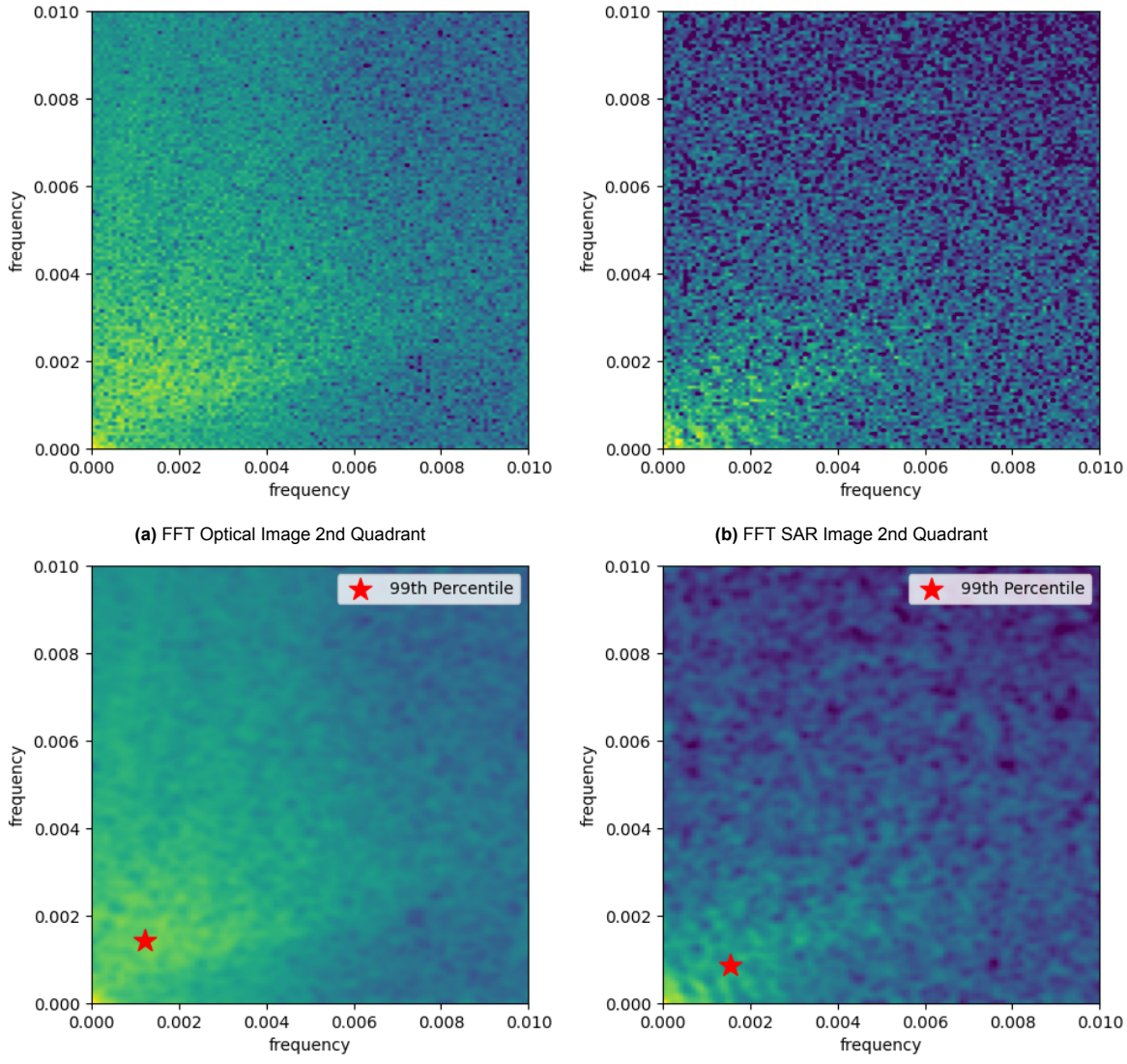

(a) FFT Optical Image 2nd Quadrant

(b) FFT SAR Image 2nd Quadrant

(c) FFT Optical Image 2nd Quadrant with Smoothing Filter

(d) FFT SAR Image 2nd Quadrant with Smoothing Filter

Figure 4.8: Comparison of FFT results between Optical and SAR satellite images for the 2nd quadrant only containing the signal along with the smoothed image used to determine the sand wave characteristics as discussed in Section 3.3 by taking the 99th percentile of values present.

The process was repeated for the MBES for the same AOI as seen in Figure 4.9. The horizontal and vertical lines present in the FFT of the MBES are due to the distinct lines in the data due to the merging of the datasets where it does not line up. Compared to the FFT from the optical and SAR images, the

signal is much more distinct because there are no other sources of noise such as clouds, ships, and speckle noise. However, the FFT does resemble that of the optical image seen in Figure 4.8 (c). A reason why the signal is spread out is because all the irregular sand waves are visible so the signal is the average of all these angles. The resulting wavelength is 427.4 meters and an angle of 34.6 degrees.

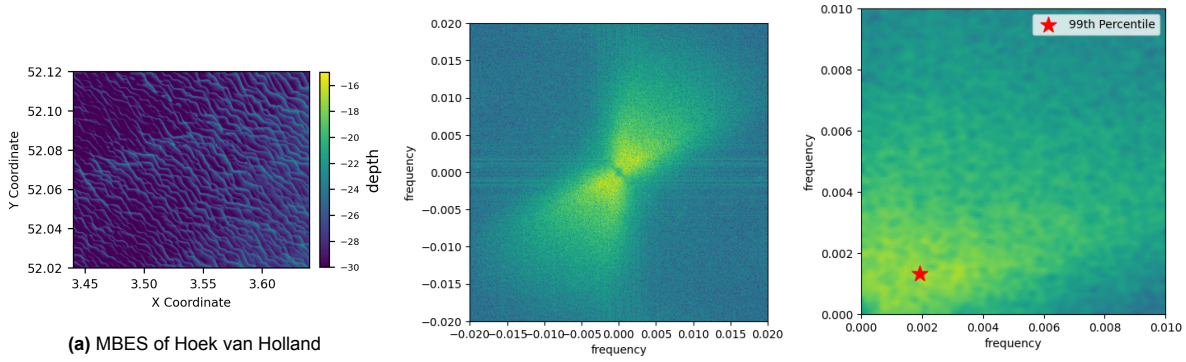

(a) MBES of Hoek van Holland

(b) FFT of MBES

(c) FFT MBES 2nd Quadrant with Smoothing Filter

Figure 4.9: Process of getting sand wave characteristics from MBES at Hoek van Holland

The second AOI to be looked at was at Holland Kust Zuid and the satellite images are shown in Figure 4.10. The sand waves at HKZ have a longer wavelength and are more regular than at HvH. In the optical image the sand waves that can be seen do not follow the entire crest line of the sand wave because the signal is not visible. In addition to visible sand wave signals, the optical image also contains smaller clouds as well as a Cirrus cloud which looks like a streak across the image and is labeled with the letter A. The SAR image has much more distinct sand waves than what is visible in optical. This is the opposite case compared to HvH, where the sand waves were much more visible in the optical image compared to SAR. Also, while in the optical image, the sand waves are presented as a solid line of lower reflectance, in the SAR image, both the smoother and rougher sea surface can be seen for each sand wave. In the SAR image a small ship is labeled with A, and an area where there are no sand waves visible in the northwest is labeled with B.

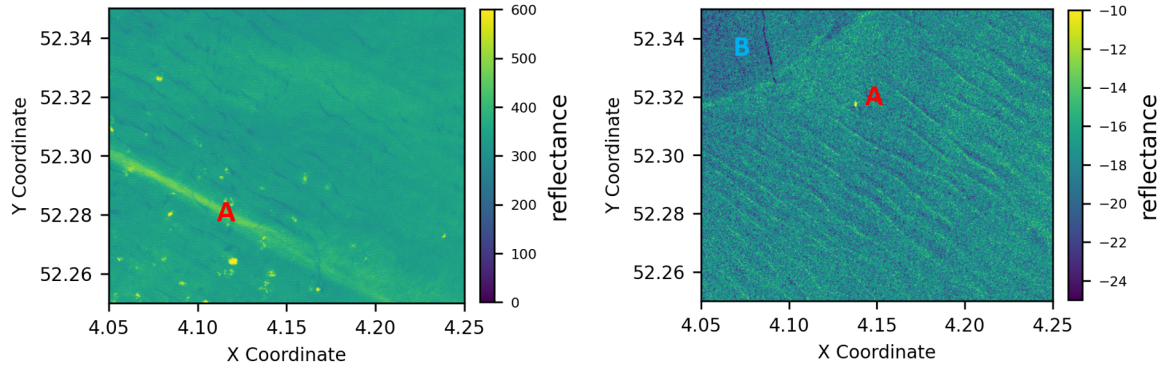

(a) Holland Kust Zuid Optical Satellite Image 2021

(b) Holland Kust Zuid SAR Satellite Image 2021

Figure 4.10: Optical and SAR satellite images at Holland Kust Zuid

The sand wave characteristic calculation by finding the center of the signal is shown in Figure 4.11. The signal in the FFT for SAR is very clear and results in a sand wavelength of 843.9 meters and angle of 38.1 degrees. The signal for the optical image is affected by by clouds, and the effect clouds has is further discussed in Section 4.1.3. The calculated wavelength is 895.3 meters and the angle is 27.7 degrees.

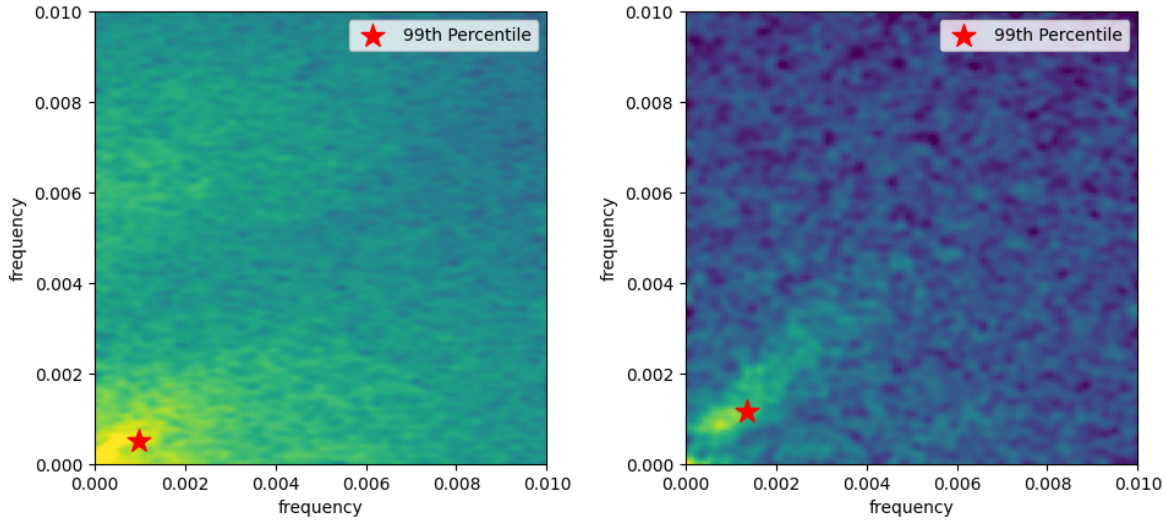

(a) FFT Optical Image at HKZ 2nd Quadrant with Smoothing Filter

(b) FFT SAR Image at HKZ 2nd Quadrant with Smoothing Filter

Figure 4.11: Comparison of Optical and SAR FFT for 2nd quartile at Holland Kust Zuid used to determine the sand wave characteristics

Once again, the process is repeated over the same AOI for a MBES. Seen in the FFT for the MBES is the ideal situation in which there is a very clear and defined signal. This clear signal comes from the strong pattern found in the regular sand waves at Holland Kust Zuid. The resulting wavelength is 738 meters and angle is 45.9 degrees. Unfortunately, the quality of data derived from the satellite images is lower than from MBES and the sand wave signals are much less distinct and there are more sources of noise. Also, irregular sand waves are common in the North Sea like at HvH, which means the conditions to have as clear of a signal as the FFT of the MBES is not always met.

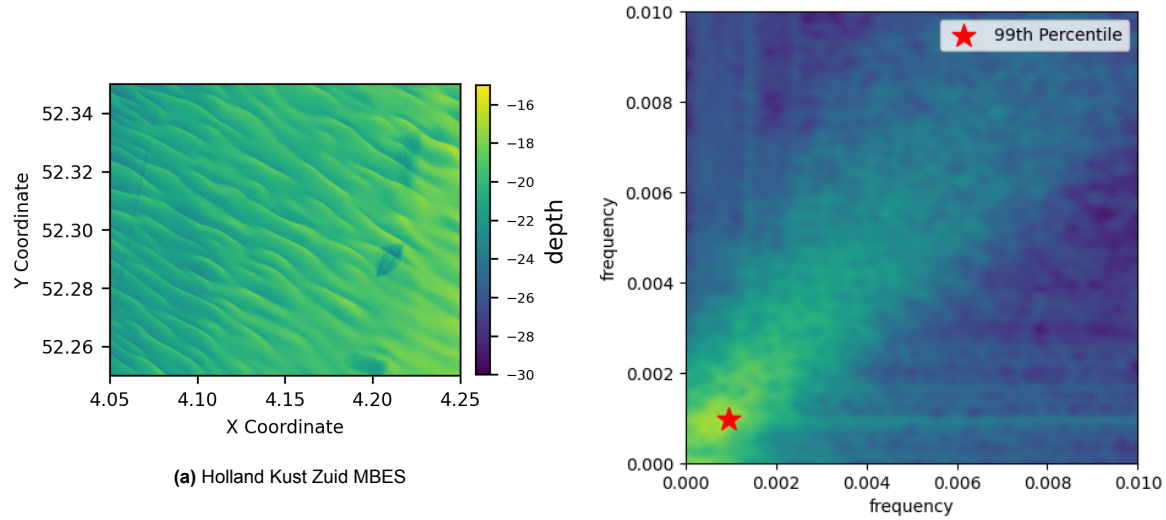

(a) Holland Kust Zuid MBES

(b) FFT MBES Image 2nd Quadrant with Smoothing Filter

Figure 4.12: MBES at Holland Kust Zuid and FFT results for the 2nd quadrant only containing the signal along with the smoothed image used to determine the sand wave characteristics

The last AOI discussed is Alkmaar. When a location contains no sand waves such as Alkmaar seen in Figure 4.13, there should be no distinct signal present in the FFT. However, as a result of the methodology to calculate the location of the 99th percentile point, the sand wave characteristics can still be calculated and have a resulting wavelength and wave angle. In this thesis the method to differentiate whether or not an area contains sand waves has not been determined and is mentioned in the Recom-

mendations in Chapter 7. The optical images contains two instances of clouds labeled A and B. The SAR image contains ships labeled with A, and a less distinct unknown signal labeled with B.

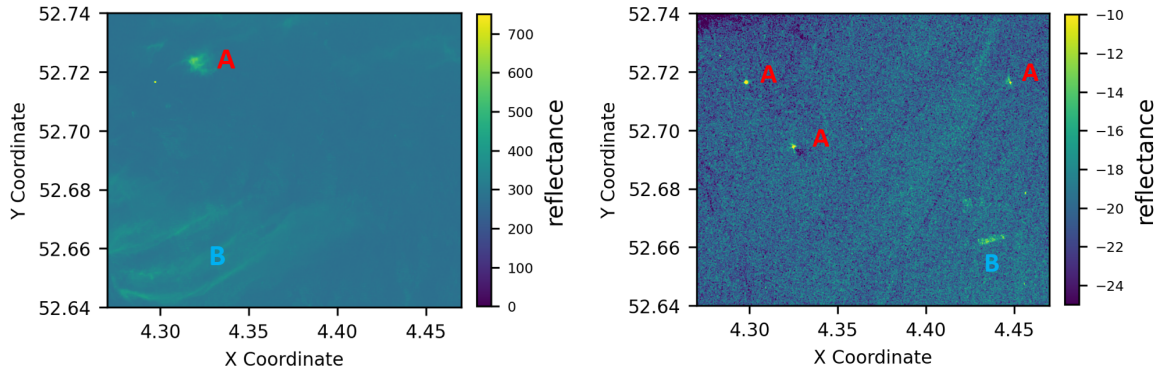

(a) Alkmaar Optical Satellite Image 2021

(b) Alkmaar SAR Satellite Image 2021

Figure 4.13: Optical and SAR satellite images at Alkmaar

Unlike what was expected, there is a signal present in the FFT for the optical image as seen in Figure 4.14. This is due to the clouds present in the optical image. The clouds show up as a signal around the origin and when looking at the second quadrant the signal looks like that of a sand wave. At the same location for the year 2022, the FFT looks very similar to that of SAR. The FFT for the SAR image contains no distinct signals and the calculated point does not match and spots of brightness. The calculated wavelength and wave angle for optical is 1134.6 meters and 33.8 degrees and for SAR is 329.2 meters and 44.1 degrees. While the sand wave angle does not differ much, there is a significant difference in the calculated wavelength of over 800 meters. This could be in part because of the additional signals in the optical FFT due to clouds, or a difference in the distribution of values between the optical and SAR FFT.

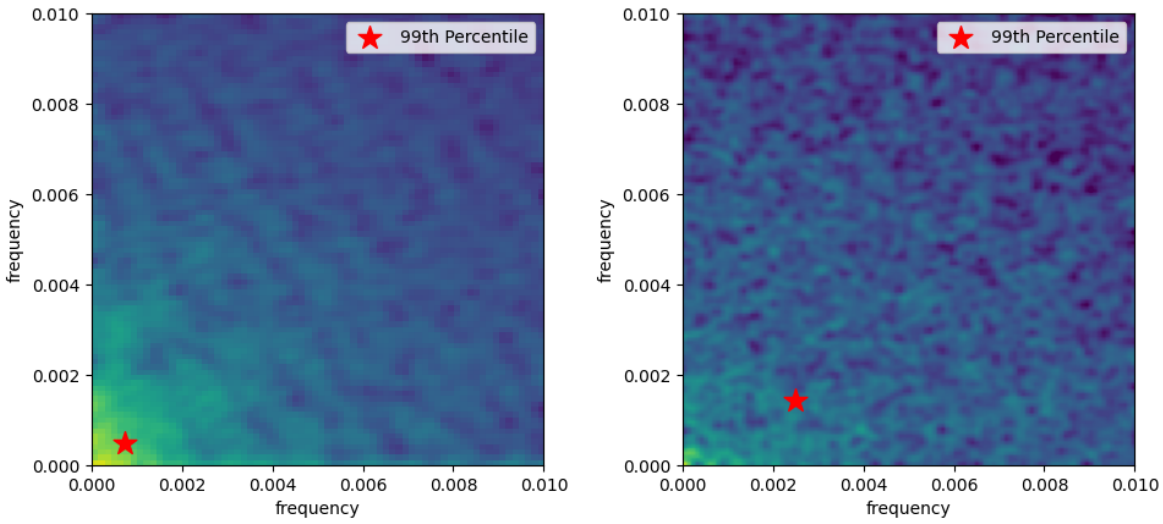

(a) FFT Optical Image at Alkmaar 2nd Quadrant with Smoothing Filter

(b) FFT SAR Image at Alkmaar 2nd Quadrant with Smoothing Filter

Figure 4.14: Comparison of Optical and SAR FFT for 2nd quartile at Alkmaar used to determine the sand wave characteristics

Once again, the process was repeated for the MBES. The water depth at Alkmaar is shallower than the two other cases. The FFT for Alkmaar contains a bright signal at the origin but no other distinct signals from sand waves. The calculated wavelength is 719 meters and sand wave angle is 71.7 degrees.

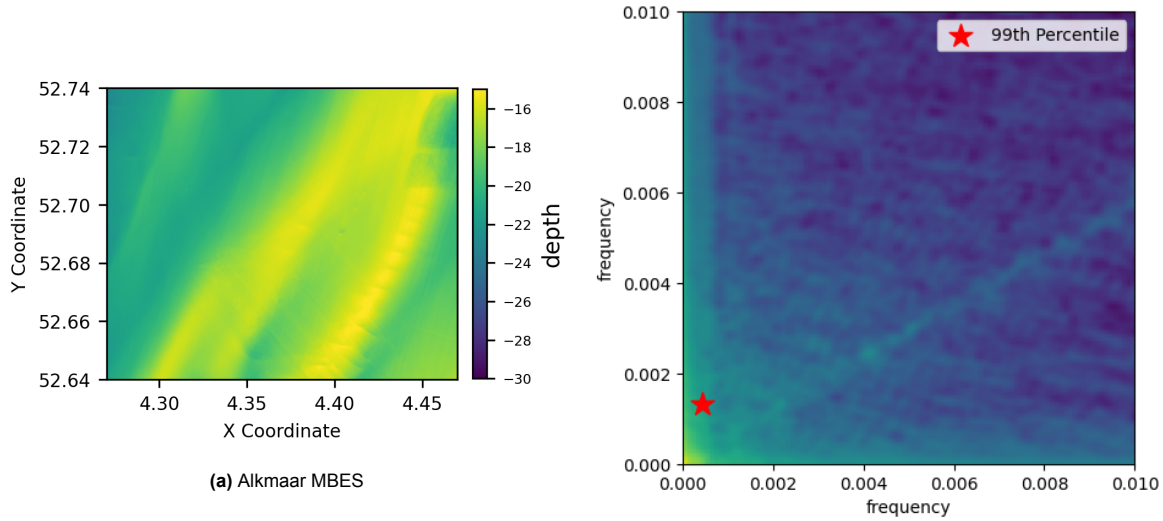

(a) Alkmaar MBES

(b) FFT MBES Image 2nd Quadrant with Smoothing Filter

Figure 4.15: MBES at Alkmaar and FFT results for the 2nd quadrant only containing the signal along with the smoothed image used to determine the sand wave characteristics

The results for the sand wave calculations at Hoek van Holland, Holland Kust Zuid, and Alkmaar are compiled in Table 4.2. The wavelength calculated through all three methods is lower at HvH than at HKZ as expected. At HvH, the sand waves are shorter and more irregular while at HKZ they are longer and more regular. The difference in the signal due to regular and irregular sand waves is further discussed in Appendix C. At both HvH and HKZ, the wavelength calculated using an optical and SAR image differs by about 30-50 meters, while by MBES is 100 meters less for both locations. Therefore, the remote sensing methods tends to overestimate the wavelength compared to MBES. Alkmaar is the unique case because there are no sand waves present here. The sand wavelengths calculated here vary the most, where the optical image is 400 meters greater than the MBES, and SAR is 400 meters less than the MBES. The greatest distance between wave angles also occurs at Alkmaar, where the optical and MBES wave angle varies by 40 degrees.

Table 4.2: Resulting sand wave characteristics

Location	Type	Wavelength [m]	Wave Angle [deg]
Hoek van Holland	Optical	533.2	49.6
	SAR	561.9	29.1
	MBES	427.4	34.6
Holland Kust Zuid	Optical	895.3	27.7
	SAR	843.9	38.1
	MBES	738.0	45.9
Alkmaar	Optical	1134.6	33.8
	SAR	329.2	44.1
	MBES	719.0	71.7

To get more detailed information the average wavelength and the standard deviation were determined for Hoek van Holland and Holland Kust Zuid. This was done by determining the wavelength between each sand wave along a trajectory in QGIS. At HvH the average wavelength is 340 meters and the standard deviation is 119 meters. For all three methods, optical, SAR, and MBES, the wavelength calculated over the area is larger than the average value. The optical and SAR image are within one standard deviation of the MBES wavelength value. The overestimation of the wavelengths for the remote sensing methods can be due to wind and current conditions for the AH model. It is possible that only the sand waves with the largest heights within an area will be visible, and the smaller sand waves are not visible. This will lead to longer wavelengths. However, if the conditions are ideal, it is possible to have all sand waves visible within an area which would lead to a lower wavelength if all the

signals are captured. At HKZ, the average wavelength is 700 meters and the standard deviation is 208 meters. At HKZ, all three remote sensing methods are within one standard deviation of the average wavelength. The longer sand wavelength and the regularity of the sand waves allows for clearer visibility in the satellite images and the FFT to get a more concentrated signal for the calculation of sand wave characteristics.

The results in Table 4.2 lead to another finding, the signals in the resulting FFT from sand waves is very important. Many factors can impact the value of the sand wave characteristics. Different sources of noise can change the signals in the FFT in different ways. The quality, like the amount of speckle noise in a SAR image, of the image is also a very important factor. The visibility of sand waves within an image will change the clarity of the signal in the FFT and also where the signal is located. Also, the size of the area used for the FFT can have an impact.

4.1.3. Sensitivity Analysis

Comparison for different Tile Sizes

The overall image was split into smaller tiles of different sizes to investigate if a smaller area will still read the correct signals in the FFT and allows for a finer data grid. To determine the best size, the images were split into tiles of 1, 2, 3, 4 and 5 kilometers and for each tile the wavelength and wave angle of the sand waves were calculated and the results compared to each other. This is shown in Figure 4.16 for both an Optical Image and a SAR Image at HvH for the sand wave length and angle characteristics. Since both the optical and SAR image at HvH contain a ship, the tile containing the ship will be the largest outlier as discussed later in Section 4.1.3. The results for the comparison for different area sizes for HKZ is in Figure B.1.

The full area represents the results for the entire area that is considered in Subsection 4.1.2. At this larger area size the calculation for the sand wavelength and wave angle is averaged over a large area and the influence of noise or weaker signals becomes less significant. Although at an area of 1 km, the range for the wavelength for the optical and SAR image is the smallest with the lowest standard deviation of 72.7 and 125.1 meters respectively, the angle at this area size has inversely has the largest range and greatest stand deviation of 20.5 and 23.6 degrees respectively. The value of the sand wave angle also reaches 0 degrees which is not wrong for this location. Another reason that 1 km is too small of an area is that the sand wavelength can be up to 1000 meters, or 1 km. At this wavelength it is possible that only a single wave will be present within a tile area, causing there to be no clear sinusoidal signal within the image to calculate the FFT for. The whiskers for each box plot indicates the variability outside the upper and lower quartile which is contained within the box. The length of the whiskers decreases as the area size increases for the wavelength of both optical and SAR. The range of the wave angle data becomes smaller starting at an area of 3 km for optical and 4 km for SAR.

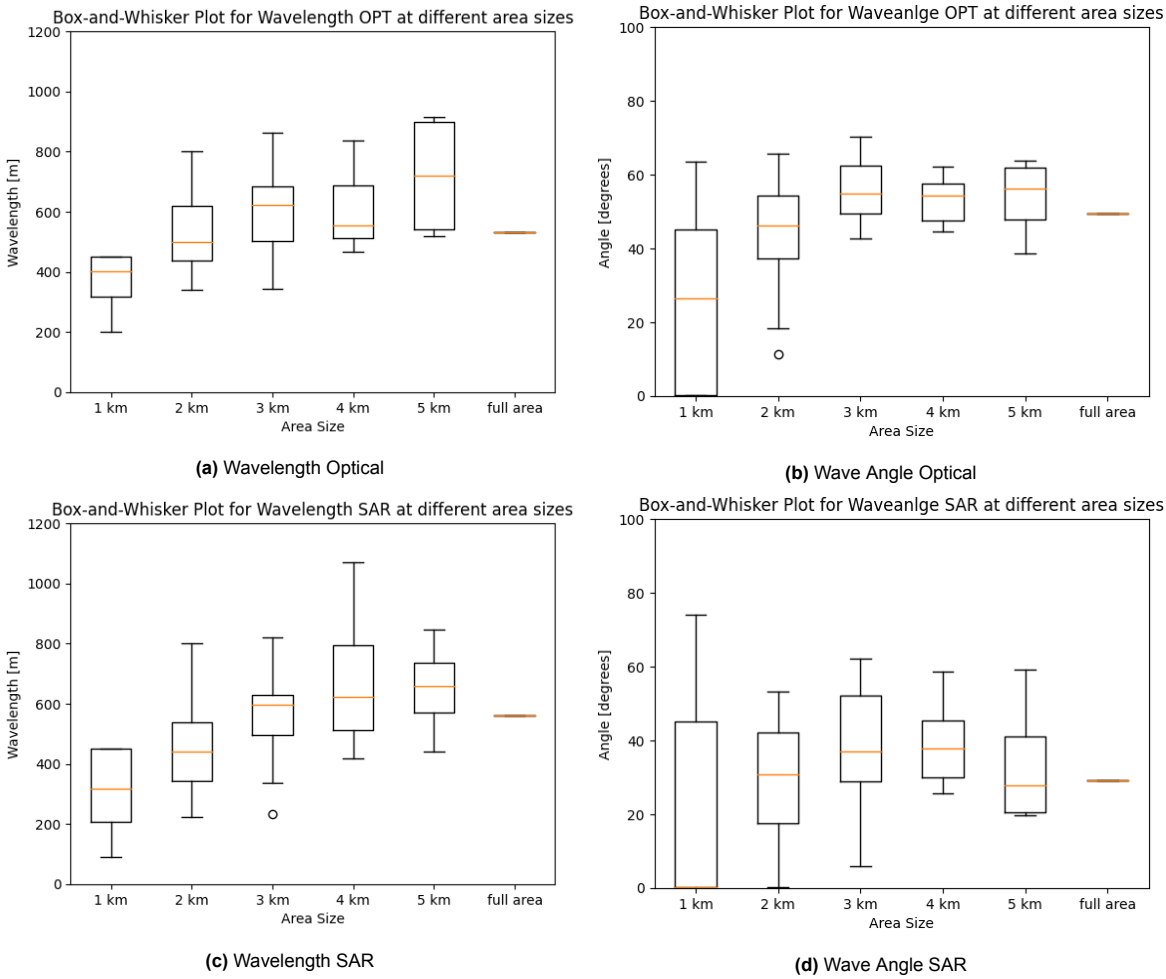

(a) Wavelength Optical

(b) Wave Angle Optical

(c) Wavelength SAR

(d) Wave Angle SAR

Figure 4.16: Comparison of different tile sizes and the effect on sand wave characteristics at Hoek van Holland for an Optical and a SAR Image

As a benchmark, the same process was repeated for MBES for the same area as seen in Figure 4.17. Compared to the results for optical and SAR, the average value for wavelength is closer to that of the full image and has less overall spread in the data with less outliers. This is due to quality of data of the MBES compared to that of the optical and SAR images. Not only is there more noise present such as speckle noise or clouds, the signal present in satellite images is weaker and less distinct than in MBES. It is also expected to have low variability in the wavelength because the area of interest is not large enough to contain significant change in the sand wave characteristics. The greater spread of the wave angle data at the lower area size is due the MBES capturing the entirety of the signal from the very irregular sand waves present at HvH. This spread in the data is not present in the results for the tile comparison at HKZ which has much more regular waves as seen in Appendix B Figure B.1.

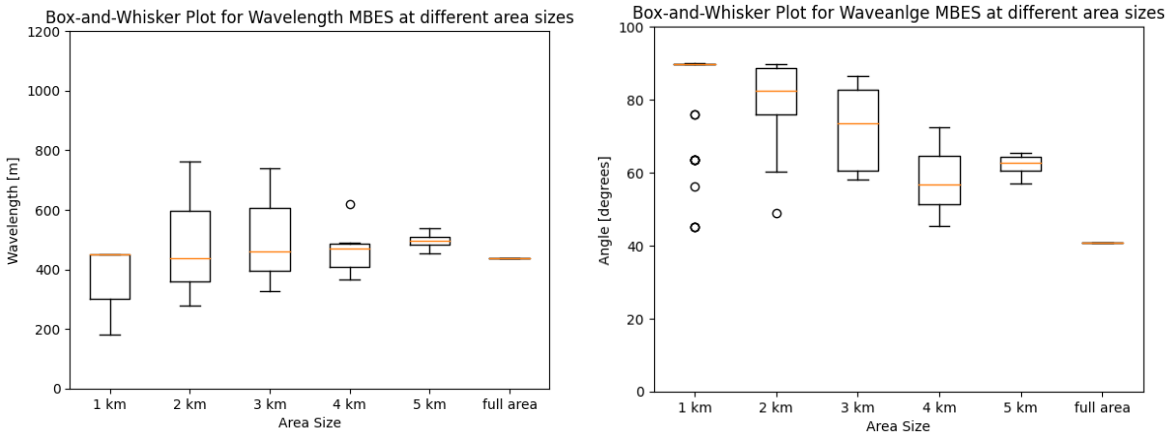

(a) Wave Length

(b) Wave Angle

Figure 4.17: Comparison of different tile sizes and affect on sand wave characteristics at Hoek van Holland for MBES

The tile size comparison was also performed for the optical and SAR images and MBES at HKZ as seen in Figure B.1 with similar results to that of HvH. It was decided to move forward with a tile size of 5 by 5 km. This area was the smallest area that was still in relative agreement with the results over the full image, along with a lower amount of variance in the data and less outliers. Low variance is wanted because the sand waves are all present in a single area and have similar characteristics. The full area is not large enough to contain significantly different sand waves. At HvH, all the sand waves have a shorter wavelength and are irregular. Also, there is no significant change in depth or environmental parameters either so the conditions are expected to stay the same. Depending on the area size that is considered for the FFT, different signals are detected. This explains why the wavelength tends to increase as the area size increases. Also, it is important to note that at small area sizes such as 1 and 2 kilometers, the signal that is read is not always the sand wavelength, which is further explained in Chapter 5

Effect of Noise

The ideal FFT signal for sand waves is a pair of dots as seen in Figure 2.5, however due to the natural characteristics of sand waves like irregularity, speckle noise due to the remote sensing method, and other sources of noise, additional signals are present. To determine the effect that different sources of noise (like ships and wind farms) have on the FFT, 5 by 5 km areas were found containing both sand waves and a noise source. The FFT was performed on the area to determine the sand wave characteristics as well as to analyze how the FFT signal has changed due to noise.

In Figure 4.18, an optical and a SAR image are shown for the same location containing a wind farm. The sand wave signals are very distinct in the optical image and less distinctive in the SAR image. However, the turbines of the wind farm are presented as small points in the optical image and are much larger signal points in the SAR image.

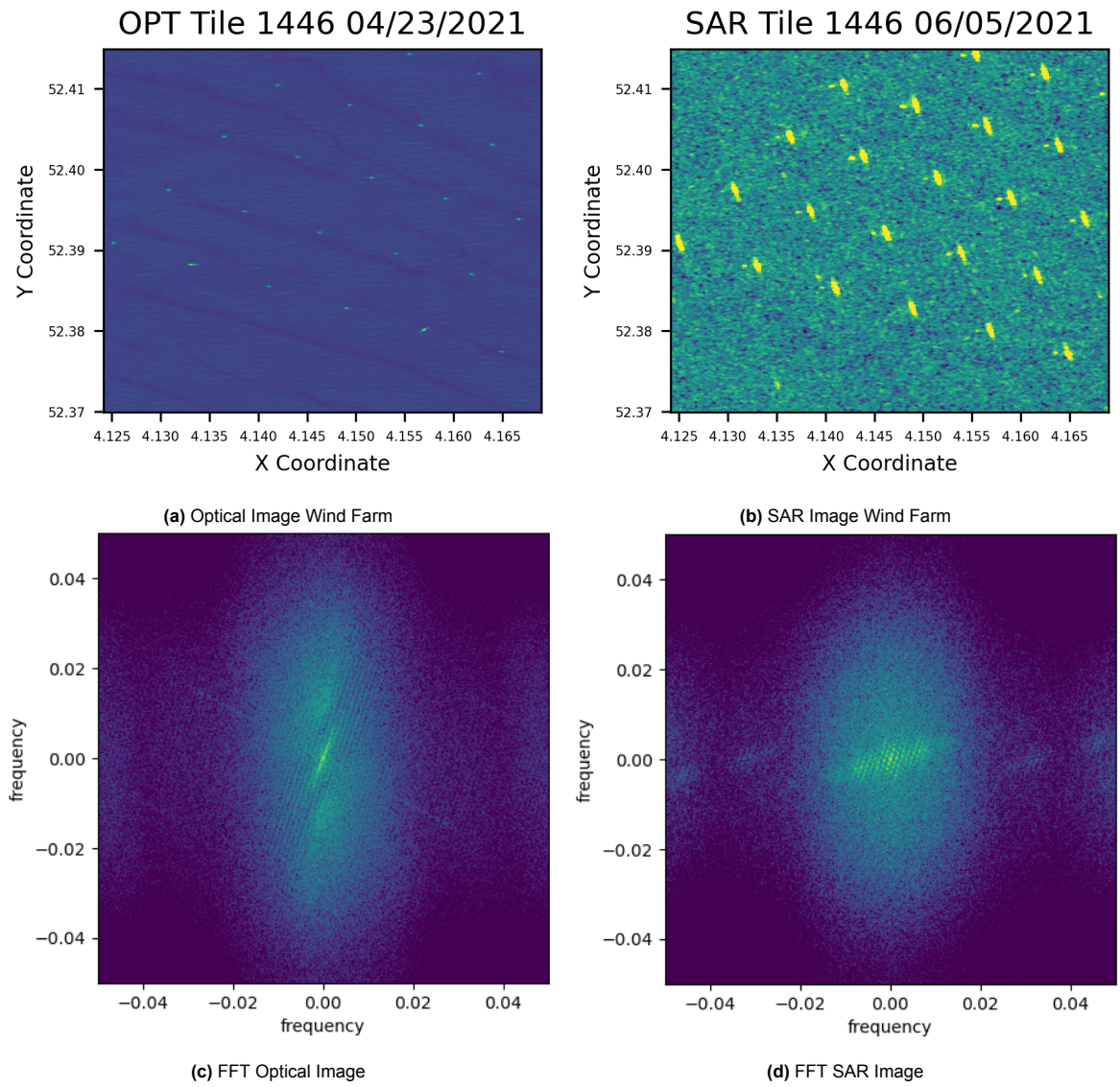

(a) Optical Image Wind Farm

(b) SAR Image Wind Farm

(c) FFT Optical Image

(d) FFT SAR Image

Figure 4.18: Optical and SAR image containing a wind farm with the resulting FFT

The FFT for both images contain what looks like a grid of points near the origin which can be seen in Figure 4.19. The Gaussian filter applied to the FFT smooths the effect of the additional signals. The wavelength calculated for optical is 516 m and for SAR is 392 m, which is both lower than what is expected in this area. The wave angle seen for the signal in the FFT for optical matches better with the angle the sand waves make in the satellite image, while the angle seen in the SAR image is much lower. Comparing the effect on the FFT between optical and SAR, optical imagery seems less affected by the presence of the wind farm, especially for the wave angle. The strong impact of wind turbines in the SAR image causes the sand waves to be less visible in the image and therefore weaker in the FFT.

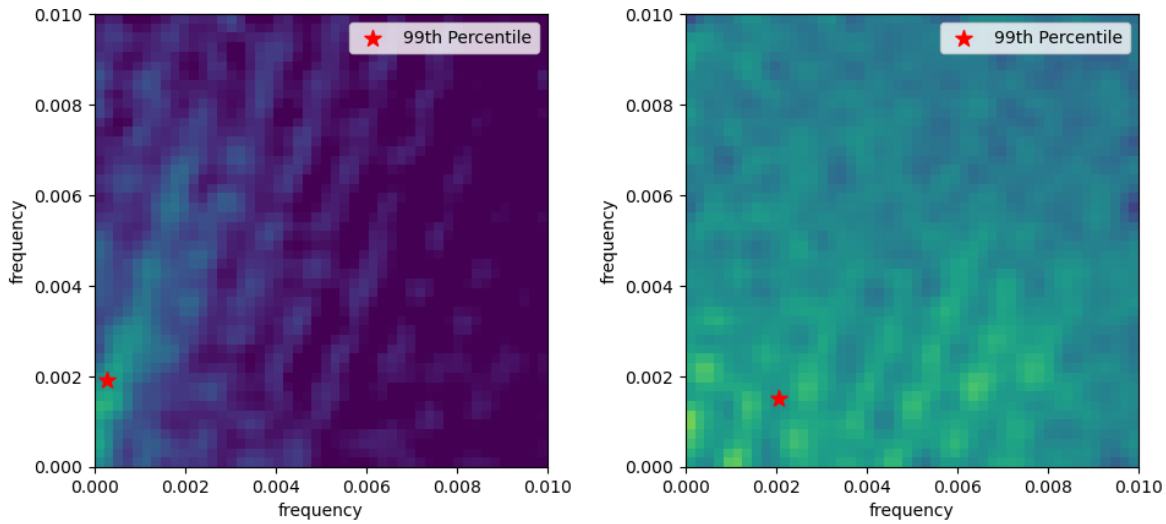

(a) FFT Optical Image Quadrant 2

(b) FFT SAR Image Quadrant 2

Figure 4.19: Optical and SAR image FFT smoothed quadrant 2 containing a wind farm

The next source of noise observed is that of a ship. Both images in Figure 4.20, contain a ship. In the optical image it was observed that the ship is traveling towards the southwest evident by the wake behind the ship. Also, the ship is more distinct in the optical image compared to the SAR image where the ship is brighter, with less sharp lines and no visible wake. The ship in the optical image has a significant effect on the FFT by adding an ellipse with a very strong signal tends to cover that of the sand wave signal. The SAR FFT contains no strong signals.

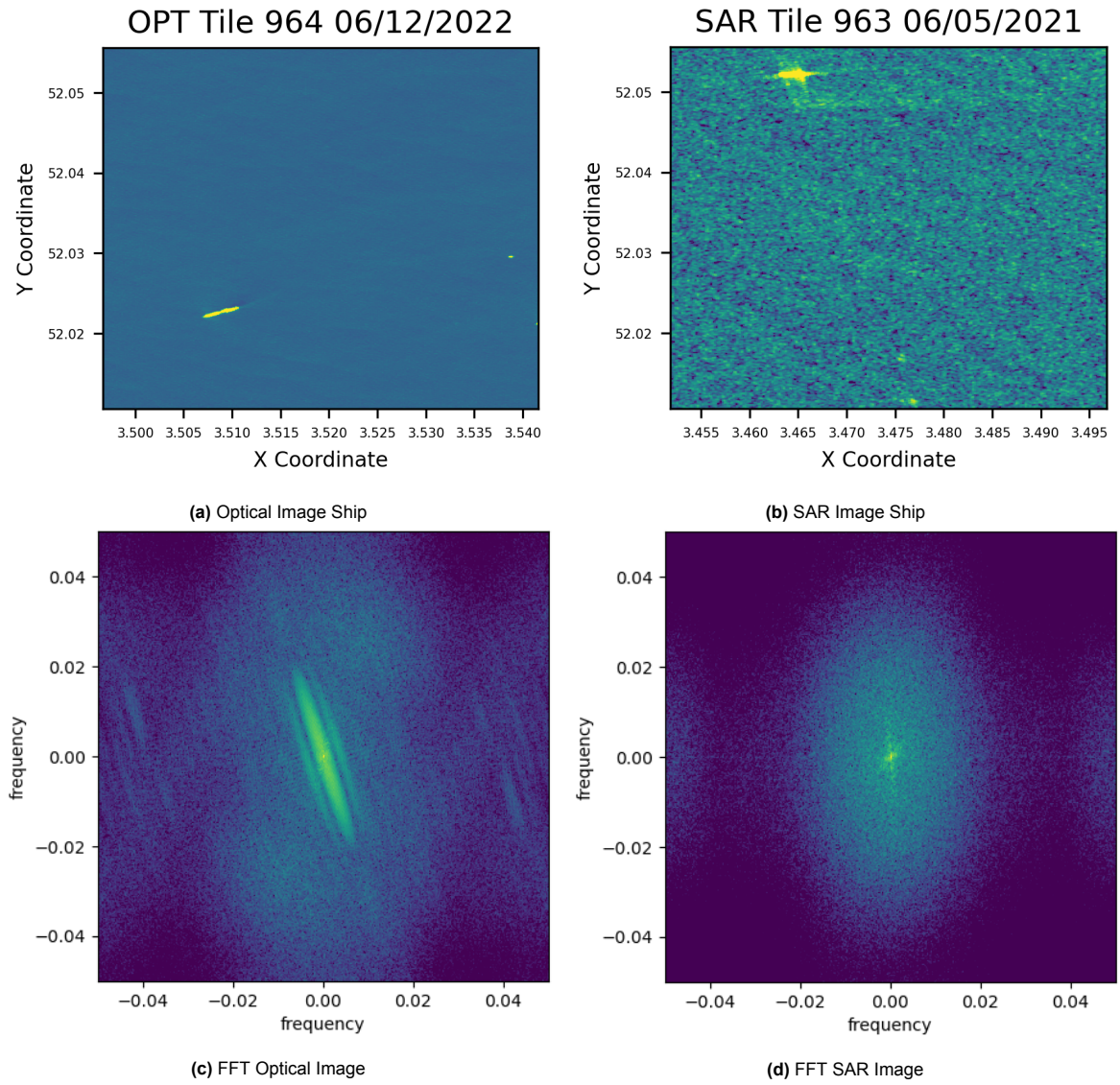

(a) Optical Image Ship

(b) SAR Image Ship

(c) FFT Optical Image

(d) FFT SAR Image

Figure 4.20: Optical and SAR image containing a ship with the resulting FFT

The optical image results in a wavelength of 1074 m. However, where the signal of the sand waves should be, the signal due to the ship overshadows it in quadrant 2 of the FFT as seen in Figure 4.21. So the sand wavelength that is calculated is due to the signal from the ship instead. The SAR image results in a wavelength of 1154 m with a signal that is strongest around the origin. Both these values are significantly larger than what is expected at this location and it can be concluded that ships have a strong effect on the calculation of the sand wave characteristics. The signal of the ship in the FFT covers that of the sand wave in both methods. A recommendation on how to remove tiles affected by ships is given in Chapter 7.

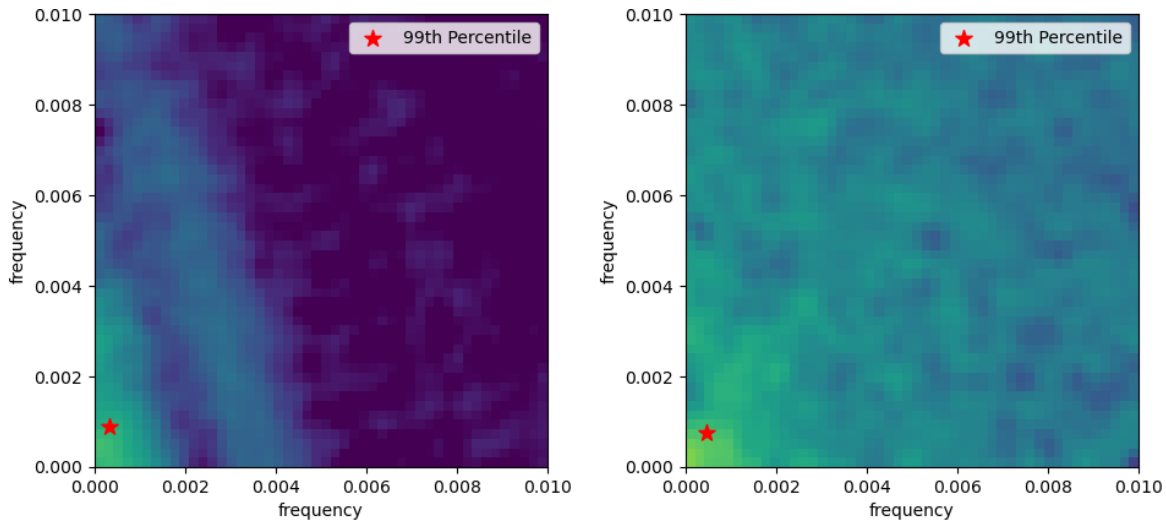

(a) FFT Optical Image Quadrant 2

(b) FFT SAR Image Quadrant 2

Figure 4.21: Optical and SAR image FFT smoothed quadrant 2 containing a ship

Another example of how a ship can affect the sand wave characteristic is seen in Figure 4.22. For optical, the calculated wavelength is 621 meters which is a reasonable value, however, the calculated sand wave angle is 3.6 degrees which is very low. This very low wave angle value is another indicator that noise is present. This is the same for the SAR image which contains three ships. The calculated sand wavelength is 1002 meters and the wave angle is 17.4 degrees. While the angle is not as low as that in the optical image, it is lower than expected. Also, the effect on the FFT is very different between the optical and SAR image. For the optical image it has created a very strong pattern that occurs throughout the FFT while in the case of SAR, it has caused a bright signal around the origin.

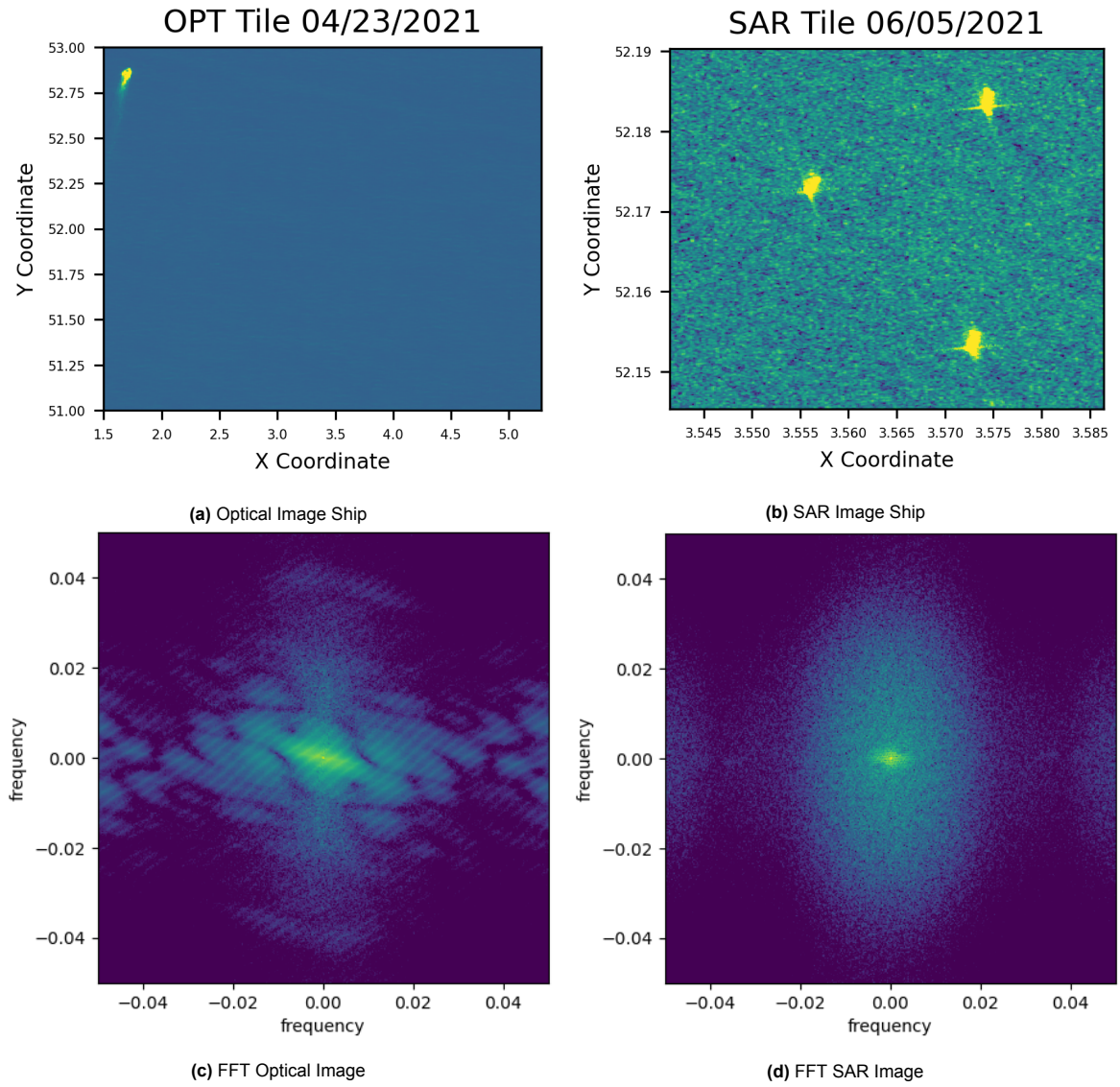

(a) Optical Image Ship

(b) SAR Image Ship

(c) FFT Optical Image

(d) FFT SAR Image

Figure 4.22: Additional example for Optical and SAR image containing a ship with the resulting FFT

Due to the nature of optical images, they are affected by clouds while SAR is not. An image with a small amount of clouds is chosen because the overall time step the satellite pass is chosen for should already have little to no clouds present. When looking at the corresponding FFT image in Figure 4.23 (b), the resulting signal is strongest around the origin, but the signal due to sand waves can still be observed. The strong signal at the origin would cause a shift in the location of the calculated center of the point to be closer to the origin than it actually is.

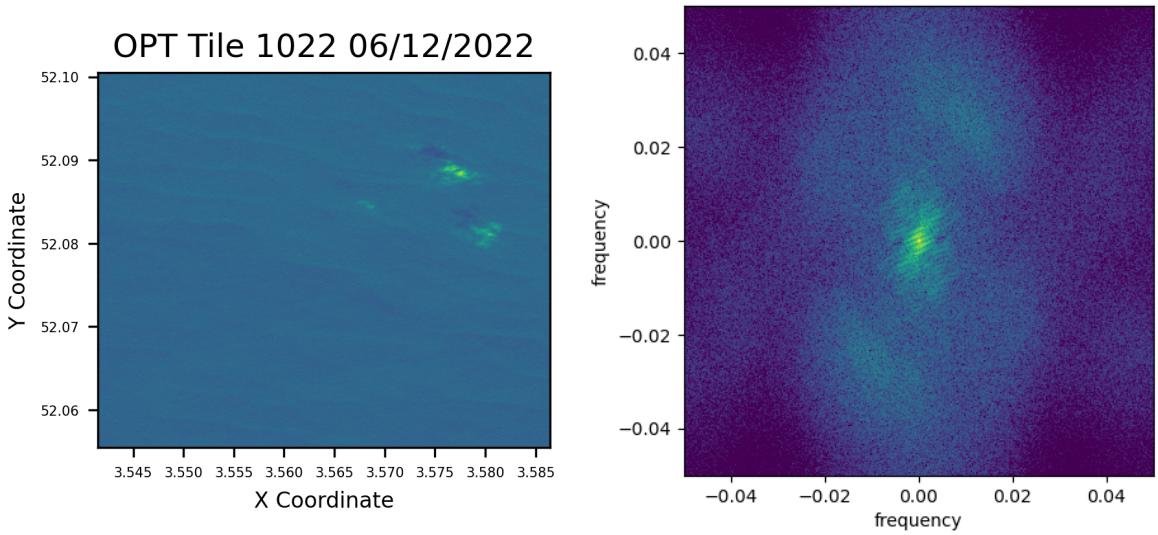

(a) Optical Image Clouds

(b) FFT Optical Image

Figure 4.23: Optical image containing clouds with the resulting FFT

Due to the shift in signal due to the bright signal at the origin from the clouds present the wavelength calculated was 714 m as seen in Figure 4.24 and larger than what is expected at this location. This is confirmation that when filtering the collection and choosing images clouds should avoided as much as possible for optical satellite images.

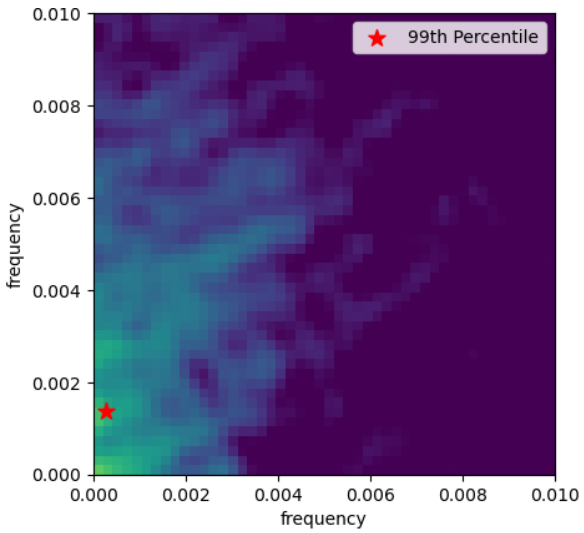

Figure 4.24: Optical image FFT smoothed quadrant 2 containing clouds

Suspended sediment in the water column (turbidity plume), like clouds, is also visible in optical images like the one seen in Figure 4.25. The sediment moves in the direction of the current which is perpendicular to that of the sand wave crests. The FFT also shows the typical signal of the sand wave from the bottom left to the right quadrants, while there is a fainter signal from the sediment in the top left and bottom right quadrants.

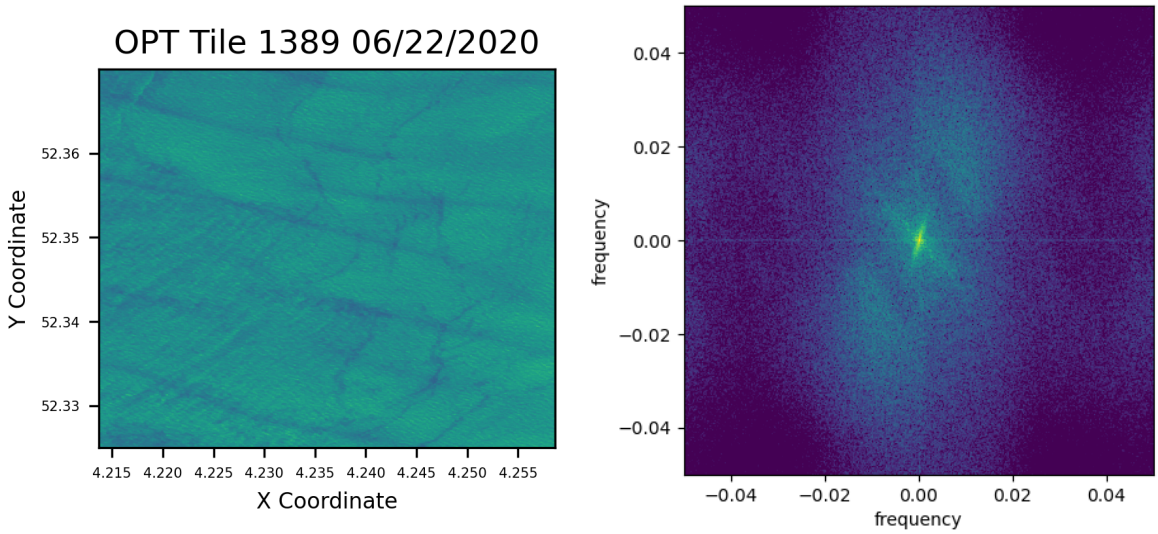

(a) Optical Image Sediment

(b) FFT Optical Image

Figure 4.25: Optical and SAR image containing suspended sediment transport with the resulting FFT

The calculated wavelength is 611 m. The only signal visible in quadrant 2 in Figure 4.26 is due to the sand waves. As a result, suspended sediment in optical images does not have much affect on the calculation of the sand wave characteristics because the quadrant used to make the calculations will never contain the signal.

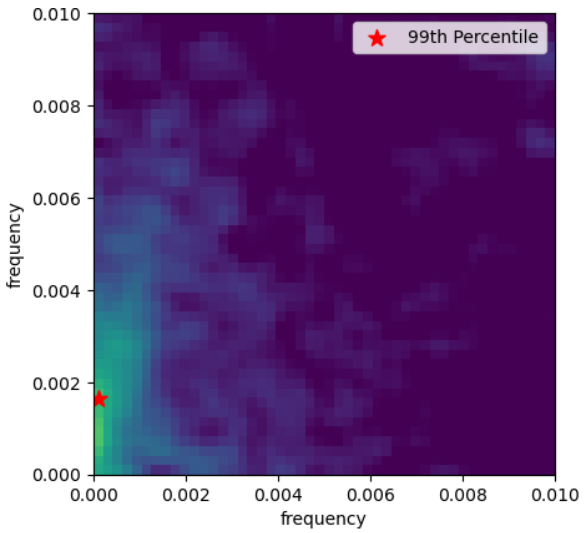

Figure 4.26: Optical image FFT smoothed quadrant 2 containing suspended sediment transport

Areas of lower reflectance values can occur in SAR images as seen in Figure 4.30 on the west side (dark colored patch). Multiple phenomena present themselves as dark patches, such as rain cells, upwellings, internal waves, and oil spills (Liu et al., 2022). The benefit of SAR compared to optical imagery is that it is dependent upon less environmental parameters like the mean glint angle and cloud cover, yet weather patterns are still indirectly visible. The dark patch blocks the visibility of sand waves within the satellite image, and therefore there is no strong signal visible within the FFT seen in Figure 4.27, however it is very faint.

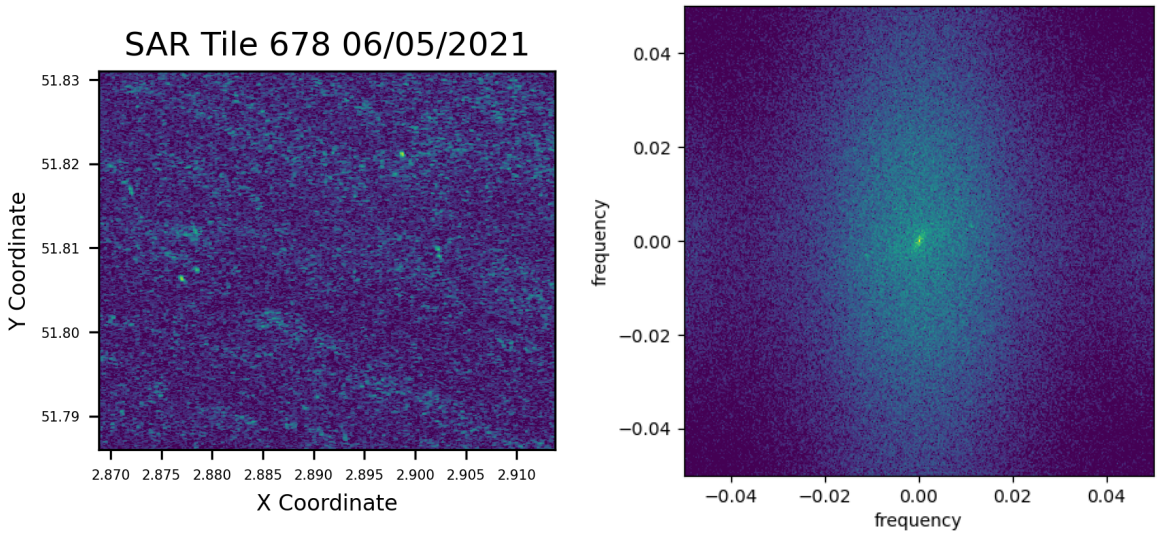

(a) SAR Image Low Reflectance

(b) FFT SAR Image

Figure 4.27: SAR image at a low reflectance area with the resulting FFT

The resulting wavelength from Figure 4.28 is 793 meters which is about twice as large as expected. The second quadrant of the FFT shows that the signal in the FFT is very indistinct and does not actually look like the signal of a sand wave. Therefore, if the dark patches are visible in a SAR image, this area should be disregarded for calculation of sand wave characteristics.

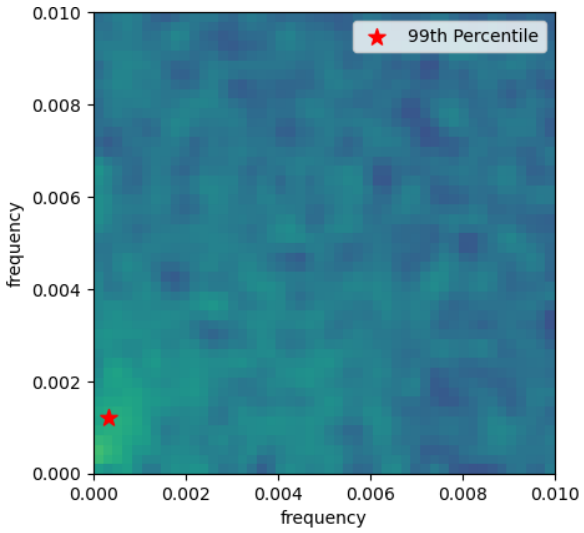

Figure 4.28: SAR image FFT smoothed quadrant 2 at location of low reflectance

The resulting wavelength, wave angle, and wave density was compiled into Table 4.3. In addition to the sand wave characteristics calculated through remote sensing, a column was added containing the wavelength measured manually using the MBES and averaged over the same area as each tile. Due to different sources of noise, the sand wavelength and wave angle can vary largely from the expected characteristics in an area. This is most strongly seen for optical and SAR images containing ships with a wavelength 700 meters greater than expected. On the other hand, the calculated wavelength for the optical image at the wind farm is not very affected by the source of noise and the wavelength is only 75 meters smaller. Therefore, as stated earlier, sand wave characteristics can be calculated at wind farms when using optical satellite images only. There are two examples shown for the case where the source for noise is from a ship for optical images, because the location of the ship within the image

and the shape affected the sand wave characteristics differently. In one case, the sand wavelength is significantly larger than expected but the angle is reasonable, while in the other case the wavelength is reasonable and the sand wave angle is very low in value. For both examples of ships for SAR, a very high wavelength was calculated. While sediment has little effect on the sand wavelength and angle, clouds have a large effect and should be avoided for optical images. Dark patches in SAR images should also be avoided because it blocks the visibility of sand waves within the satellite image and the resulting calculated sand wave characteristics do not correspond to the actual sand waves present.

Table 4.3: Sand Wave Characteristics derived from 5km tiles containing different sources of noise. The actual wavelength was determined using the MBES in QGIS and manually measuring the distance of wavelengths

Source of Noise	Satellite Type	Wavelength [m]	Wavelength QGIS [m]	Wave Angle [deg]	Wave Density [-]
Wind Farm	OPT	515.8	590	82.4	9.8
	SAR	392.2	590	36.2	15.8
Ship	OPT	1074.0	295	70.2	5.0
	OPT	621.0	422	3.6	1.6
	SAR	1154.4	315	58.7	5.1
	SAR	1002.2	426	17.4	1.0
Sediment	OPT	611.1	740	86.1	8.2
Clouds	OPT	713.8	386	79.5	7.1
Dark Patch	SAR	793.4	416	74.7	6.6

Due to noise it is important to determine whether or not a source of noise is present within an image. This is because it can cause a false value for sand wave characteristics, such as in the case of the ships in satellite images or the dark patch in the SAR image. A reasonable value for wavelength can be calculated, however it is due to the signal of the noise in the FFT, and not due to visible sand waves.

4.2. Upscaling

The next section considers the upscaling of the methodology for the North Sea. The same methodology that was used to calculate the sand wave characteristics in Section 4.1.2 for 5 km areas is used to create a grid of data. A single satellite pass-over was used by assuming similar environmental conditions across the larger area of interest and therefore visibility of sand waves. The dates for the images for the pass-over were chosen from the results obtained by filtering the image collection with the process seen in Section 4.1.1, where sand waves were visible at both HvH and HKZ.

4.2.1. Post Processing for Sand Wave Characteristics

Seen in Figure 4.29 is the grid at which optical and SAR satellite images are downloaded. This gives a coverage of the North Sea between the Netherlands and England, the primary location of the sand wave field defined in Figure 1.2, at 5 km intervals.

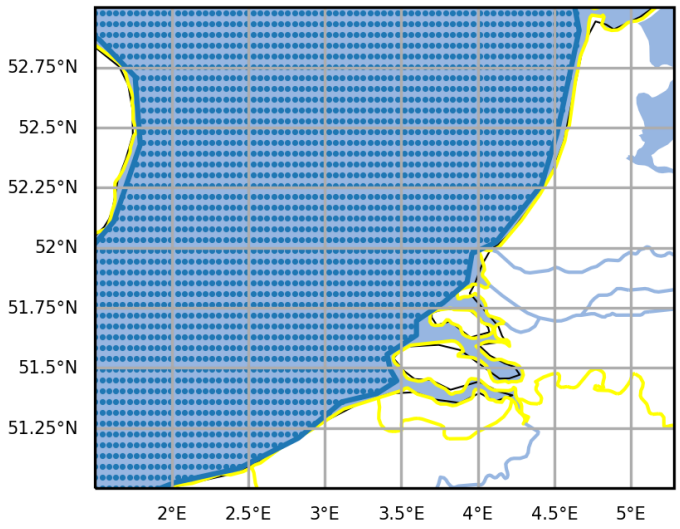

Figure 4.29: Grid points to download satellite data every 5 km in the North Sea between the West coast of the Netherlands and East of England

To better understand where the sand waves occur, the outline of the sand wave field as defined by Nemeth seen in Figure 1.2 was added to the figures. Only the solid area where the sand wave field is uninterrupted and not scattered was taken into account. Due to the satellite trajectory over the North Sea (and its swath width) there is not always complete coverage in a single pass as seen in the south-west of the SAR image in Figure 4.30. Additionally, due to the variability in weather it is possible that the North Sea is partially covered by clouds, impacting the usefulness of optical images. Images for the year 2021 are further analysed below while the analyses for the years 2020 and 2022 are reported in Appendix B, both these years contain an incomplete pass over of the North Sea for SAR.

The optical image was taken on April 23rd, 2021 and the SAR image was taken on June 5th, 2021. There is some evidence of clouds in the optical image as seen in Figure 4.30 (a) in the upper right as bright spots. labeled with A The dark patch in the left of the SAR image labeled with A in Figure 4.30 is most likely due to a rain cell since rain is a typical weather condition in the North Sea region. The effect that the dark patch has on the visibility of sand waves is discussed for Figure 4.27. The SAR image is also not a complete pass of the North Sea and is missing coverage in the Southwest of the image. The optical image has fuller coverage but is missing some data along the East side close to the Dutch coast.

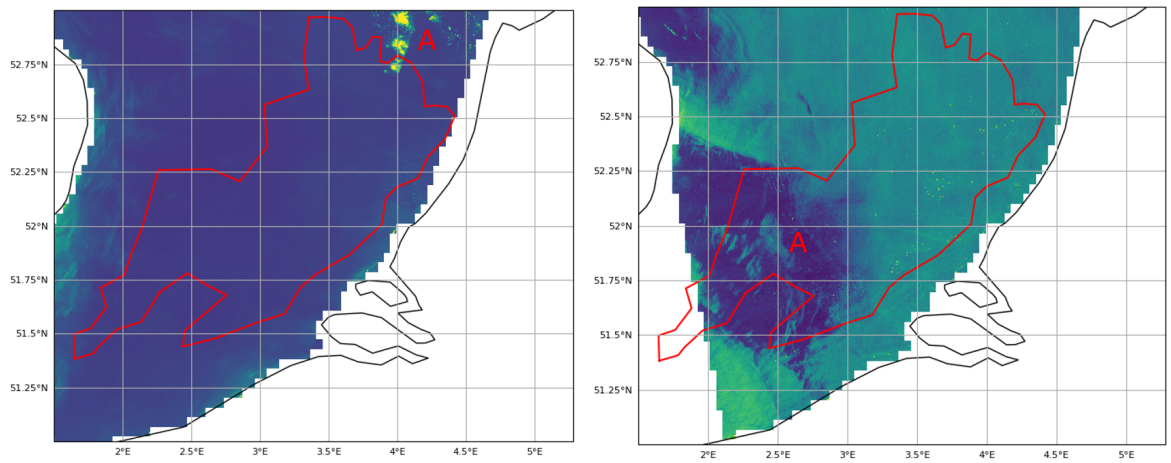

(a) Optical Image 04/23/2021

(b) SAR Image 06/06/2021

Figure 4.30: Optical and SAR satellite image for the entire North Sea using a single pass-over

The wavelength of sand waves in the North Sea is considered to be in the range from 100 to 1000 meters, the data points that do not meet these requirements were removed. The majority of points removed for the optical results were greater than 1000 meters which is understandable when looking at the resulting wavelength for Alkmaar in Table 4.2, where there are no sand waves present. The optical method calculated a large wavelength. The SAR method at Alkmaar resulted in a lower wavelength of 330 meters, which will not be removed by the filter, and is consequently the reason why more data points are still visible in Figure 4.31 (d).

The distribution of data points for the optical image as seen in Figure 4.31 (c) when filtered on wavelength matches the sand wave field boundaries on the west, east, and north boundaries. This is also consistent for the years 2020 and 2022 for the optical images as seen in Figure B.4.The scattering of points with data along the northwest is in the location where there are inconsistent sand waves present. For the resulting wavelengths for the optical image, the wavelength is lower towards the south and increases moving towards the north, with points of high wavelength values scattered throughout the area. The resulting wavelengths for the SAR image is larger in the south and smaller in the north. The high wavelength area in the south corresponds to where the area with lower reflection occurs in Figure 4.30 (b). Both wavelength images, but especially SAR, exhibit higher wavelengths along the eastern border of the sand wave field.

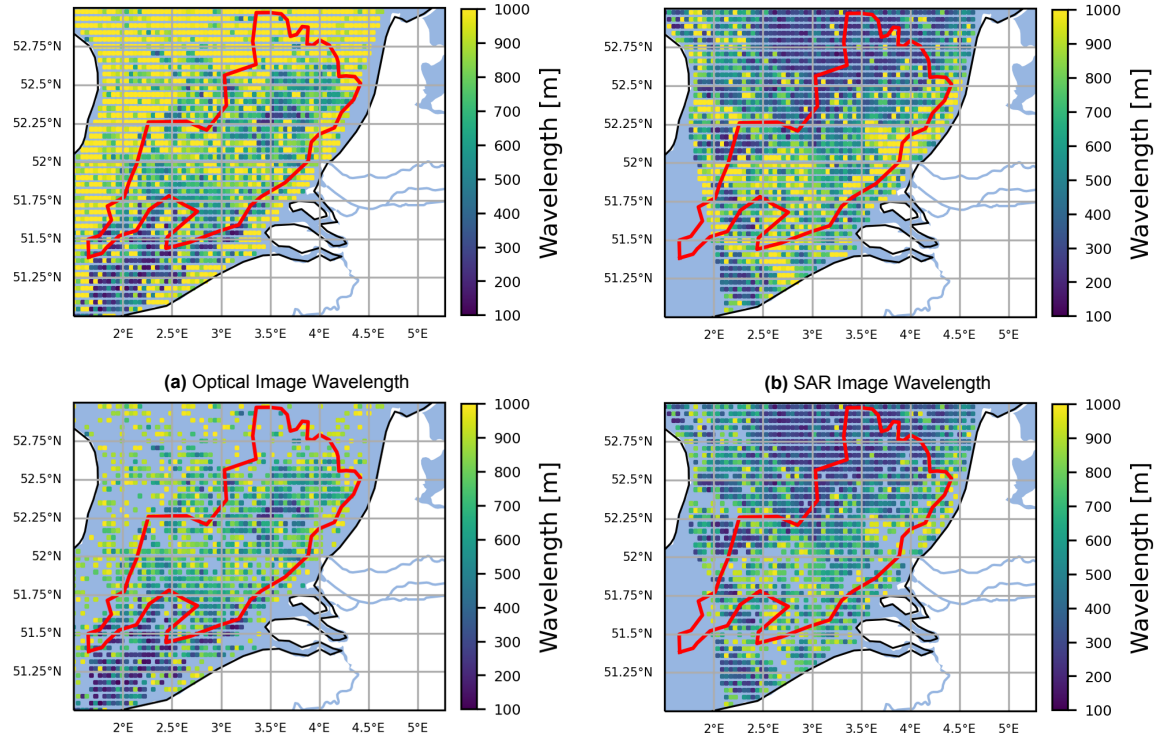

(a) Optical Image Wavelength

(b) SAR Image Wavelength

(c) Optical Image Wavelength Filtered

(d) SAR Image Wavelength Filtered

Figure 4.31: Optical and SAR results for sand wavelength for 2021 in (a) and (b) and with filtering for a wavelength between 100 and 1000 meters in (c) and (d)

In Damen et al., 2018 the sand wave characteristics were calculated using a 2D FFT for a MBES of the Dutch Continental Shelf. The wavelength is around 100 to 200 meters in the South and gradually increases moving North. The largest wavelength at around 900 to 1000 meters occurs around the North and Eastern borders. The MBES dataset used in Damen et al., 2018 does not have complete coverage over the entire sand wave field in the North Sea as defined by Nemeth, 2003. To compare the results the wavelength data from Damen et al., 2018 was re-sampled to the grid used for both optical and SAR and shown in Figure 4.32. The wavelengths from Damen et al., 2018, looks like it has a lower value of wavelengths in general across the entire area. This is because it measures the wavelength of

each individual waves which can have shorter wavelengths. All three figures show a higher value for wavelength in the Northeast and a lower value in the Northwest. In the South the wavelength calculated from the satellite images has a higher wavelength around 1000 meters. These high values could be due to a high number of ships in this area due to a popular shipping route leaving from Rotterdam.

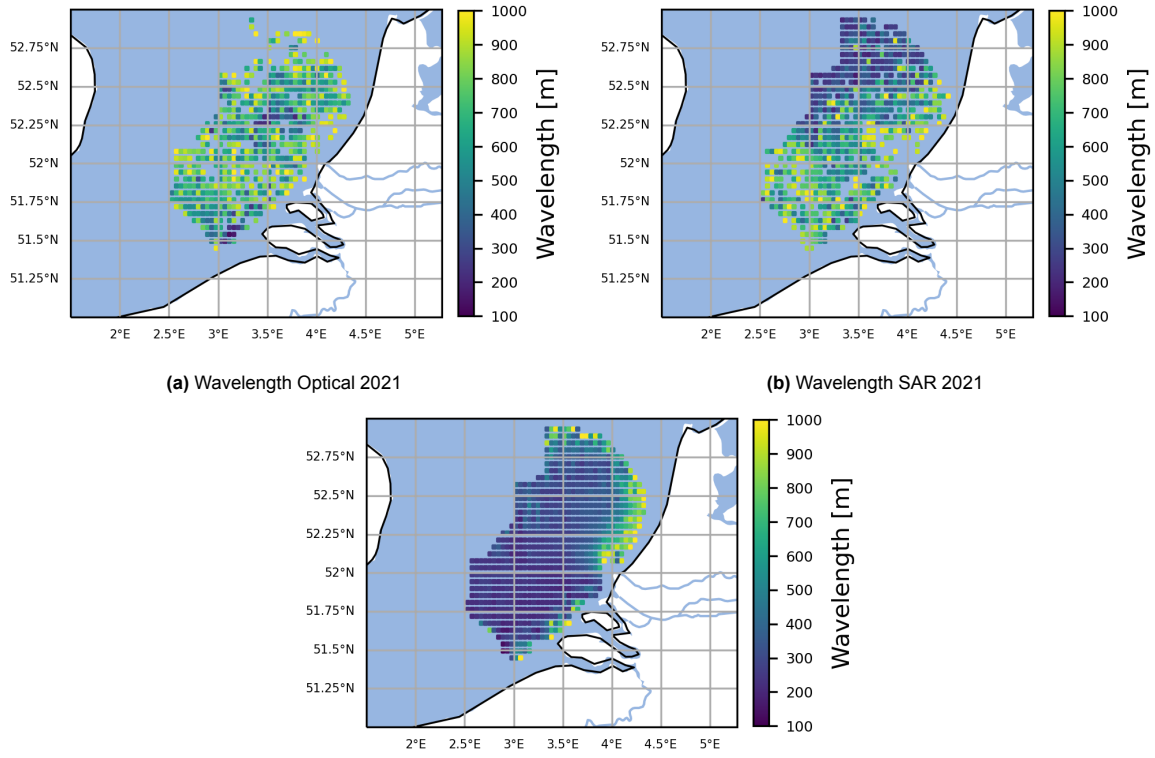

(a) Wavelength Optical 2021

(b) Wavelength SAR 2021

(c) Wavelength Damen et al., 2018

Figure 4.32: Comparison of wavelengths obtained from Optical Image, SAR Image, and Damen et al., 2018 for 2021

Correlation for the optical image resulting wavelength and Damen et al., 2018 wavelength is 0.156 and for SAR is 0.015. The data is visualized in Figure 4.33 with the wavelength from the satellite data on the x-axis and wavelength from Damen et al., 2018 data in the y-axis. A positive trend is seen for the optical image and a negative trend for the SAR image. The wavelength from Damen et al., 2018 tends to have a low value of around 100 to 400 meters with fewer values greater than 400 meters. Both the optical and SAR wavelengths has data from 100 to 1000 meters, however SAR is more densely populated at lower wavelength values and optical at higher values, which causes the negative correlation for SAR and positive correlation for optical. The negative correlation should theoretically not occur. However, when no sand waves are present in a SAR image, the calculated wavelength from the FFT signal is around 200 to 300 meters. Although the correlation is still low for the optical image, it has better agreement than SAR does with the wavelength data.

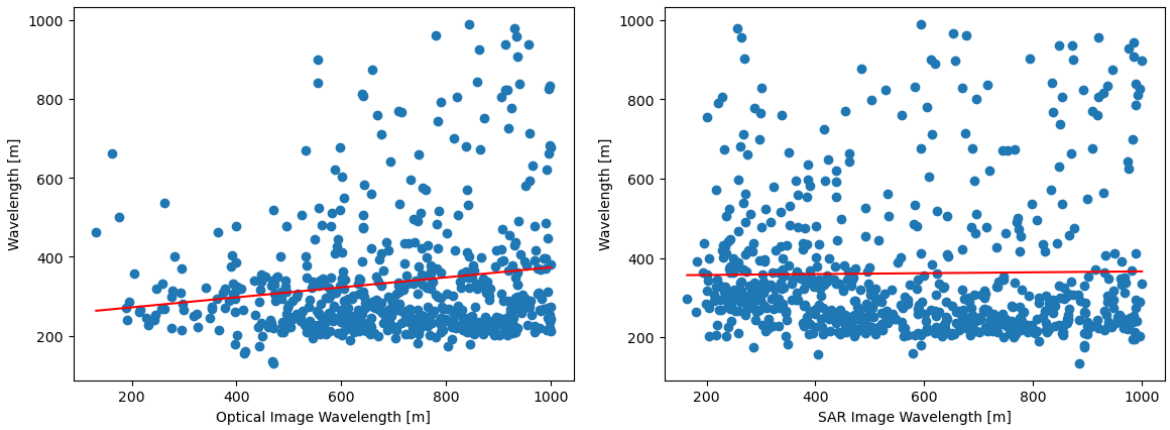

(a) Optical **(b)** SAR

Figure 4.33: Optical and SAR wavelength results correlation with wavelength data from Damen et al., 2018

On average, the wave angle determined from the optical satellite image is about 10 to 20 degrees higher than that from SAR. This means that the sand waves determined in SAR is more in the northeast direction while in the optical image is north-northeast. In both images in Figure 4.34, the wave angle smoothly transitions from one point to the next in value with the exception of outliers with values close to zero degrees. Seen in Figure B.2, the sand wave angles for the optical image that were removed because the wavelengths were not between 100 and 1000 meters were very small, between 0 and 20 degrees which is another method to differentiate areas containing sand waves compared to areas containing no sand waves or sources of noise.

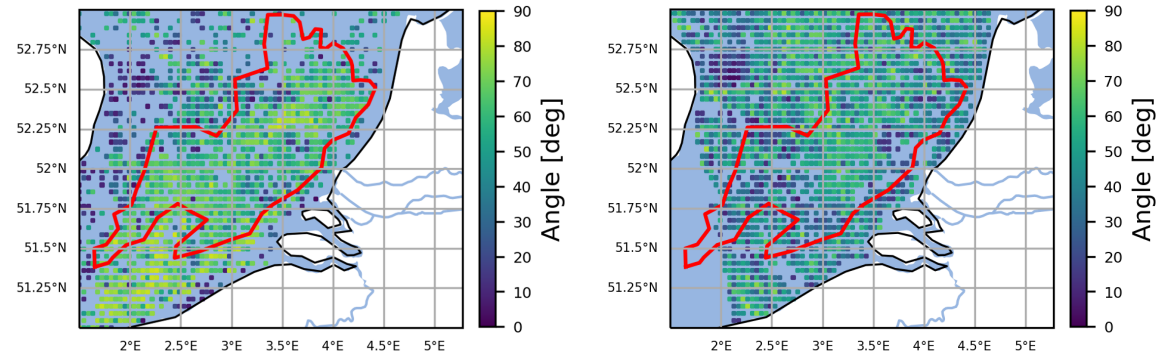

(a) Optical **(b)** SAR

Figure 4.34: Optical and SAR results for sand wave angle 2021. Wave angle is measured with respect to due East.

The wave density is calculated by dividing the length of the tile by the sand wavelength for every tile. When wavelengths are short, the sand wave density is high, and when wavelengths are long, the density is low. The wave density ranges mostly between 10 and 15 within the defined sand wave field. However, in the SAR image results there is a large area in the North with a very high density. This is the same location where the sand wavelength is around 100 to 200 meters. This could be because the way SAR calculates wavelength when there are no sand waves present as seen for the case of Alkmaar in Subsection 4.1.2. SAR tends to have very lower wavelength results when there is no clear signal in the FFT.

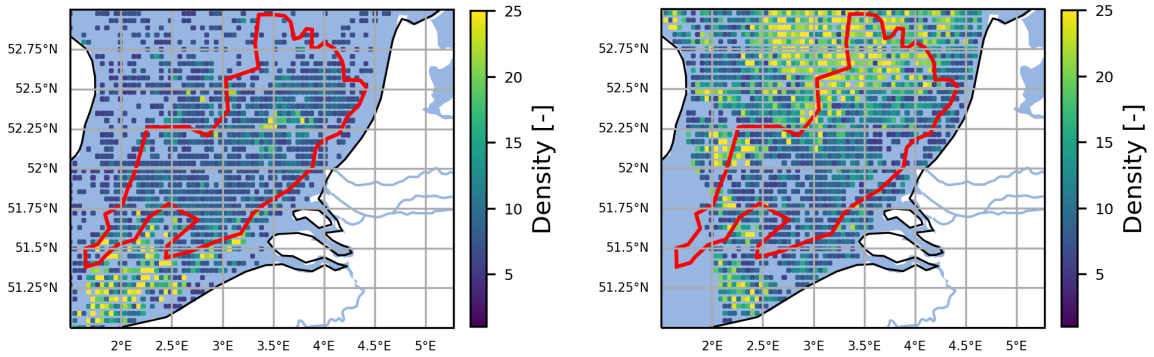

(a) Optical **(b)** SAR

Figure 4.35: Optical and SAR results for sand wave density over the area of the 5 by 5 km tile for 2021

The spatial frequency takes the wave density and divides it by length of the tile which in this case is 5 kilometers. The resampled results to match that of optical and SAR from Damen et al., 2018 can be seen in Figure 4.36. There is higher sand wave frequency in the South around 4 to 5 km^{-1} and decrease to between 3 to 4 km^{-1} moving North. The lowest frequency occurs on the Eastern border of the sand wave field at around 1 to 2 km^{-1}. The optical image has a relatively low spatial frequency of about 1 to 2 km^{-1} across the entire area considered with occasional location with higher values. The results from the SAR image has a similar frequency to that of the optical image, however in the Northwest corner there is an area of spatial frequency greater than 4 km^{-1}. All three figures have a low frequency of around 1 km^{-1} in the Northeast corner starting at about 52 degrees latitude. This is in agreement with the sand wavelength in this region as seen in Figure 4.31.

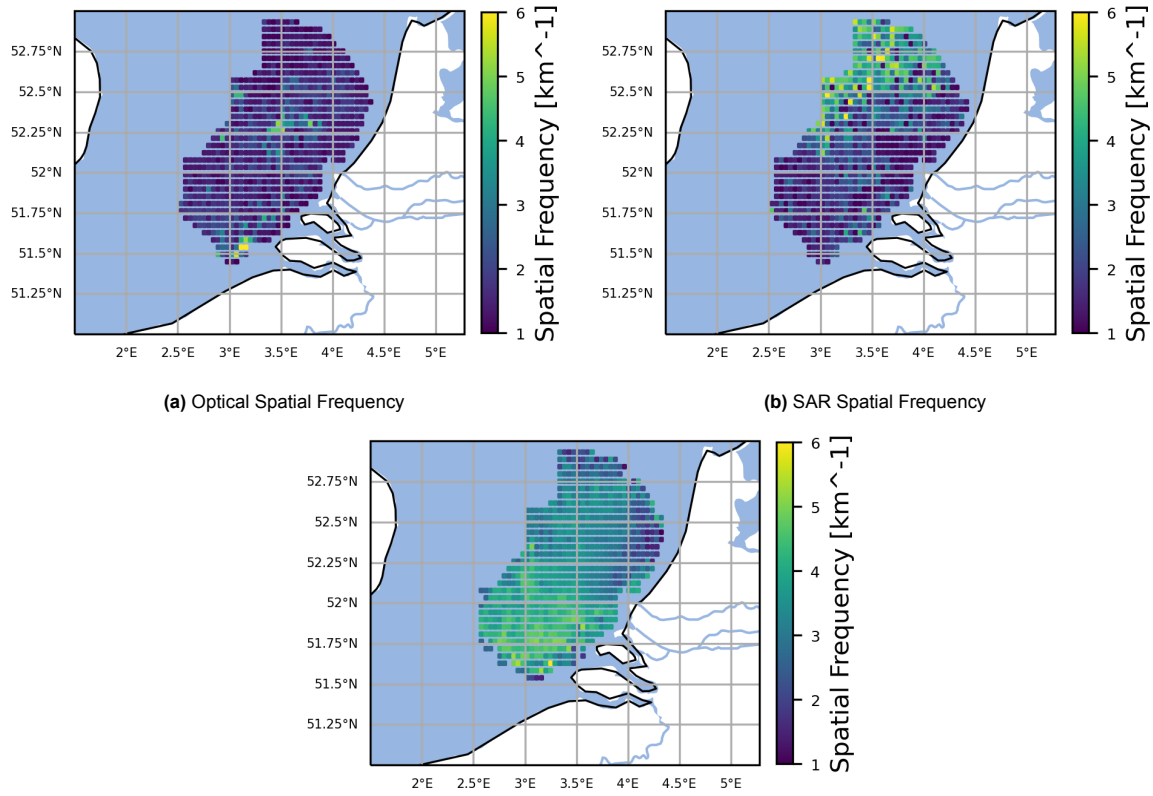

(a) Optical Spatial Frequency **(b)** SAR Spatial Frequency

(c) Spatial Frequency from Damen et al., 2018

Figure 4.36: Optical and SAR results for sand wave frequency for 2021 with the spatial frequency from Damen et al., 2018

The requirements for wind speed is between 3 and 12 m/s. If the sea surface is completely smooth due to low wind speeds, the sea surface roughness will not change due to the current interaction with bed forms, and if the wind speed is too high, it causes too much noise. As seen in Figure 4.37, the date and time for the SAR image meets these requirements across the entire area. However, at the date and time of the optical image the values are on the boundary of the lower threshold.

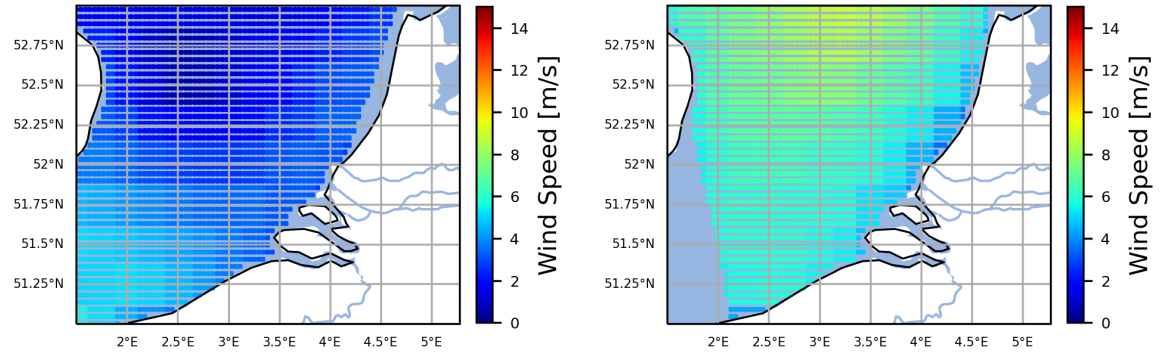

(a) Optical **(b)** SAR

Figure 4.37: Wind Speed for the same time as Optical and SAR image

The required current speed to detect sand waves according to the Alpers Hennings (AH) model as discussed in Section 2.3 is greater than 0.4 m/s. As seen in Figure 4.38 the current speed at the date and time the SAR image was taken satisfies this condition over the entire North Sea. However, the optical image has current speeds very close in value to the threshold or slightly below, however sand waves are still visible at this time. Therefore, there is a balance between the sand wave characteristics such as height and wavelength, and the environmental parameters of wind and current speed that make them visible in satellite images. It could also be that the thresholds are different for optical and SAR, because sand waves are visible in both methods for 2020 to 2022, however the current speed is always much greater at the point of time for SAR as seen in both Figure 4.38 and Figure B.8.

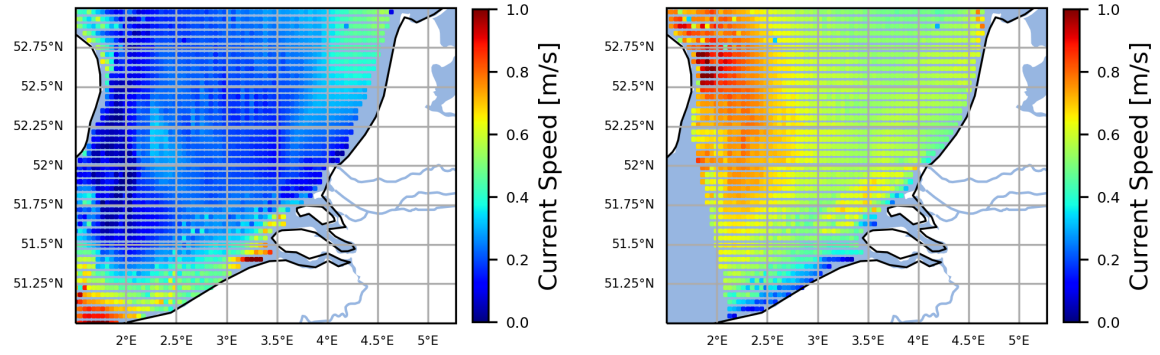

(a) Optical **(b)** SAR

Figure 4.38: Wind Speed for the same time as Optical and SAR image

In addition to wind and current speed, the depth also has impact on the visibility of sand waves in satellite imagery. The depth of the North Sea is shown in Figure 4.39. Along the East half of the sand wave field (on the Dutch Continental Shelf) the water depth ranges from 20 to 30 meters and in the West half the depth ranges from 40 to 50 meters. The western half is significantly deeper which makes it less likely to be able to detect sand waves here. This is explained by the AH model, which states that the sea surface roughness is affected by the current over the sand waves. If the water is too deep and the current not strong enough the bed forms will no longer have an effect on the surface roughness. It is possible that more sand waves were visible for SAR in 2021 because in the deeper channel in the West the current speed for that date and time was significantly higher, ranging from 0.8 to 1.0 m/s. A very

strong current will allow the sand waves to be visible at deeper depths which is also shown in Li et al., 2010, where bathymetric features at a depth greater tan 500 meters were visible in SAR due to the Gulf Stream with a current greater than 2 m/s. However, these bathymetric features had a wavelength of 2.3 kilometers which is significantly larger than the wavelengths of the sand waves found in the North Sea.

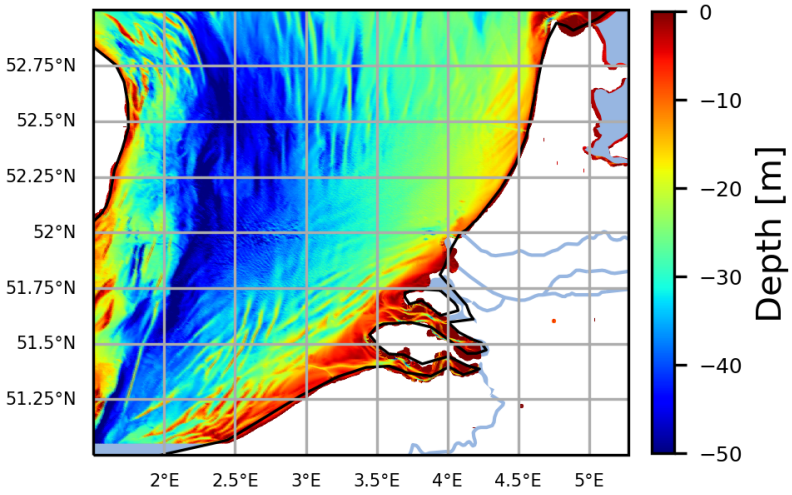

Figure 4.39: North Sea depth from the European Marine Observation and Data Network (EMODnet).

Difference in Sand Wave Characteristics between Years

The absolute difference between each year for every sand wave characteristic (sand wave angle, length and density) was calculated per tile. The difference between 2021 and 2022 for optical images is shown in Figure 4.40. For the wavelength the difference within the sand wave field is largely around 200 meters with some areas around 400 to 600 meters difference. The average difference in wavelength within the sand wave field is 329 meters and a standard deviation of 233 meters. The large difference in values can be due to noise occurring within an area like ships or clouds which are not constant over time. The average sand wave angle in the sand wave field in 2021 is 53.3 degrees and in 2022 is 58.7 degrees. The sand wave angle can be averaged over the entire sand wave field unlike wavelength and wave density because it typically does not vary as much since the direction is due to the current direction. Within the sand wave field the sand wave angle mostly varies up to 10 degrees, however there are scattered points where the difference is much larger, most likely also due to noise. This causes the average difference in wave angle to be 21 degrees and a standard deviation of 16.5 degrees. The average difference in wave density is 4.2 and with a standard deviation of 4.2.

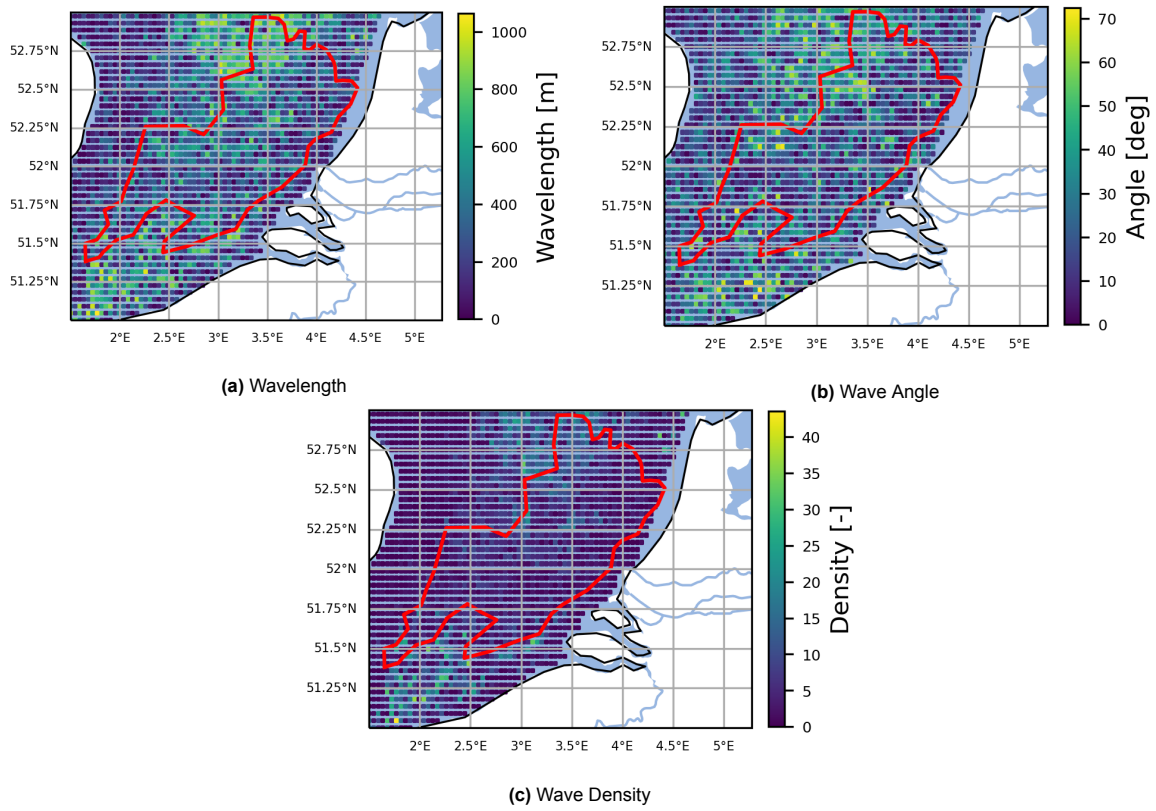

(a) Wavelength

(b) Wave Angle

(c) Wave Density

Figure 4.40: Difference between results from year 2021 and 2022 Optical Images

The resulting difference between 2021 and 2022 for SAR images does not cover the entire sand wave field due to the SAR image from 2022 in Figure B.4 not being a complete pass-over of the North Sea for that date. However, it is the most complete image for that year. The difference in wavelength is mostly less than 200 meters, and occasionally up to 600 meters. The average value of the difference of the wavelength for the points within the sand wave field is 225 meters with a standard deviation of 203 meters. Just like for optical images, this could be due to sources of noise that are not constant in time such as ships or dark patches. The average wave angle for the sand wave field for 2021 is 43.8 degrees and for 2022 is 56.1 degrees. The difference in wave angle between years tends to be 10 degrees but can be up to 50 degrees. The average difference for the sand wave angle is 18 degrees, lower than that of optical, and a standard deviation of 14 degrees. The average wave density is 4.6 and the standard deviation is 4.5.

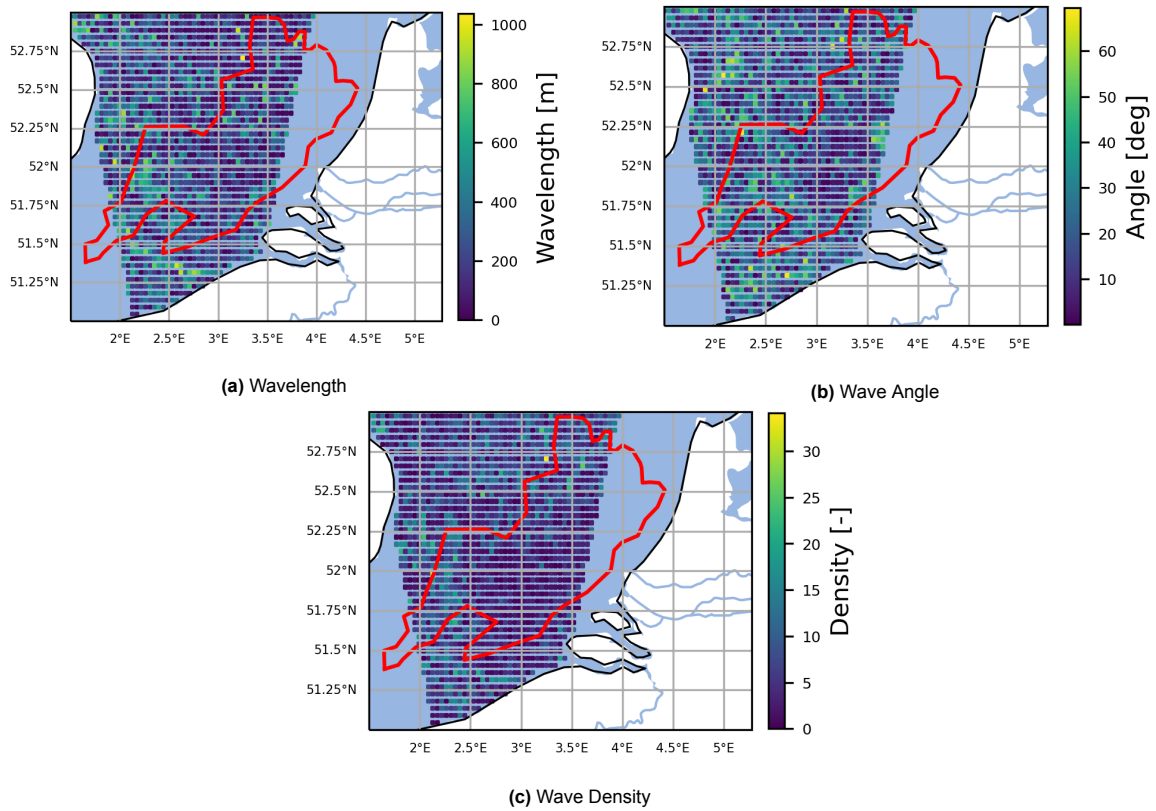

(a) Wavelength

(b) Wave Angle

(c) Wave Density

Figure 4.41: Difference between results from year 2021 and 2022 SAR Images

Time Series of Sand Wave Characteristics

To find a different way to visualize the change in value of sand wave characteristics, for 10 points across the sand wave field as seen in Figure 4.42, the sand wave characteristics were extracted for the years 2020, 2021, and 2022. The points along the Eastern border of the Polygon (like Point 3 and 7) are expected to perform better in terms of derivation of the sand wave characteristics due to the water depth being shallower.

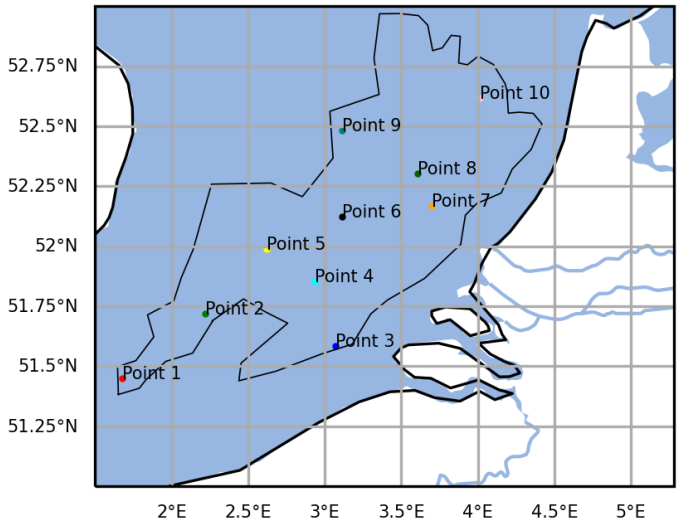

Figure 4.42: Locations within sand wave field for which time series of sand wave characteristics are computed

Dashed lines in Figure 4.43 indicate the points that are at deeper locations off of the Dutch Continental Shelf and come with more uncertainty. For the time series for the optical results, only points 1 and 5 have values greater than 1000 meters which is considered the upper limit for sand waves within the North Sea and both are on the West side of the sand wave field. For SAR, this is points 4, 5 and 7. Point 7 for SAR lies within the East half of the sand wave field and it is expected accurately calculate the sand wavelength at this location. This is true for the year 2020 and 2022, however in 2021 the value is just above 1000 meters which is unexpected. The tile for point 7 is seen in Figure 4.22 and contains three ships within the image which is the reason for the high value for the calculated wavelength.

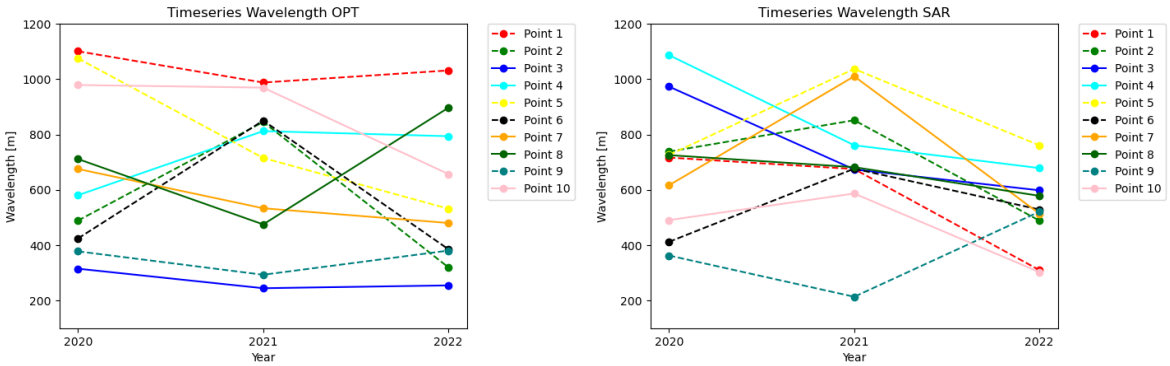

(a) Optical Images Time Series Wavelength

(b) SAR Images Time Series Wavelength

Figure 4.43: Optical and SAR time series of wavelength over years 2020, 2021, and 2022

The sand wave angle is shown in Figure 4.44. Although the wavelength for Point 7 in optical only varied about 100 meters over all three years, the wave angle experienced a drastic decrease in 2021 to 20 degrees while in 2020 and 2022 the angle is close to 70 degrees. Such a change can also be due to a ship within the area of the image. The resulting angle can be very low in value as seen in Figure 4.22. This also hold true for the value of the wave angle at Point 7 for SAR which changes drastically in 2021, like what happened for the wavelength during this year as well. This is also due to ships acting as a source of noise. However, another time when a wave angle has a low value is when no sand waves are visible in an image.

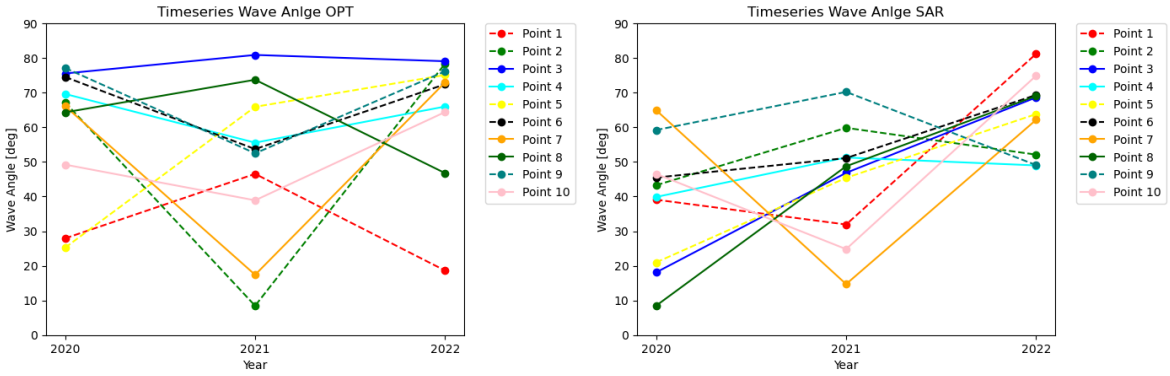

(a) Optical Images Time Series Wave Angle

(b) SAR Images Time Series Wave Angle

Figure 4.44: Optical and SAR time series of wave angle over years 2020, 2021, and 2022

The change in wave density year to year is expected to stay very small. The migration rate of sand waves in the North Sea is not high enough to expect any significant change within a 3 year time period considering the area of the tiles is 5 by 5 km, unless there is an outside source of noise. Over the time series, the density for the majority of the points remains mostly constant. The largest difference in value occurs for point 9, which is in the Northwest of the sand wave field. This is mostly due to the way

density is calculated and that there is more significant change when wavelength is short, which ranges from 200 to 400 meters at this location.

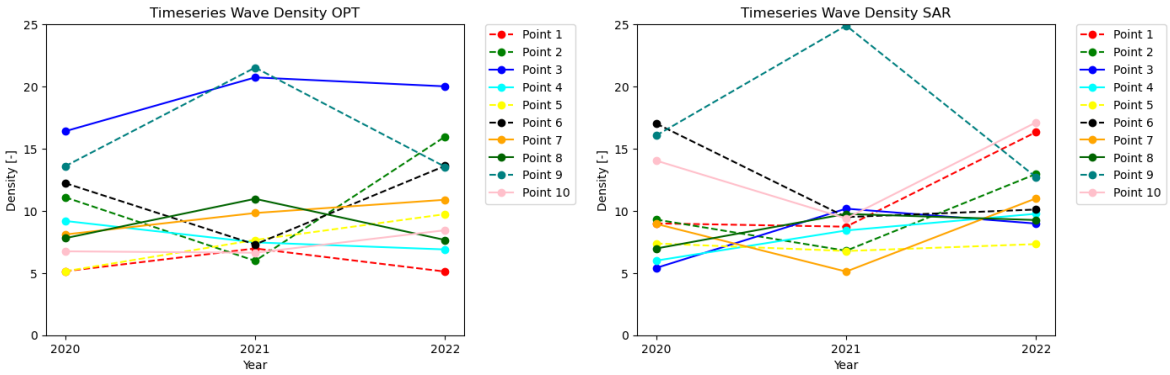

(a) Optical Images Time Series Wave Density

(b) SAR Images Time Series Wave Density

Figure 4.45: Optical and SAR time series of wave density over years 2020, 2021, and 2022

4.3. Summary of Results

In this section the results for Chapter 4 are summarized. Section 4.1 applies the methodology to three areas of interest, Hoek van Holland, Holland Kust Zuid, and Alkmaar. Each area has different sand wave properties, shorter irregular sand waves, long regular sand waves, and no sand waves, respectively. First, in Subsection 4.1.1 the filtering process was applied to each of the areas for the year 2021 for an optical image collection and a SAR image collection. The results of the filtering indicated that even if the conditions set for the environmental parameters are met, the results do not always contain sand waves. The lack of visibility of sand waves even though the conditions are met can be because of stricter thresholds necessary or due to additional parameters that are not considered in this thesis. Also, there are fewer optical satellite images that contain sand waves compared to SAR, and they occur between April and July, while SAR images containing sand waves can occur year-round. This acts as a temporal limitation because there is no guarantee that an image will be taken when the right conditions are met, Also, This means for optical images that there is no data availability during autumn and winter.

Then in Subsection 4.1.2 a FFT was performed for an optical and SAR image in 2021, as well as a MBES of the same area, to calculate the sand wave characteristics of wavelength and wave angle. The calculated sand wavelength between MBES and the remote sensing methods was within a range of 150 meters, and the wave angle within about 15 degrees for the locations containing sand waves. When comparing to the manually calculated average wavelength for these locations, the wavelength is better captured at Holland Kust Zuid where the sand waves have a longer wavelength and are more regular. A comparison of the calculated sand wave characteristics depending on area size was performed to determine which area size to apply for the upscaling. The area size decided on was 5 by 5 km. In Subsection 4.1.3, the effect of different sources of noise was explored to understand how the sand wave characteristics change in response. Wind farms have a significant effect on SAR images, and less of an effect optical images, making it a viable choice to use optical images at locations with wind farms. Ships have a strong effect on both optical and SAR images and should be avoided, or a method to successfully remove them from images is required. Optical images can also contain suspended sediment transport which does not affect the results because the resulting signal is always perpendicular to that of sand waves. Clouds, which also only affect optical images have a similar effect to ships in optical images and should be avoided. Dark patches in SAR images, due to rain cells in the North Sea, cover the signals of sand waves in satellite images, and therefore there is no resulting signal in the FFT.

Once the area size and the effect of noise was established an upscaling of the methodology over the North Sea was performed in Section 4.2. The results for a pass-over of the North Sea for a date in 2021 are shown in Subsection 4.2.1. This includes the calculated sand wave characteristics for sand wavelength, wave angle, and wave density. A comparison to results for sand wavelength and spatial frequency from Damen et al., 2018 was done to calculate the correlation. The environmental parame-

ters of wind and current speed for the same date and time were found to determine their effect in the visibility of sand waves. This process was repeated for 2020 and 2022 and the results are shown in Appendix B, and the difference in sand wave characteristics between 2021 and 2022 are compared for optical and SAR. Additionally, the time series of the sand wave characteristics for multiple points within the sand wave field were calculated. The entire process of upscaling to the North Sea shows that noise has a very strong effect on the results.

5
Discussion

This chapter discusses the different limitations in spatial and temporal scale that affect both remote sensing methods. The limitations of the methodology are important to understand because it affects the filtering process for satellite images to obtain sand waves and the results for the calculated sand wave characteristics. Also, a comparison between the availability of data and the process of calculating sand wave characteristics between optical and SAR images is discussed.

5.1. Spatial Limitations

5.1.1. Pixel Resolution

The resolution of satellite images has an effect on how the data can be worked with. The resolution of 10 meters for both Sentinel-1 and Sentinel-2 means that a high/low pass filter on the FFT for the specific wavelengths leaves few discernible features left in the passing image. Also, for very short sand waves of around 100 meters in wavelength, lower resolution would be an even larger problem for different satellites such as the Landsat Satellites which have a resolution of 30 meters. A satellite with higher resolution such as the Planet Dove satellites with a resolution of 3 meters will allow for satellite images with more information in it. A high/low pass filter could be applied with more success than for the current satellite images with a 10-meter resolution.

5.1.2. Noise

The amount of speckle noise present in SAR images carries over to the FFT of the image as seen in Figure 4.8 when comparing the resulting FFT for optical and SAR. Speckle noise is a strong limiting factor for SAR, especially when the goal of remote sensing of sand waves is to detect weaker signals within an image. A filter, like the Lee Filter that was applied to SAR images, smooths the effect of speckle noise to make sand wave signals clearer, especially for the FFT. However, the noise can be too strong to see the signals in the first place.

5.1.3. Area Size of Interest

Another spatial limitation is the difference in calculated sand wave characteristics due to the area size. As seen in Figure 4.16 the detected wavelength is different depending on the tile size. The size of the tile is important to which signals are most prominent in the FFT of the image. When the area is small, the signal that gets picked up is the width of the rougher or smoother patch of the ocean due to the sand wave's effect on the current based on the Alpers Hennings Model. The distance from the crest line to where the signal changes from rough to smooth is shown in Figure 2.3 as ΔL_2. This signal does not give the distance between sand waves which is needed for the wavelength. When the area considered is larger, the number of sand waves typically increases and the pattern created from the signals becomes more prominent. Then instead of the FFT taking the width of the signal, it instead represents the distance between signals, equating to the wavelength. This is why the wavelength measurement increases as the area increases and the average is a better match to the full area calculation. However, the area can also not be too large. This is because a large area is less homogeneous compared to a smaller area in sand wave characteristics, water depth, and environmental parameters.

5.1.4. Environmental Conditions

The most prominent spatial limitation is perhaps the water depth in conjunction with the environmental parameters. As discussed in Chapter 2, the method for detecting sand waves in satellite images works through the Alpers Hennings Model where the current interacts with the bed form which eventually in turn affects the sea surface roughness. For the sea surface roughness to change enough to be

discernible in satellite images, the current speed needs to be strong enough. As the depth increases so does the necessary current speed required for viewing sand waves. On the Dutch Continental Shelf where the depth ranges from 20 to 30 meters, the satellite images can capture sand waves present here. However, in deeper waters of the channel as seen in Figure 4.39, there are no sand waves seen. To be able to see sand waves, the threshold for current speed should be set higher. It was possible to observe bed forms with a wavelength of 2.3 kilometers at over 500 meter depth in SAR images with a strong current speed of 2 m/s (Li et al., 2010). Therefore, if the conditions of the other environmental parameters are met and a high enough threshold for the current speed is set it should be possible to view sand waves at deeper locations.

5.2. Temporal Limitations

5.2.1. Environmental Conditions

Remote sensing using optical images has limitations imposed by the environmental parameters, most significantly the mean glint angle and cloud cover. Due to these conditions, optical images containing sand waves typically only occur between April and August. Either the mean glint angle is too low, or the weather conditions during specific times of year means there is significant cloud cover making the FFT unsuitable. These factors limit the amount of available data containing sand waves for optical images.

Another temporal limitation is due to the data used for the environmental parameters when filtering the image collection for the correct conditions where sand waves should be visible. The source of data that was used for the environmental parameters of wind and current are both gained from models. Both datasets provide hourly data and the time at which the satellite image is taken and rounded to the nearest hour to get the corresponding wind and current speed values. This means that there can exist a difference of up to half an hour between the model results and the time at which an image is taken. Current speeds experience less significant variability compared to wind speed in this time frame. The wind speed resulting from ERA5 can vary significantly in small space and time scales. One reason for this is that wind gusts sustained over a 3 second time period can cause higher wind speeds over a specific area at the time the satellite image is taken and not be taken into account by the model data.

An additional limitation is due to the satellites themselves. The pass over time for Sentinel-1 over the North Sea is every 6 days and for Sentinel-2 is every 5 days. The perfect environmental conditions can occur at any given time at high frequency, however the chances that the satellite image is captured at this exact time is low. The use of additional satellites over a location would increase the amount of data available and the chances of a satellite image taken a time where the environmental conditions are met and sand waves are visible.

5.3. Comparison of Remote Sensing Methods

When comparing the two remote sensing methods of sand waves there are multiple factors to consider. First, the number of images that contain sand waves after filtering based on the environmental parameters. SAR is less limited by the parameters and has more available images year-round, while there only tends to be one or two usable optical images for areas within the North Sea. However, SAR, while more numerous, tends to have lower quality in images due to speckle noise, which tends to mask weaker signals such as sand waves, which does not affect optical images.

Secondly, optical and SAR images are affected differently by sources of noise which changes the resulting FFT and affects the calculations in sand wave characteristics. This means that there are different situations for which one method is more suitable than the other. For wind farms, the optical image handles the noise better than the SAR image does. The FFT for optical is less affected by the additional signals caused by the turbines leading to a better result. On the other hand, both methods do not handle ships well, with a ship having a strong signal and causing a drastic change in the value of wavelength and wave angle at a 5 kilometer scale. It is better to not include data when a ship is present at this scale. Unlike SAR, optical images can visually contain suspended sediment in the water column and therefore be affected by sediment. Sediment has little impact on the calculation of the sand wave characteristics because the signal created in the FFT is perpendicular to that of sand waves because of the direction of the current. Optical images are also the only ones to be affected by clouds,

which do have a larger impact on the FFT and need to be minimized by filtering data for a low cloud cover percentage. This makes it difficult to find suitable images in general, but especially difficult to find a single pass over of the North Sea with minimal clouds. A source of noise unique to SAR is dark patches where the reflectance is especially low compared to the surroundings which can be caused by multiple sources such as internal waves or rain cells. The most likely cause in the North Sea is rain cells.

Either remote sensing method can be used for any location worldwide that contains sand waves but multiple factors would change which method is best used. For example, an area of interest at latitude would likely also have weather patterns with a lot of clouds. This typically means that the amount of available optical images containing sand waves will be less than SAR because of the mean glint angle and cloud cover conditions not being satisfied. Also, as seen in Figure 4.31, the results for the optical image can be used to define the sand wave field to some extent. When removing points where the sand waves are either smaller than 100 meters or larger than 1000 meters, the results were relatively within the bounds of the sand wave field. Another difference is the effect of noise as explained in the paragraph above. Optical images can be used to determine sand wave characteristics in locations with wind farms while SAR cannot. However, SAR is not affected by clouds as a source of noise. When there are smaller and more irregular sand waves present, they are more likely to be seen in an optical image compared to a SAR image as seen in Figure 4.6 due to speckle noise.

5.4. Applications of Remote Sensing

Remote sensing of sand waves through satellite images from both SAR and Optical can be used to detect sand wave characteristics including wavelength, wave angle and density. Between Optical and SAR, there are differences for how effective it will be. For example, optical images can be used to supplement MBES data for wind farms because it is less affected by the source of noise. Remote sensing provides an alternative method to get a preliminary assumption on sand wave characteristics within an area. It can also be used to look back in time at an area before surveys were performed or to supplement data poor areas, especially if there were only single-beam sonar surveys available at a location, since the data provided by the methodology is two dimensional.

Another option to get better quality data for a time frame is to combine the results from different satellite images. This allows for a easy way to remove data points that either do not capture sand waves due to the environmental conditions, or calculate wrong due to additional signals in the FFT from noise. The mosaic of the results for the North Sea can be created from multiple years because of low migration rates compared to the area size of 5 by 5 kilometer considered.

6
Conclusions

Sand waves impact offshore activities such as offshore wind farms and therefore having knowledge of what is happening on the seabed is important. The purpose of this thesis was to develop a methodology to calculate sand wave characteristics using satellite data and understand the limitations of this process. This led to the following research question:

To what extent can satellite data be used to detect sand waves in different environments?

This research question was answered through three sub-questions. The first step was to determine which existing methods there are for utilizing satellite data. Then, a method to filter satellite image collections over a period of time and area of interest for Sentinel-1 and Sentinel-2, SAR and optical images respectively, was developed. The filtering depends on four environmental parameters, mean glint angle, cloud cover, wind speed, and current speed, where the first two parameters only pertain to optical image collections. Then, a Fourier Transformation is applied to the resulting images containing sand waves. A process to determine sand wave characteristics including the sand wavelength, sand wave angle, and density, from the resulting signal in the FFT. The results were used to answer the following questions:

1. What methods are there for detecting sand waves through satellite data and what are the different processes they require?

The different methods of detecting sand waves through remote sensing with satellites was discussed in Chapter 2. These methods include directly viewing sand waves through the blue band of optical images and measuring the sea surface roughness directly through SAR Images, or indirectly using sun glint through Optical Images. The sea surface roughness change can be explained through the Alpers-Hennings Model which works in three steps. The first is that a current will be affected by seabed forms such as sand waves, and this current variation will in turn affect the surface currents, which will then change the sea surface roughness.

2. How can these methods be applied to sand wave fields in different environments?

Remote sensing of sand waves is a viable method to obtain sand wave characteristics, including wavelength, wave angle, and density, by applying a Fourier Transformation to an image containing sand waves. This can be done for both regular and irregular sand waves. Also for a range of wavelengths as sand waves in the North Sea can range from 100 to 1000 meters in length. However it requires very specific conditions for it to work and is still strongly impacted by the quality of the data. Different sources of noise such as ships, clouds, and wind farms need to be accounted for because it affects the calculation of sand wave characteristics.

3. What is the accuracy of the methods and what are the limitations regarding spatial and temporal scale?

The accuracy of the sand wave characteristics is negatively impacted by different sources of noise such as wind farms, ships, and clouds, that can be present within the satellite image. These different sources of noise introduce additional signals within the FFT and cause the sand wave characteristics to be calculated based on the signals created from the noise rather than the sand waves. When comparing the resulting sand wavelength for the North Sea to values determined by MBES data by Damen et al., 2018, the correlation between datasets is low, indicating that there can still be improvements

in calculating sand wave characteristics. Further research is required to determine whether this improvement can be achieved by removing sources of noise, better quality of satellite images, or another reason.

There are multiple temporal and spatial limiting factors. Temporal limiting factors for both optical and SAR images are the conditions necessary from the environmental parameters of wind speed, current speed, mean glint angle, and cloud cover. Optical images are most affected by the mean glint angle and the cloud cover. The mean glint angle for the North Sea is only satisfactory for a few months per the year and optical images containing sand waves were found only between April and July, and only one or two images per year. SAR images are more numerous considering these are only dependent on wind and current speed and therefore images are found throughout the year. The spatial limitations that affect the remote sensing methods is the resolution of the satellite images. Higher resolution allows for more information to be captured including shorter sand waves. A limitation that only affects SAR images is the speckle noise caused by the interference of the back scatter of the signal. This effect can be stronger than the signal of sand waves, effectively covering them. The most limiting factor is the depth in conjunction with the current speed. Although the upscaling of the methodology was applied to the North Sea, sand waves were only reliably visible up to depths of 40 meters. Sand waves are only visible with strong current speeds and to see sand waves in deeper waters it needs to be even stronger.

Final Conclusion

To answer the research question of this thesis, to what extent can satellite data be used to detect sand waves in different environments, the answers to the three sub-questions are combined. Based on the Alpers-Hennings Model, in which the sea surface roughness changes due to current interactions with sand waves, they are visible in both optical and SAR satellite images. It is possible to determine sand wave characteristics such as sand wavelength, wave angle, and wave density over an area by using a Fourier transformation. This method is better suited for regular sand waves with a longer wavelength. The irregularity of sand waves and a shorter wave length causes more deviation from the actual sand wave characteristics. By upscaling the same methodology, it is possible to determine these sand wave characteristics for the sand wave field in the North Sea for 5 by 5 kilometer areas. The methodology is limited by environmental parameters and noise that can be present in the satellite images. As discussed, for SAR images to have visible sand waves there are specific current and wind speed conditions, and while optical images also require these same conditions it is also dependent on the mean glint angle and cloud cover. Sources of noise that can effect the resulting sand wave characteristics includes ships, wind farms, dark patches for SAR images, and clouds for optical images. Therefore, it is possible to apply the process for determining sand wave characteristics over an entire sand wave field, like that of the North Sea, however, the results are dependent on the environmental conditions and present noise. The process is not fully automated because there is still a need to manually check the filtered image collection for whether or not it contains sand waves. To allow for further automation of the process more conditions should be considered for filtering the image collections.

7 Recommendations

Recommendations for future research to expand on the results of this thesis are listed bellow. Additional research will allow for further understanding on the application of remote sensing for sand waves.

Additional Conditions
To improve the results from filtering of the original image collection, another environmental parameter that could be filtered for is swell. Swell can have the same period as the sand waves at a location which mimics the signal of a sand wave. Also, even if the swell has a different period it is typically a stronger signal than that of sand waves and would prevent it from being seen. By removing dates when swell is present this problem would be avoided, however it would be necessary to have another dataset as input like that of current and wind speed. This could either be real world observations from buoys, or model output.

As seen in Section 4.1.3, ships can have a strong effect on the resulting FFT, which is more prevalent for optical images compared to SAR. To remove this problem the tiles containing ships would be flagged. Data on ship position can be obtained with the Automatic Identification System (AIS) required for most vessels. Using the exact date and time for a satellite image pass over to get the exact locations of ships within the area of interest, the data points can be removed. Another method to address noise is to remove it from the satellite image before taking the Fourier transformation. This would mean that there is more satellite data available rather than images containing sand waves being removed from the collection for containing ships, and better able to use the methodology at wind farms. One method to accomplish this Otsu's method which splits pixels based on a threshold value.

Another important step is to be able to determine whether or not sand waves are detected. This could be accomplished through machine learning or from the resulting FFT. The FFT for an area that contains no sand waves presents differently than if there are sand waves. This visual difference means there should be a method to discern a difference in the FFT containing sand waves from those without. It would better define the limits of a sand wave field as well as give more information on the limitations of the methodology, such as depth. It can also be used for a single pass over can be sorted based on the presence of sand waves the methodology can be upscaled even more to apply to even larger areas.

Mosaic Data
As seen in Figures 4.30 and B.3, the satellite images can contain clouds or dark patches. Sometimes, sand waves are not visible throughout an entire area due the environmental conditions. Other times, sources of noise like ships are present that effect thee calculation of sand wave characteristics. To overcome this, multiple satellite images over an area can be compiled together. An average image will not suffice because the sources of noise will still be present. Also, the presentation of sand wave signals in the satellite image will change due the environmental parameters, for example, the location will change if the wind and current are in the same direction compared to if they are in opposite directions. The best option would be to mosaic the images, taking the best quality data for each tile.

Other Locations
As discussed in Chapter 2, there are multiple locations with sand wave fields containing sand waves with different characteristics and environmental conditions. For example, in the Taiwan Banks, the sand waves are very symmetrical unlike in the North Sea, which could make them more or less visible. Also, the conditions for mean glint angle and the amount of expected cloud cover per year is going to be different than the North Sea considering it is at a much lower latitude as different weather conditions affecting cloud cover. Another location of interest would be the sand wave fields on the East Coast of

the United States of America by Connecticut, where the migration of sand waves is higher than in the North Sea.

Satellites
The image collections for Sentinel-1 and Sentinel-2 are limited by a few factors. The first is that the frequent pass over rate is about 6 days over Europe and lower elsewhere in the world. Also, it only contains images dating back to 2014 and 2015 and has a resolution of 10 meters. Although a lower pass over rate and lower resolution of 25 meters, Landsat-4 was launched in 1982, with multiple newer Landsat satellites launched at later dates, having a total number of images that can be used to detect satellites up to over 5 million. This would allow for the detection of sand waves into the past for locations with a lack of data. Another option to improve the dataset is to use satellite with much higher resolution, such as Planet Dove with an optical image resolution of three meters or TerraSAR with a SAR image resolution of one to three meters. Higher resolution data will allow for more accuracy and the possibility to use a high or low pass filter at a smaller scale without losing too much data to make it legible.

Determine Crest Location
As seen in Figure 4.10 (a), sand waves can be very easily identified. In this thesis the method of extracting sand wave characteristics like wavelength and wave angle was accomplished by applying a 2D FFT to the satellite images. However, another method of obtaining the sand wave characteristics would be by identifying the locations of the sand wave crests. This would also result in knowing the general location of sand waves. More research is needed into understanding the effect of current and wind on the shift in location of the crest location as seen in Figure 2.3 with ΔL_2, the distance from the crest location to the point where the sea surface roughness changes from smooth to rough, which is most prominent in satellite images.

Machine Learning
Another option for moving forward in the remote sensing of sand waves is by applying machine learning. The method of obtaining images now is by setting threshold values based on environmental parameters and then filtering an image collection. At this point, there are still factors unaccounted for when filtering for images containing sand waves because the resulting collection after filtering contains a combination of images containing sand waves and those without. A way to get around this is machine learning for which the training data is satellite images containing sand waves. Then, the ideal model would be able to determine the satellite images that contains sand waves.

Reflectance Model to Predict where Sand Waves should be
In Haakman, 2023 a reflectance model was used to recreate Kelvin wakes from ships. It is based on the solar zenith and azimuth angles as well as surface slopes of wind waves necessary for the reflectance to occur based on the wind speed. The expected reflectance of the Kelvin wake can be calculated from these values. This model could be applied to satellite images to make the signals from sand waves more clearer. This can be potentially used in the same way it was used in Haakman, 2023, to find the ideal conditions to view sand waves, rather than a trial by error.

References

4COffshore. (n.d.). Global offshore renewable map. https://map.4coffshore.com/offshorewind/

Agrawal, S., & Khairnar, G. B. (2019). A comparative assessment of remote sensing imaging techniques: Optical, sar and lidar. *International Archives of the Photogrammetry, Remote Sensing and Spatial Information Sciences - ISPRS Archives*, *42*, 1–6. https://doi.org/10.5194/isprs-archives-XLII-5-W3-1-2019

Alpers, W., & Hennings, I. (1984). Theory of the imaging mechanism of underwater bottom topography by real and synthetic aperture radar. *Journal of Geophysical Research*, *89*, 10529–10546. https://doi.org/10.1029/JC089iC06p10529

Basu, M. (2002). Gaussian-based edge-detection methods- a survey. *IEEE Transactions on Systems, Man, and Cybernetics, Part C*, *32*, 252–260. https://doi.org/10.1109/TSMCC.2002.804448

Bergsma, E. W., & Almar, R. (2020). Coastal coverage of esa' sentinel 2 mission. *Advances in Space Research*, *65*, 2636–2644. https://doi.org/10.1016/j.asr.2020.03.001

Besio, G., Blondeaux, P., Brocchini, M., Hulscher, S. J., Idier, D., Knaapen, M. A., Németh, A. A., Roos, P. C., & Vittori, G. (2008). The morphodynamics of tidal sand waves: A model overview. *Coastal Engineering*, *55*, 657–670. https://doi.org/10.1016/j.coastaleng.2007.11.004

Damen, J. M., Dijk, T. A. G. P. V., & Hulscher, S. J. M. H. (2018). Spatially varying environmental properties controlling observed sand wave morphology. *Journal of Geophysical Research*. https://doi.org/10.4121/uuid:0d7e016d-2182-46ea-bc19-cdfda5c20308

Gagliardini, D. A., Dogliotti, A. I., Karszenbaum, H., & Grings, F. (2004). Comparison of bathymetric features detected by ers2 sar and landsat tm data over san matías gulf, argentina. *Gayana (Concepción)*, *68*. https://doi.org/10.4067/s0717-65382004000200036

Giglio, L., Descloitres, J., Justice, C. O., & Kaufman, Y. J. (2003). An enhanced contextual fire detection algorithm for modis. *Remote Sensing of Environment*, *87*, 273–282. https://doi.org/10.1016/S0034-4257(03)00184-6

Gorelick, N., Hancher, M., Dixon, M., Ilyushchenko, S., Thau, D., & Moore, R. (2017). Google earth engine: Planetary-scale geospatial analysis for everyone. *Remote Sensing of Environment*, *202*, 18–27. https://doi.org/10.1016/j.rse.2017.06.031

Gruppetta, S. (2021). How to create any image using only sine functions | 2d fourier transform in python. https://thepythoncodingbook.com/2021/08/30/2d-fourier-transform-in-python-and-fourier-synthesis-of-images/

Haakman, K. (2023). Estimation of surface currents using optical satellite imagery of kelvin wakes. http://repository.tudelft.nl/.

Harmel, T., Chami, M., Tormos, T., Reynaud, N., & Danis, P. A. (2018). Sunglint correction of the multi-spectral instrument (msi)-sentinel-2 imagery over inland and sea waters from swir bands. *Remote Sensing of Environment*, *204*, 308–321. https://doi.org/10.1016/j.rse.2017.10.022

He, X., Chen, N., Zhang, H., Fu, B., & Wang, X. (2014). Reconstruction of sand wave bathymetry using both satellite imagery and multi-beam bathymetric data: A case study of the taiwan banks. *International Journal of Remote Sensing*, *35*, 3286–3299. https://doi.org/10.1080/01431161.2014.902551

Hennings, I., Matthews, J., & Metzner, M. (1994). Sun glitter radiance and radar cross-section modulations of the sea bed. *Journal of Geophysical Research*, *99*. https://doi.org/10.1029/93jc02777

Hulscher, S. J. M. H. (1996). Tidal-induced large-scale regular bed form patterns in a three-dimensional shallow water model. *Journal of Geophysical Research*, *101*.

Hulscher, S. J., & Dohmen-Janssen, C. M. (2005). Introduction to special section on marine sand wave and river dune dynamics. *Journal of Geophysical Research: Earth Surface*, *110*. https://doi.org/10.1029/2005JF000404

Jackson, C. R., & Alpers, W. (2010). The role of the critical angle in brightness reversals on sunglint images of the sea surface. *Journal of Geophysical Research: Oceans*, *115*. https://doi.org/10.1029/2009JC006037

Kay, S., Hedley, J. D., & Lavender, S. (2009). Sun glint correction of high and low spatial resolution images of aquatic scenes: A review of methods for visible and near-infrared wavelengths. *Remote Sensing*, *1*, 697–730. https://doi.org/10.3390/rs1040697

Kras, E., Luijendijk, A., White, R., Roetert, T., & Overes, P. (2022). *Cable-seabed interaction*. Deltares.

Li, X., Yang, X., Zheng, Q., Pietrafesa, L. J., Pichel, W. G., Li, Z., & Li, X. (2010). Deep-water bathymetric features imaged by spaceborne sar in the gulf stream region. *Geophysical Research Letters*, *37*. https://doi.org/10.1029/2010GL044406

Liu, X., Li, Y., Liu, X., & Zou, H. (2022). Dark spot detection from sar images based on superpixel deeper graph convolutional network. *Remote Sensing*, *14*. https://doi.org/10.3390/rs14215618

Nemeth, A. A. (2003). *Modelling offshore sand waves*. s.n.]

Painam, R. K., & Manikandan, S. (2021). A comprehensive review of sar image filtering techniques: Systematic survey and future directions. *Arabian Journal of Geosciences*. https://doi.org/10.1007/s12517-020-06416-1/Published

Rijksoverheid. (2018). *Kabinet maakt plannen bekend voor windparken op zee 2024-2030*. Retrieved March 28, 2023, from https://www.rijksoverheid.nl/actueel/nieuws/2018/03/27/kabinet-maakt-plannen-bekend-voor-windparken-op-zee-2024-2030

Rijksoverheid. (2020). *Offshore wind energy*. Retrieved March 28, 2023, from https://www.government.nl/topics/renewable-energy/offshore-wind-energy

Roetert, T., Raaijmakers, T., & Borsje, B. W. (2017). *Cable route optimization for offshore wind farms in morphodynamic areas be safe view project sandbox-smart and sustainable design for offshore operations in a sandy seabed view project*.

Shao, H., Li, Y., & Li, L. (2011). Sun glitter imaging of submarine sand waves on the taiwan banks: Determination of the relaxation rate of short waves. *Journal of Geophysical Research: Oceans*, *116*. https://doi.org/10.1029/2010JC006798

Shao, H., Li, Y., & Li, L. (2014). Priori knowledge based a bathymetry assessment method using the sun glitter imagery: A case study of sand waves on the taiwan banks. *Acta Oceanologica Sinica*, *33*, 120–126. https://doi.org/10.1007/s13131-014-0375-z

Taskesen, E. (2020). Denoise. https://erdogant.github.io/findpeaks/pages/html/Denoise.html

UNFCCC. (2015). The paris agreement.

van Santen, R. B., de Swart, H. E., & van Dijk, T. A. (2011). Sensitivity of tidal sand wavelength to environmental parameters: A combined data analysis and modelling approach. *Continental Shelf Research*, *31*, 966–978. https://doi.org/10.1016/j.csr.2011.03.003

Zhang, H., Lou, X., Li, Y., Shi, A., Li, D., & Fu, B. (2015). Whitecap features induced by submarine sand waves in stereo optical imagery. *Journal of Geophysical Research: Oceans*, *120*, 6225–6233. https://doi.org/10.1002/2015JC010947

Zhang, H., Lou, X.-L., Shi, A.-Q., He, X.-K., Guan, W.-B., & Li, D.-L. (2014). Observation of sand waves in the taiwan banks using hj-1a/1b sun glitter imagery. https://doi.org/10.1117/1.JRS.8

Zhang, H., Yang, K., Lou, X.-L., Li, D.-L., Shi, A.-Q., & Fu, B. (2015). Bathymetric mapping of submarine sand waves using multiangle sun glitter imagery: A case of the taiwan banks with aster stereo imagery.

Zhang, H., Yang, K., Lou, X., Li, Y., Zheng, G., Wang, J., Wang, X., Ren, L., Li, D., & Shi, A. (2018). Observation of sea surface roughness at a pixel scale using multi-angle sun glitter images acquired by the aster sensor. *Remote Sensing of Environment*, *208*, 97–108. https://doi.org/10.1016/j.rse.2018.02.004

A
Fourier Transformation Sensitivity

To determine which parameters will most accurately capture the center of the signal from the sand waves presented within the FFT a sensitivity analysis was performed for a SAR and optical image from June 2022 at Hoek van Holland. The FFT is split into four quadrants and the quadrant containing the positive signal is used which in this case where the waves have an orientation from southwest to north-east the second quadrant is used

The center of the signal is determined by taking the nth percentile of the remaining data and calculating the mean location of this point. A range of percentiles was used from 65th to 99th percentile as seen in the following figure. In this figure the signal is visually best captured by the 99th percentile.

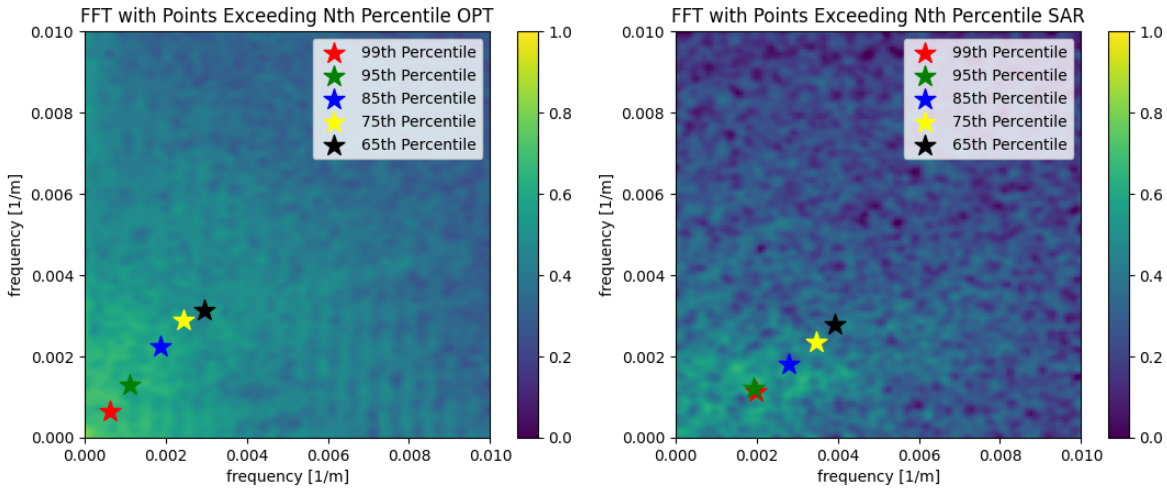

Figure A.1: FFT with calculated center of signal at for different percentile for optical image (left) and SAR image (right)

Another factor for determining the center of the signal is done by setting limits to the FFT to disregard outliers that can occur. This is done by cutting off the array and then calculating the center of the signal for the 99th percentile as seen in the following figure. At lower percentile values there was an increase in visual matching to the center of the signal as the limit decreased, however for the 99th percentile the change in the location of the center of the signal is very small. The limit decided on was 0.01 which is equivalent to a wavelength of 1000 meters along the x or y axis which is the maximum expected wavelength of sand waves in the North Sea.

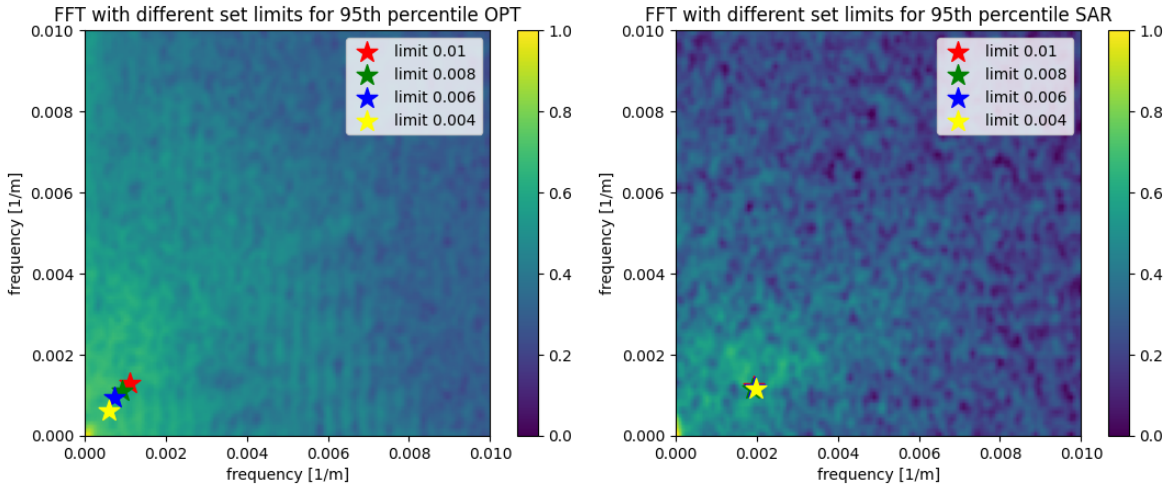

Figure A.2: FFT with calculated center of signal using the 99th percentile at different limits for optical image (left) and SAR image (right)

B Additional Results

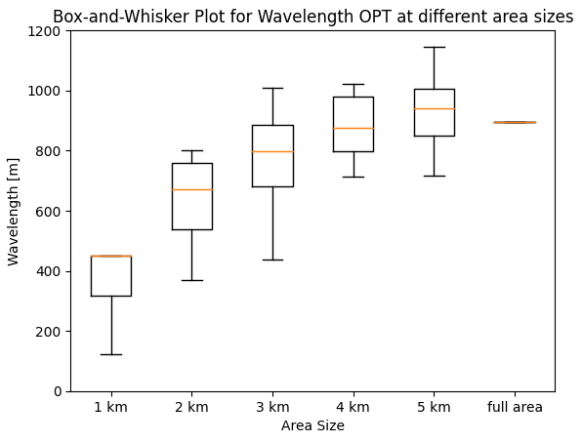

(a) Wave Length Optical

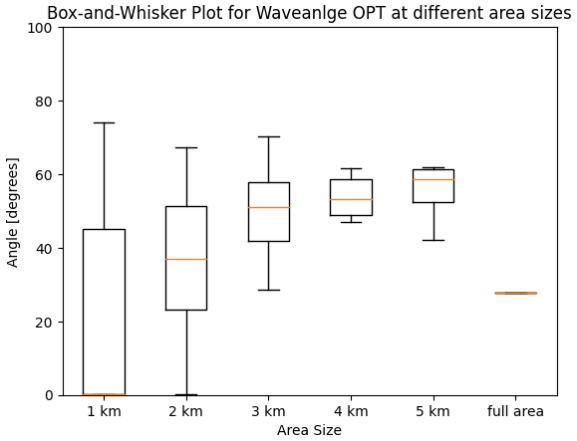

(b) Wave Angle Optical

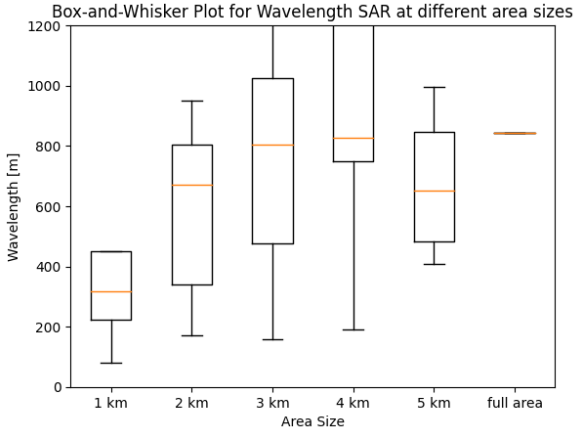

(c) Wave Length SAR

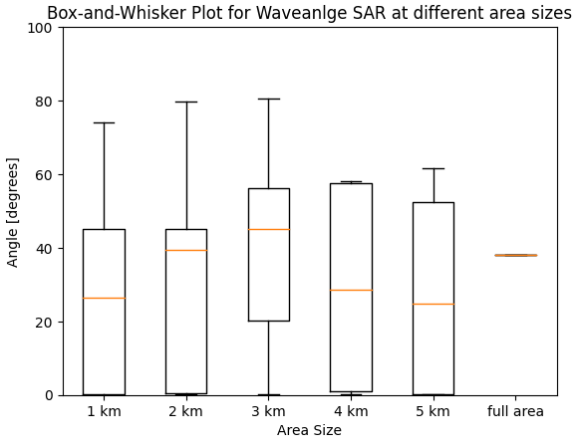

(d) Wave Angle SAR

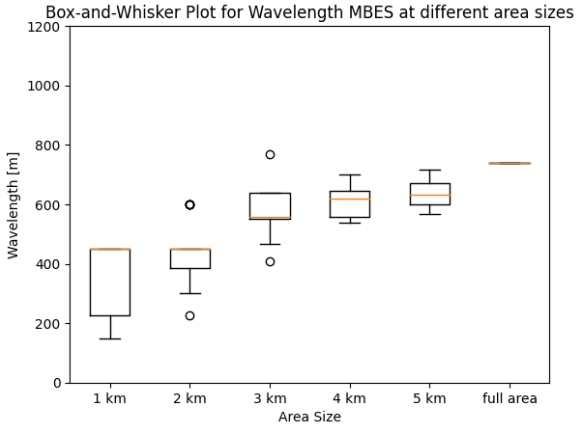

(e) Wave Length MBES

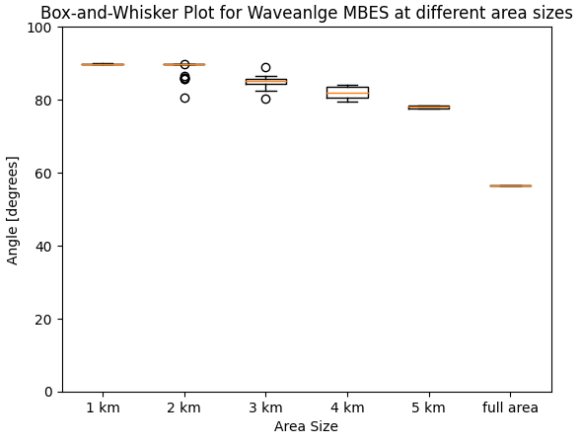

(f) Wave Angle MBES

Figure B.1: Comparison of different tile sizes and effect on sand wave characteristics at Holland Kust Zuid for Optical and SAR Image and MBES

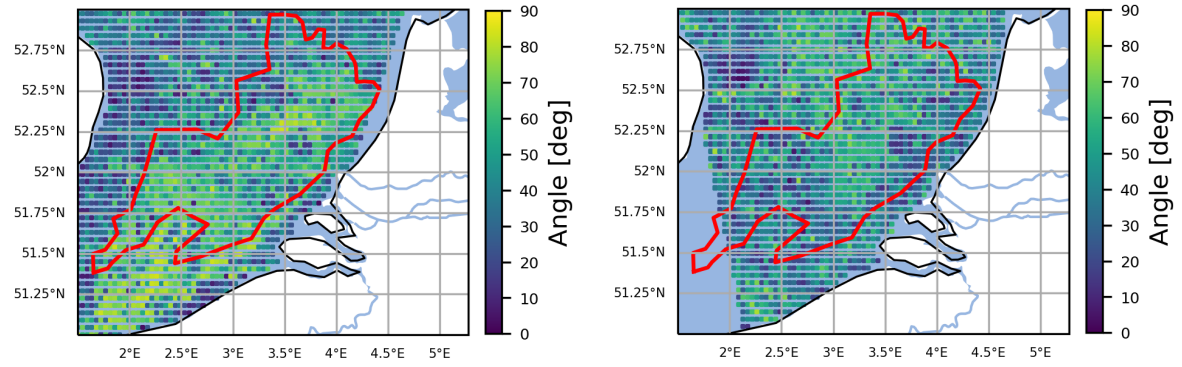

(a) Optical Image Wave Angle

(b) SAR Image Wave Angle

Figure B.2: Optical and SAR results for sand wavelength 2021 without filtering for a wavelength between 100 and 1000 meters

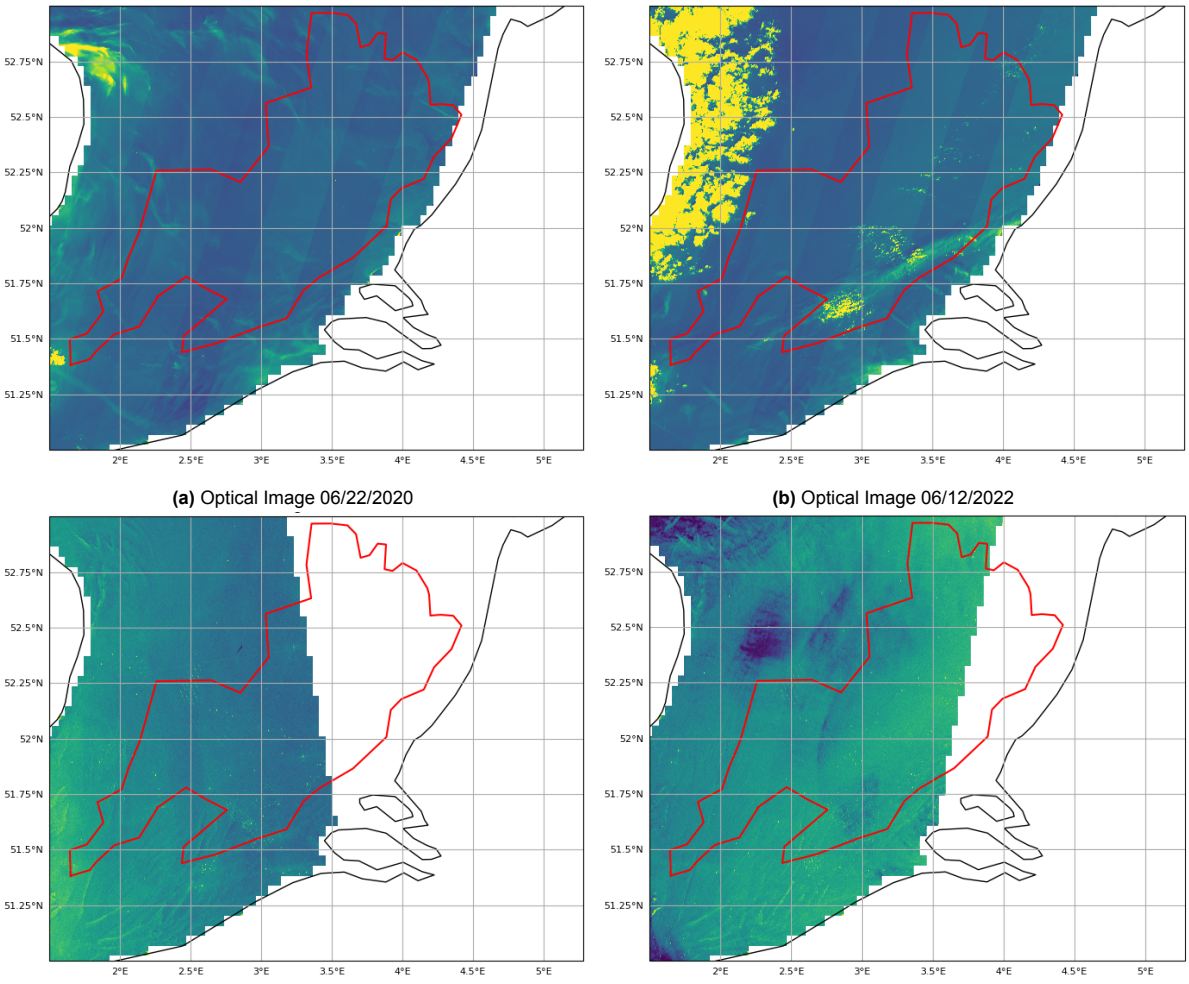

(a) Optical Image 06/22/2020

(b) Optical Image 06/12/2022

(c) SAR Image 06/03/2020

(d) SAR Image 06/14/2022

Figure B.3: Optical and SAR satellite image over the entire North Sea using a single pass over

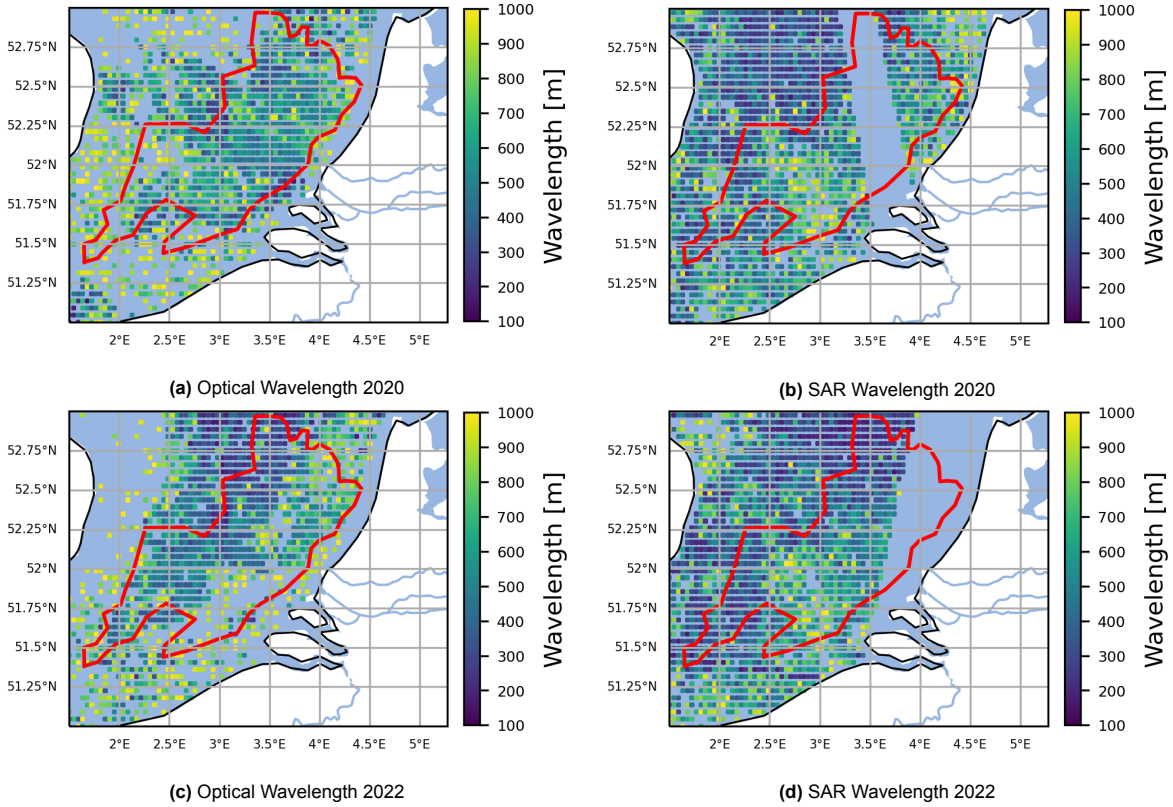

(a) Optical Wavelength 2020

(b) SAR Wavelength 2020

(c) Optical Wavelength 2022

(d) SAR Wavelength 2022

Figure B.4: Optical and SAR results for sand wavelength for years 2020 and 2022

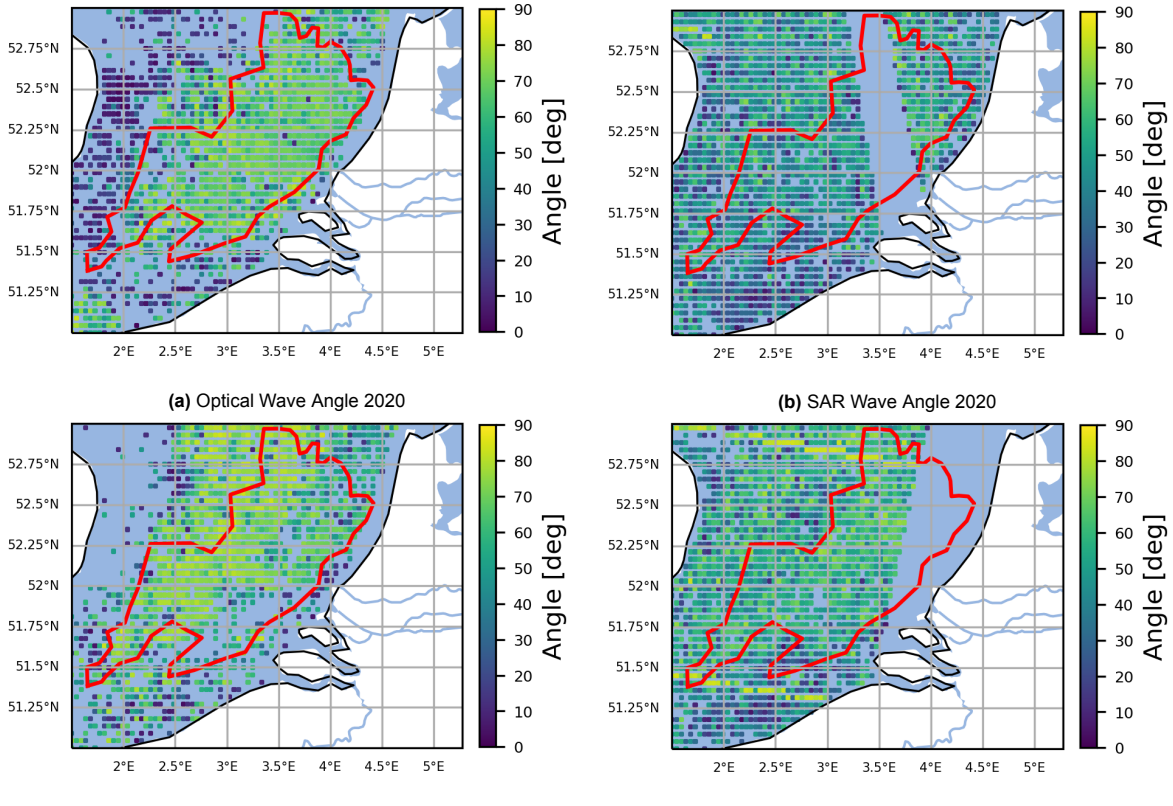

(a) Optical Wave Angle 2020

(b) SAR Wave Angle 2020

(c) Optical Wave Angle 2022

(d) SAR Wave Angle 2022

Figure B.5: Optical and SAR results for sand wave angle for years 2020 and 2022

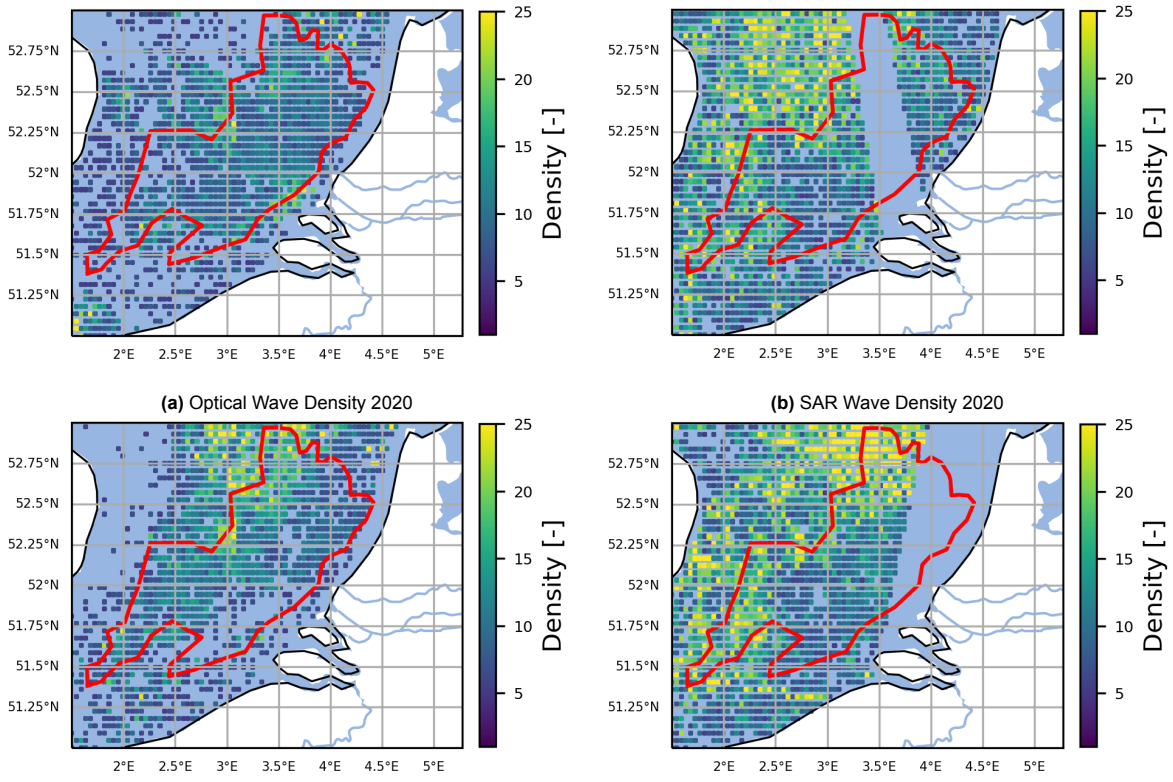

(a) Optical Wave Density 2020

(b) SAR Wave Density 2020

(c) Optical Wave Density 2022

(d) SAR Wave Density 2022

Figure B.6: Optical and SAR results for sand wave density over a length of 1 km for years 2020 and 2022

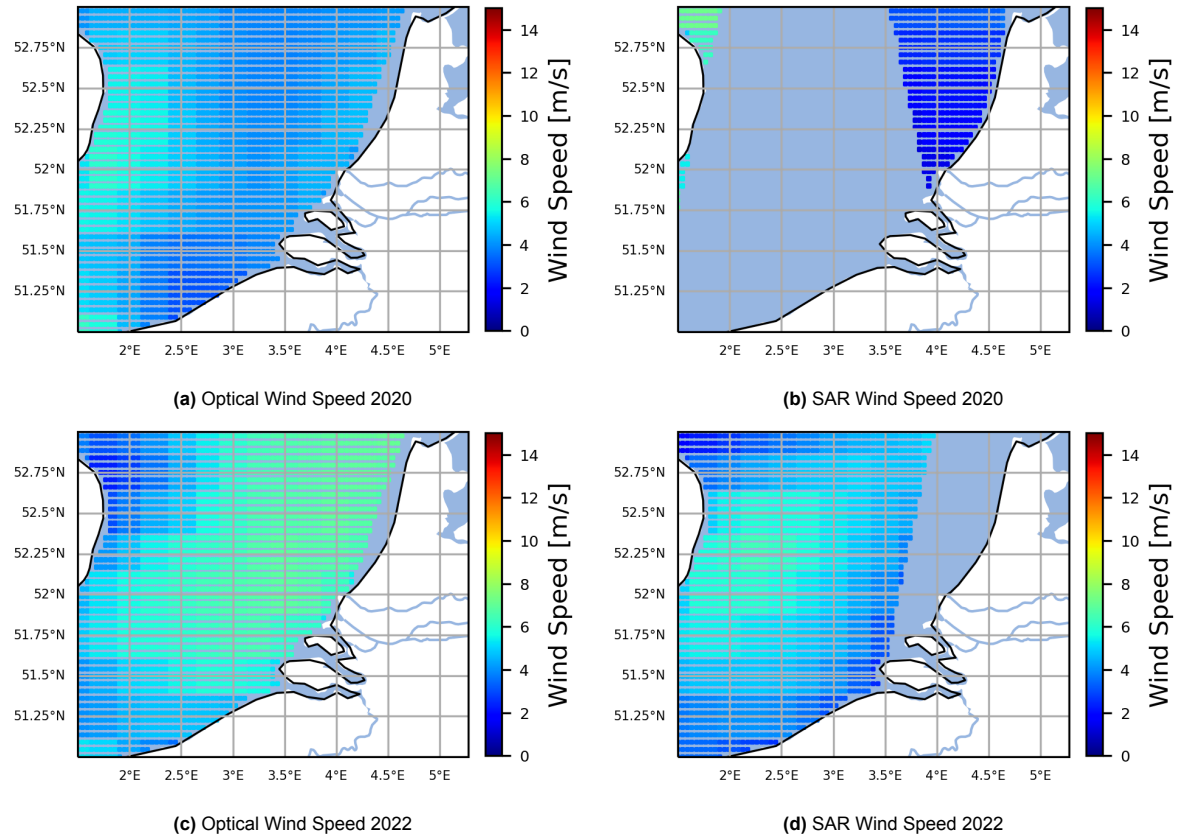

(a) Optical Wind Speed 2020

(b) SAR Wind Speed 2020

(c) Optical Wind Speed 2022

(d) SAR Wind Speed 2022

Figure B.7: Wind Speed for the same time as Optical and SAR image for years 2020 and 2022

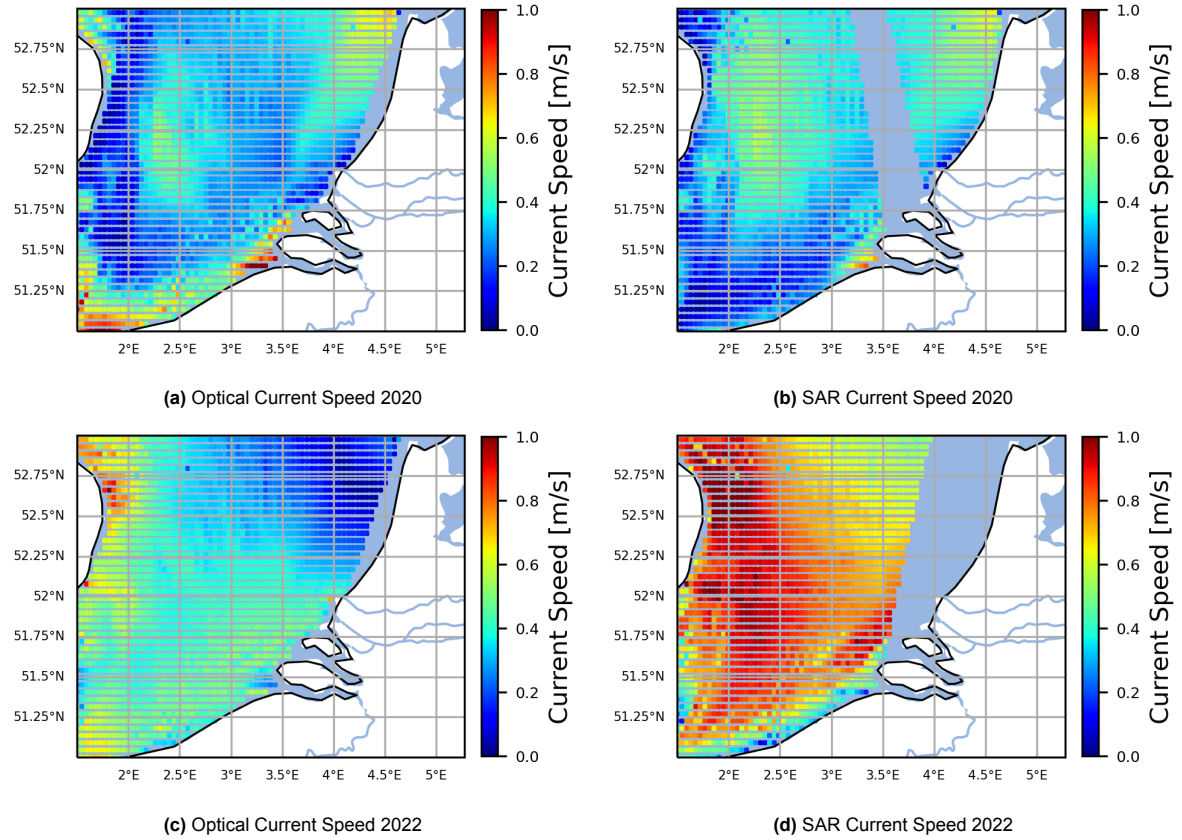

(a) Optical Current Speed 2020

(b) SAR Current Speed 2020

(c) Optical Current Speed 2022

(d) SAR Current Speed 2022

Figure B.8: Wind Speed for the same time as Optical and SAR image for years 2020 and 2022

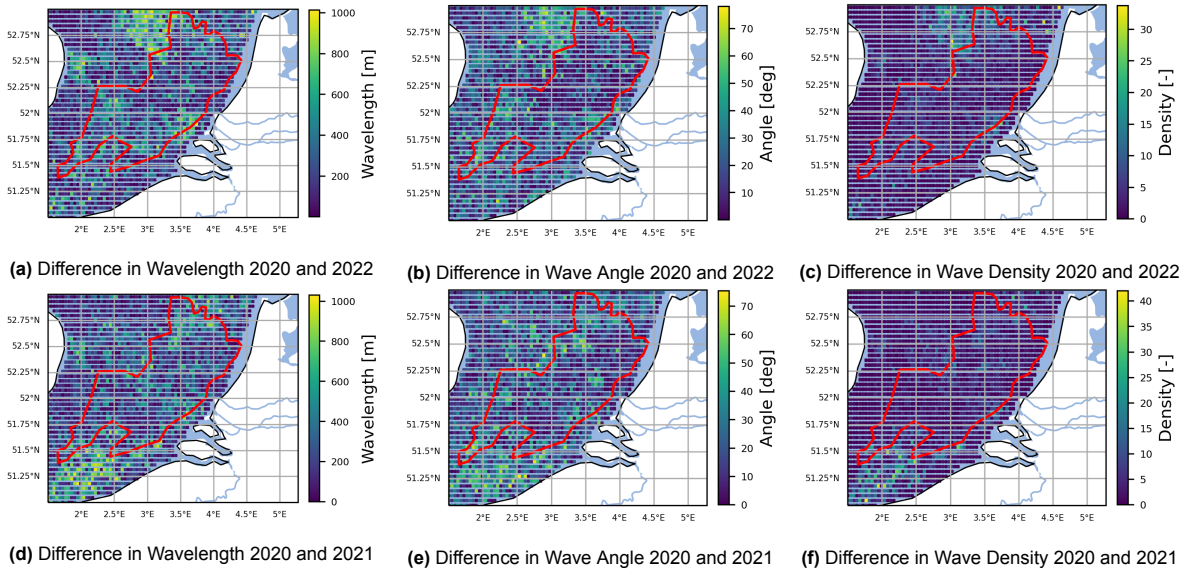

(a) Difference in Wavelength 2020 and 2022

(b) Difference in Wave Angle 2020 and 2022

(c) Difference in Wave Density 2020 and 2022

(d) Difference in Wavelength 2020 and 2021

(e) Difference in Wave Angle 2020 and 2021

(f) Difference in Wave Density 2020 and 2021

Figure B.9: Difference between results Optical Images

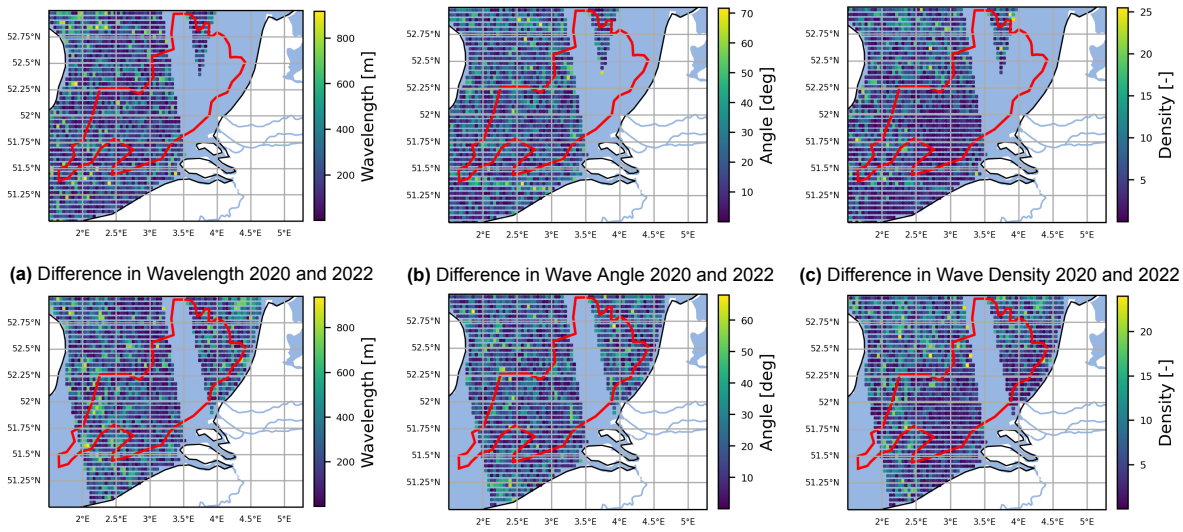

(a) Difference in Wavelength 2020 and 2022

(b) Difference in Wave Angle 2020 and 2022

(c) Difference in Wave Density 2020 and 2022

(d) Difference in Wavelength 2020 and 2021

(e) Difference in Wave Angle 2020 and 2021

(f) Difference in Wave Density 2020 and 2021

Figure B.10: Difference between results SAR Images

C
Irregular and Regular Waves

When comparing the sand waves at Holland Kust Zuid (HKZ) and Hoek van Holland (HvH) there are differences in the characteristics. The sand waves present HKZ are regular waves with long wavelengths and a similar wave angle while at HvH the sand waves are much more irregular with shorter wavelengths and a larger range of wave angles. This can be seen in the resulting signal from the Fourier Transformation in Figures 4.11 and 4.8 for HKZ and HvH respectively. The signal at HKZ is much more concentrated at a single point while the signal for HvH is spread out more.

This is also reflected in the difference of the probability density function for the FFT between regular and irregular waves as seen in Figure C.1. The difference is most visible for the optical images, where the peak for regular sand waves is much higher, as more concentrated. Similarly, the distribution for regular waves for SAR has a higher overall density compared to irregular waves.

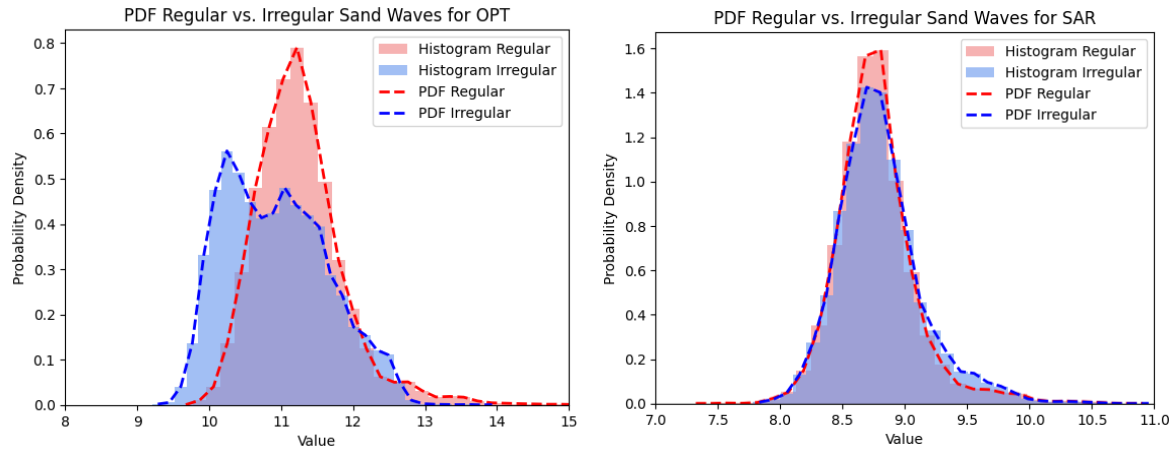

(a) PDF OPT

(b) PDF SAR

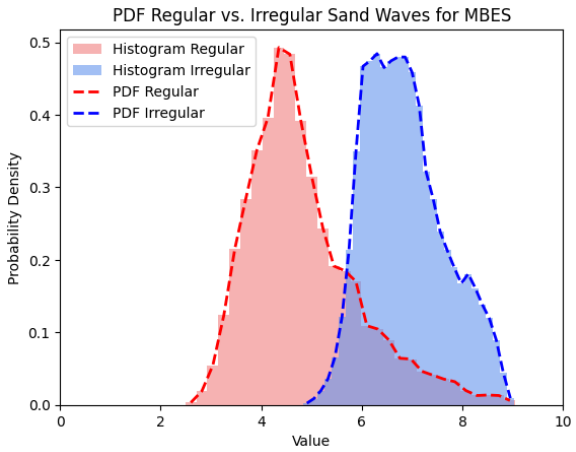

(c) PDF MBES

Figure C.1: Comparison between regular and irregular waves at Holland Kust Zuid and Hoek van Holland respectively for optical images, SAR images, and MBES